Asian Power Electronics Journal

PERC, HK PolyU

First edition Dec. 2018 Printed in Hong Kong by Reprographic Unit
The Hong Kong Polytechnic University

Published by

Power Electronics Research Centre
The Hong Kong Polytechnic University
Hung Hom, Kowloon, Hong Kong

ISSN 1995-1051

Disclaimer

Any opinions, findings, conclusions or recommendations expressed in this material/event do not reflect the views of The Hong Kong Polytechnic University

Editorial board

Table of Content

Theoretical Analysis of Isolated Bidirectional Dual Full Bridge ZVS DC-DC Converter with Novel Triple Phase-shift Control 27
Kuiyuan Wu, William G.Dunford and Clarence W.de Silva

Performance Comparison of Asymmetric Carrier Random and Dual Random PM Algorithms for Variable Speed Drives 36
P.Sasanandam, P.Pooanm Upadhyay and A.Jayalaxmi

Performance of Modular PFC Boost Converter using Average Current Control Techniue for improving EMI 41
Syed Mujtaba Mahdi Musassir, Gulam Amer and Shaik Mohammed Mukassir

Investigation of Modulation Strategy for Cascaded H-bridge Multi level fed Induction Motor Drive 47
Ravi kumar Bhukya and P.Satish kuman

Comparison of Aircraft System Using Fuzzy Logic Control and Traditional Control Scheme 53
Saifullah Khalid

Performance of PV System for Maximum Power Point Traking 58
Bipin Singh, Arunima Verma and V.K.Gin

Author Index 64

Theoretical Analysis of Isolated Bidirectional Dual Full Bridge ZVS DC-DC Converter with Novel Triple Phase-shift Control

Kuiyuan Wu[1] William G.Dunford[1] Clarence W.de Silva[2]

Abstract-This paper analyzes the working theory of the bidirectional dual full bridge ZVS DC-DC converter with novel triple-phase-shift control. This novel control method makes the efficiency and output voltage stability of the bidirectional converter more robust (insensitive) to parameter and output power change. Based on its working theory, the converter is separated into several stages. Detailed operation in each stage is analyzed. Equivalent circuits and necessary equations are built for each stage. Then, the ratio of the output voltage and input voltage, average input active power, average output active power and efficiency are solved theoretically in this paper. Relevant simulation results are attached in this paper. The forward and backward efficiency of this bidirectional converter with novel triple-phase-shift control are very high in large load scope.

Keywords-Isolated bidirectional ZVS DC-DC converter, novel triple-phase-shift control method, equivalent circuit, periodical operation, robust (insensitive) efficiency to parameter or output power change, high efficiency in large load scope.

I. Introduction

In recent years, the development of high power and large power range isolated bidirectional dc-dc converters has become an important topic because of the requirements of electric automobile, energy storage systems and aviation power system [2], [4], [8], [13]. This project is to design a forward $1kW/200V(93\%)$ and backward $250W/48V(95\%)$ bidirectional converter. The dual active full bridge converter is symmetry in both sides of the isolation transformer. It is suitable to be used as the power circuit to transfer energy back and forth, especially for high power case [12], [14], [17]. Therefore, it is used as the power circuit for this project. There are two series inductors $L01$ and $L02$ in Fig. 1. These two inductors are mainly used to enlarge ZVS scope, eliminate the switching loss and ensure the converter have high efficiency in large load scope [1], [5], [11], [18].

There are several existing control methods for this power circuit, like single phase-shift control [3], dual phase-shift control [4]. However, the novel triple phase-shift control method will make the system with high efficiency (Higher than 97%) in large load scope, especially when parameter changes. It is very important to make the efficiency of the bidirectional converter more robust (insensitive) to parameter change and different output power because this will make the converter more suitable for different applications. This approach does not appear to have been published until now in this area.

The paper first received 31 October 2017 and in revised form 20 Jun 2018. Digital Ref: APEJ-2017-10-0521

[1]**Department of Electrical and Computer Engineering, The University of British Columbia, Vancouver, BC, V6T 1Z4, Canada,**

[2]**Department of Mechanical Engineering, The University of British Columbia, Vancouver, BC, V6T 1Z4, Canada,**

(Email: wukuiyuan2010@hotmail.com)

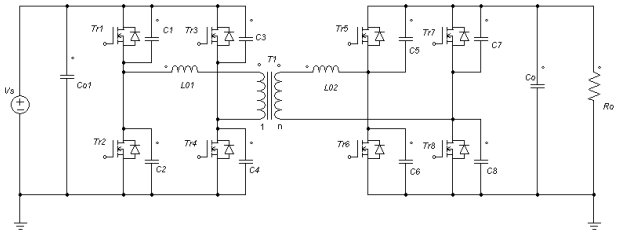

Fig. 1: The power circuit of the bidirectional converter

In novel triple-phase-shift control method, three control variables cooperate together to transfer energy. This will make the efficiency of the bidirectional DC-DC converter more robust (insensitive) to parameter change and different output powers. This project is simulated with PSIM software. Novel triple phase-shift control method is described in detail in Section II; the operation of bidirectional dual full bridge converter with novel triple phase-shift control is analyzed and equivalent circuits are derived in Section III; important equations of this bidirectional converter with novel triple phase-shift control are determined in Section IV; voltage ratio, active power and efficiency expressions of this bidirectional converter with triple phase-shift control are solved in Section V; the results obtained from theoretical analysis are validated by simulations and discussed in Section VI; finally, the main contributions of this paper are summarized in Section VII.

II. Novel Triple-Phase-Shift Control Method For Dual Active Full Bridge Converter

A. Brief Statement of this Method

This novel triple-phase-shift control method described in this paper is neither the same as common phase-shift methods in which all control signals are half duty cycle nor the same as common single phase-shift plus PWM control method in which the duty cycle of control signals can vary from zero to one [9]. In this method, four control signals $(Vg1, Vg2, Vg5, Vg6)$ with half duty cycle; another two control signals $(Vg3, Vg4)$ with duty cycle varying between zero and 50%; the last two control signals $(Vg7, Vg8)$ with another duty cycle varying between zero and 50%. This will make the controller easier to be realized with lead-lag compensator [6], [7]. Because the work theory of this new method is similar to that of common triple-phase-shift control method, it is called novel triple-phase-shift control method in this paper. This can be seen clearly in the following simulation results and work theory analysis.

In this novel triple-phase-shift controller, the first phase-shift between the primary control signal and the corresponding secondary control signal $(Vg1\ and\ Vg5)$, the second phase-shift between the diagonal control signals in the primary power circuit $(Vg1\ and\ Vg4)$ and the third phase-shift between the diagonal control signals in the secondary power circuit $(Vg5\ and\ Vg8)$ cooperate together to control energy transfer of the bidirectional DC-DC converter.

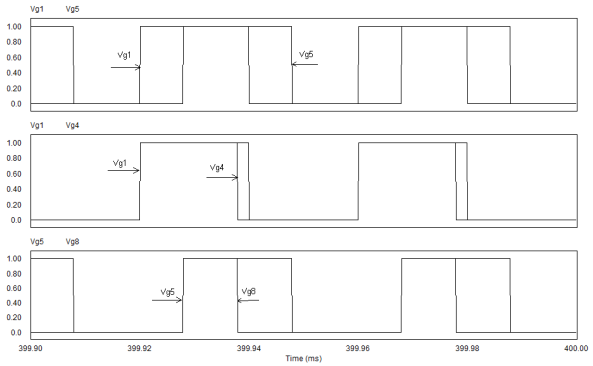

Fig. 2: Novel Triple-Phase-shift Control Signal Waveforms

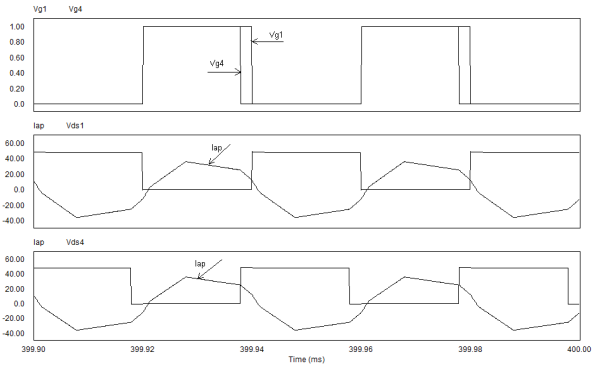

Fig. 3: Forward Control Signals, Power Switch Voltages and Primary Current with Novel Triple-Phase-shift Control

Corresponding control signal wave forms can be seen clearly in Fig. 2.

B. Forward Simulation Results of Control Signals, Power Switch Voltages and Primary Current

From Fig. 3, it can be found that the primary power circuit can realize ZVS very well because the primary current is negative when MOSFET1 and MOSFET4 turn on. This means the primary current passed through anti-parallel diodes $D1$ and $D4$ just before the power MOSFETs turn on; ZVS can be realized very well.

From Fig. 4, it can be found that the secondary power circuit can realize ZVS very well because the secondary current is positive when

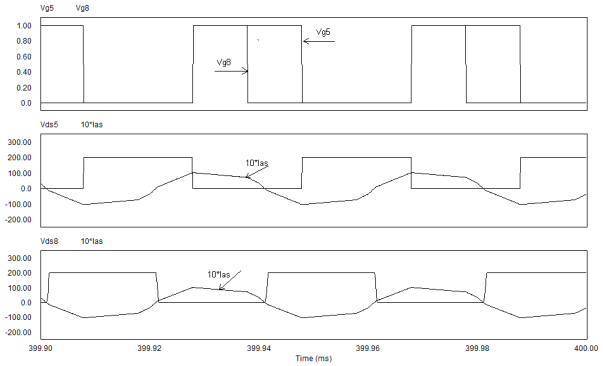

Fig. 4: Forward Control Signals, Power Switch Voltages and Secondary Current with Novel Triple-Phase-shift Control

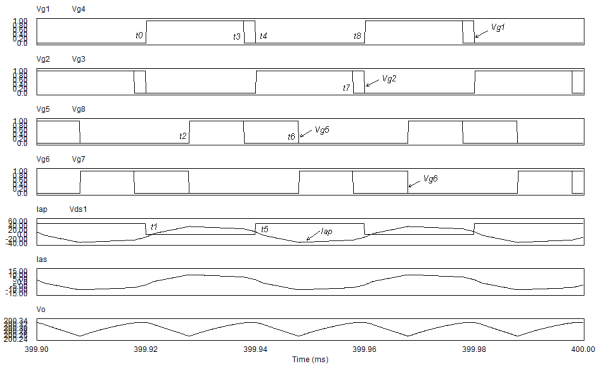

Fig. 5: Simulation Wave Forms of the Forward Bidirectional Converter with Novel Triple-Phase-shift Control for Vref1=6V

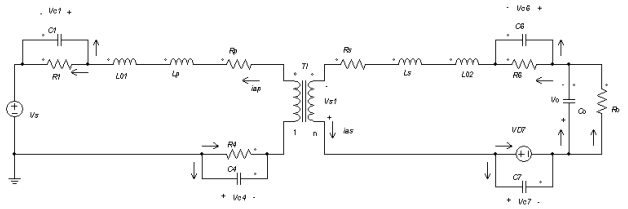

Fig. 6: Equivalent Circuit in Stage 1

MOSFET5 and MOSFET8 turn on. From the positive direction of secondary current in Fig. 1, it can be found that positive secondary current means it passed through anti-parallel diodes $D5$ and $D8$ just before the power MOSFETs turn on; ZVS can be realized very well, too. Therefore, the switching loss of this converter is eliminated [16]. For high frequency converter, switching loss is an important factor to influence efficiency [15].

III. Operation And Equivalent Circuit Of Forward Bioirectional Dual Full Bridge Converted With Novel Triple-Phase-Shift Control

The forward simulation wave-forms of bidirectional dual full bridge converter with novel triple phase-shift control are as follows.

Based Fig. 5, the forward bidirectional converter can be separated into eight stages. Corresponding equivalent circuits and necessary equations can be got in each stage. The backward converter can be analyzed similarly.

1: Stage 1 $t_0 - t_1$: Power switches $Tr1$ and $Tr4$ will turn on at $t = t_0$. Because the primary current is still negative during this period, the primary current will flow through $Tr4/Tr1$ and the inductor energy flows back to the power source.

Because $Vg5/Vg8/Vg7$ are equal to zero, $Tr5/Tr8/Tr7$ all in Off state; $Vg6 = 1$, $Tr6$ is On. $I_{as} < 0$, secondary current flows through $Tr6/D7$. The inductor $L02$ and output capacitor provide energy to the load. The output voltage reduces during this period. The equivalent circuit in this stage is Fig. 6:

2: Stage 2 $t_1 - t_2$: Because $Vg1/Vg4 = 1$, power switches $Tr1$ and $Tr4$ are in On state in this period. Because the primary current is positive during this period, the primary current will flow through $Tr1/Tr4$ and the inductor $L01$ and transformer leakage inductance. The energy will transfer from the primary side to the secondary side.

Because $Vg5/Vg8/Vg7$ are equal to zero, $Tr5/Tr8/Tr7$ all in Off state; $Vg6 = 1$, $Tr6$ is On. $I_{as>0}$, secondary current will charge

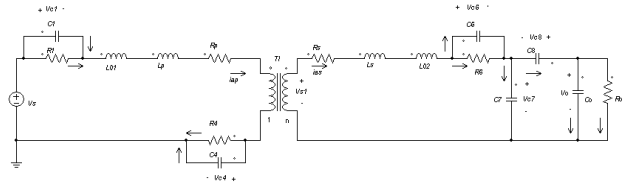

Fig. 7: C8 Discharging Equivalent Circuit in Stage 2

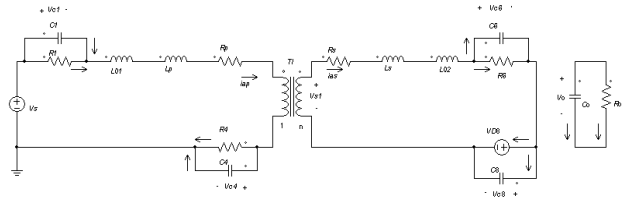

Fig. 8: Free Wheeling Equivalent Circuit in Stage 2

capacitor $C7$ and discharge capacitor $C8$ till its voltage reduces to the forward conduction voltage of diode $D8$. The equivalent circuit is Fig. 7.

Then the current flows through $Tr6/D8$. The energy is stored in the secondary inductor $L02$ and leakage inductor because this is a freewheeling period with no power transfer to the load theoretically. Output capacitor provides energy to the load and output voltage continues to reduce in this period. The equivalent circuit in this stage is Fig. 8.

$Tr6$ turns off a little before t_2. The secondary current will charge snubber capacitor $C6$ and discharge snubber capacitor $C5$. During this very short transitional time, the secondary current flows through $D8$ to charge and discharge snubber capacitors. When $C5$ is totally discharged $(Vds5 = 0)$, the secondary current will flow through $D5/D8$ and the energy will be transferred to the load. The corresponding equivalent circuits are Fig. 9-Fig. 10.

3: Stage 3 $t_2 - t_3$: The control signal $Vg5/Vg8 = 1$, power switches $Tr5/Tr8$ will turn on at t_2. Because $I_{as} > 0$ during this stage, the secondary side current will flow through $Tr5/Tr8$ and transfer energy to the load in this stage. The output voltage will increase in this stage. The equivalent circuit in this stage is shown in Fig. 11.

4: Stage 4 $t_3 - t_4$: $Vg4/Vg8 = 0$, so, $Tr4/Tr8$ will turn off at t_3.

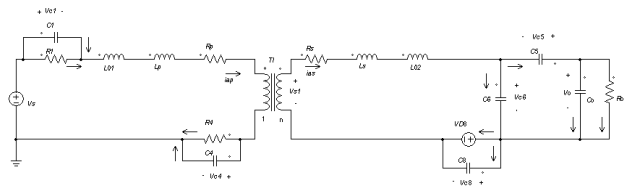

Fig. 9: Charge-Discharge Equivalent Circuit in Stage 2

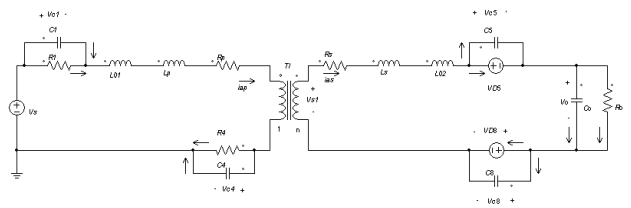

Fig. 10: Diode Conduct Equivalent Circuit in Stage 2

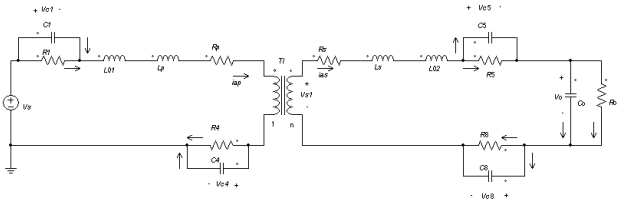

Fig. 11: Energy Transfer Equivalent Circuit in Stage 3

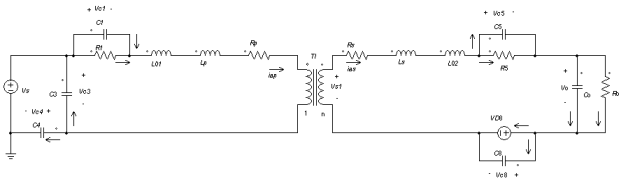

Fig. 12: C3 Discharge Equivalent Circuit in Stage 4

For the primary side, $Tr4$ turns off at t_3, The primary current will charge snubber capacitor $C4$ and discharge snubber capacitor $C3$. When $C3$ is totally discharged $(Vds3 = 0)$, the primary current will flow through $Tr1/D3$ and form a freewheeling period. No power is transferred to the secondary side theoretically.

For the secondary side, the current $I_{as} > 0$, this indicates $Tr5/D8$ will continue conduct in this period of time. The additional inductor $L02$ and secondary leakage inductance will provide energy to transfer to the load. The output voltage will continue to increase in this stage. The equivalent circuits are shown in Fig. 12 and Fig. 13.

$Tr1$ turns off a little before t_4. The primary current will discharge snubber capacitor $C2$ and charge snubber capacitor $C1$. During this very short transitional time, the current will flow through $D3$ to charge and discharge capacitors. When $C2$ is totally discharged $(Vds2 = 0)$, $D2$ will conduct and form an energy feedback to power source. This will make it feasible for $Tr2/Tr3$ to turn on under ZVS. The equivalent circuits are shown in Fig. 14 and Fig. 15.

5: Stage 5 $t_4 - t_5$: Because $Vg2/Vg3 = 1$, $Tr2/Tr3$ will turn on at t_4 under ZVS. Because the primary current $i_{ap} > 0$, the energy will feedback to the primary source in this interval.

For the secondary side, $Vg5 = 1$, so, $Tr5$ is On in this interval. $Vg6/Vg7/Vg8 = 0$, so, $Tr6/Tr7/Tr8$ will be in off state during this period of time. Because the secondary current $i_{as} > 0$, $Tr5/D8$ will conduct in this period of time. The inductor $L02$, the secondary

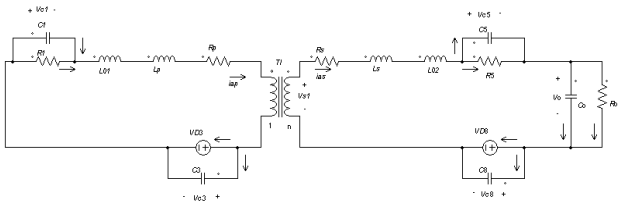

Fig. 13: Free Wheeling Equivalent Circuit in Stage 4

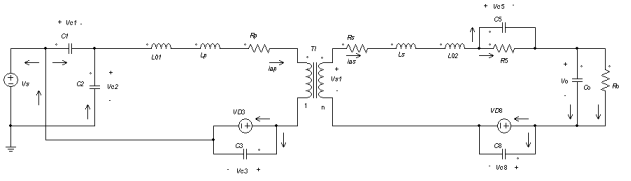

Fig. 14: C2 Discharge Equivalent Circuit in Stage 4

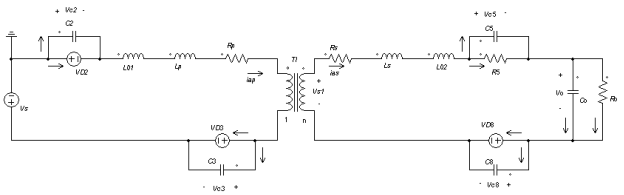

Fig. 15: Energy Feedback Equivalent Circuit in Stage 4

leakage inductor and output capacitor will provide energy to the load together in this interval. The output voltage begins to reduce in this interval. According to this analysis, the equivalent circuits in this interval can be got similarly.

6: Stage 6 $t_5 - t_6$: Because $Vg2/Vg3 = 1$, $Tr2/Tr3$ will be on in this stage. Because the primary current $I_{ap} < 0$, the energy will transfer to the secondary side again.

For the secondary side, $Vg5 = 1$, so, $Tr5$ is on state in this stage.$Vg6/Vg7/Vg8 = 0$, so, $Tr6/Tr7/Tr8$ all will be in off state during this period of time. Because the secondary side current $I_{as} < 0$, secondary current will charge capacitor $C8$ and discharge capacitor $C7$ till its voltage reduces to the forward conduction voltage of diode $D7$. Then the current flows through $Tr5/D7$ in this period of time and form a freewheeling period with no energy transferred to the load theoretically in this stage. The energy from primary source is stored in $L02$ and leakage inductor. Output capacitor provides energy to the load and output voltage will continue to reduce in this stage. The equivalent circuit can be got similarly in this stage.

7: Stage 7 $t_6 - t_7$: Because $Vg6/Vg7 = 1$, $Tr6/Tr7$ will turn on at t_6. $Vg5 = 0$, so $Tr5$ turns off a little before t_6. The secondary current will charge $C5$ and discharge $C6$. During this very short of transitional time, the secondary current flows through $D7$ to charge and discharge snubber capacitors. When $C6$ is totally discharged ($Vds6 = 0$), $D6$ will turn on and $D6/D7$ will conduct to form ZVS and transfer energy to the load. Because the secondary side current $I_{as} < 0$, $Tr6/Tr7$ will conduct in this period of time and transfer energy to the load in this stage. The output voltage will increase in this stage. The equivalent circuits in this stage can be got similarly.

8: Stage 8 $t_7 - t_8$: Because $Vg3/Vg7 = 0$ at t_7, $Tr3/Tr7$ will turn off at t_7. For the primary side, $Tr3$ turns off; the primary current will charge $C3$ and discharge $C4$. During this very short of transitional time, the primary current flows through $Tr2$ to charge and discharge snubber capacitors $C3$ and $C4$. When $C4$ is totally discharged ($Vds4 = 0$), $D4$ will turn on. $Tr2/D4$ conduct, this forms a freewheeling stage with no energy transferred to the secondary side theoretically.

Tr2 turns off a little before t_8. The energy stored in additional inductor $L01$ and transformer leakage inductance will charge the snubber capacitor $C2$ and discharge snubber capacitor $C1$. During this very short transitional time, the primary current flows through $D4$ to charge and discharge snubber capacitors. When $C1$ is discharged totally ($Vds1 = 0$), then the primary current will flow through $D4/D1$ and the inductor energy flows back to the power source.

For the secondary side, $Tr6/D7$ will continue conduct during this period of time and transfer energy to the load. This is because the secondary side current $I_{as} < 0$. The energy mainly comes from the stored energy of additional inductor $L02$ and the leakage inductance. Output voltage will continue to increase in this stage. The corresponding equivalent circuits can be got similarly according to the analysis for this stage.

IV. Important Equations For Each Stage Of Forward Bidierctional Dual Full Bridge Converter With Novel Triple-Phase-Shift Control

Based on the equivalent circuits in each stage, the corresponding equivalent inductor voltage and output capacitor current equations can be built for this bidirectional DC-DC converter in each stage.

A. Necessary Equations in Stage 1 $(t_0 - t_1)$

The necessary equation of the converter can be built according to the equivalent circuit Fig.6 in this stage as following:

$$\begin{cases} (L01 + Lp + \frac{1}{n^2} * Ls)\frac{di_{ap}}{dt} = -\frac{1}{n} * Vo - Vs - \\ \qquad (Rp + R1 + R4 + \frac{1}{n^2} * Rs + \frac{1}{n^2} * R6) * i_{ap} \\ Co\frac{dvo}{dt} = \frac{1}{n} * i_{ap} - \frac{vo}{Ro} \end{cases} \tag{1}$$

B. Necessary Equations in Stage 2 $(t_1 - t_2)$

From the previous analysis of the converter working process, it can be found there are four sub-stages and corresponding four equivalent circuits in this stage.

(1) Sub-stage of Charge-discharge of $C7$ and $C8$
According to the equivalent circuit of the converter shown in Fig. 7, the equation can be built as following:

$$\begin{cases} (L01 + Lp + \frac{1}{n^2} * L02 + \frac{1}{n^2} * Ls)\frac{di_{ap}}{dt} = -(Rp + R1 + \\ \qquad R4 + \frac{1}{n^2} * Rs + \frac{1}{n^2} * R6) * iap - \frac{1}{n} * Vc7 + Vs \\ Co\frac{dvo}{dt} = -\frac{vo}{Ro} \end{cases} \tag{2}$$

(2) Sub-stage of Free Wheeling in Stage 2
According to the equivalent circuit of the converter in freewheeling stage shown in Fig. 8, the corresponding equation can be built as following:

$$\begin{cases} (L01 + Lp + \frac{1}{n^2} * L02 + \frac{1}{n^2} * Ls)\frac{di_{ap}}{dt} = -(Rp + R1 \\ \qquad +R4 + \frac{1}{n^2} * Rs + \frac{1}{n^2} * R6) * i_{ap} + Vs \\ Co\frac{dvo}{dt} = -\frac{vo}{Ro} \end{cases} \tag{3}$$

(3) Sub-stage of $C5/C6$ Charge and Discharge in Stage 2
According to the equivalent circuit of the converter in this stage shown in Fig. 9, the corresponding equation can be built as following:

$$\begin{cases} (L01 + Lp + \frac{1}{n^2} * L02 + \frac{1}{n^2} * Ls)\frac{di_{ap}}{dt} = -(Rp + R1 + \\ \qquad R4 + \frac{1}{n^2} * Rs + \frac{1}{n^2} * R6) * i_{ap} - \frac{1}{n} * Vc6 + Vs \\ Co\frac{dvo}{dt} = -\frac{vo}{Ro} \end{cases} \tag{4}$$

(4) Sub-stage of $D5/D8$ Conduction in Stage 2
According to the equivalent circuit of the converter in this stage shown in Fig. 10, the corresponding equation can be built as following:

$$\begin{cases} (L01+Lp+\frac{1}{n^2}*L02+\frac{1}{n^2}*Ls)\frac{di_{ap}}{dt} = -(Rp+R1+ \\ \qquad R4+\frac{1}{n^2}*Rs)*i_{ap}-\frac{1}{n}*Vo+Vs \\ Co\frac{dvo}{dt} = \frac{1}{n}*i_{ap}-\frac{vo}{Ro} \end{cases} \tag{5}$$

C. Necessary Equations in Stage 3 $(t_2 - t_3)$

The energy is transferred to the DC load in this stage. According to the equivalent circuit of the converter in this stage shown in Fig. 11, the corresponding equation can be built as following:

$$\begin{cases} (L01+Lp+\frac{1}{n^2}*L02+\frac{1}{n^2}*Ls)\frac{diap}{dt} = -(Rp+R1+ \\ \qquad R4+\frac{1}{n^2}*Rs+\frac{1}{n^2}*R5+\frac{1}{n^2}*R8)*iap \\ \qquad -\frac{1}{n}*Vo+Vs \\ Co\frac{dvo}{dt} = \frac{1}{n}*iap-\frac{vo}{Ro} \end{cases} \tag{6}$$

D. Necessary Equations in Stage 4 $(t_3 - t_4)$

From the previous analysis of the converter working process, it can be found there are four sub-stages in this stage. The first two main sub-stages are analyzed here. The necessary equations can be built as following:

(1) Sub-stage of $C3/C4$ Charge and Discharge in Stage 4
According to the equivalent circuit of the converter in this stage shown in Fig. 12, the corresponding equation can be built as following:

$$\begin{cases} (L01+Lp+\frac{1}{n^2}*L02+\frac{1}{n^2}*Ls)\frac{di_{ap}}{dt} = -(Rp+R1+ \\ \qquad R4+\frac{1}{n^2}*Rs+\frac{1}{n^2}*R5+\frac{1}{n^2}*R8)*iap \\ \qquad -\frac{1}{n}*Vo+Vs \\ Co\frac{dvo}{dt} = \frac{1}{n}*iap-\frac{vo}{Ro} \end{cases} \tag{7}$$

$$\begin{cases} (L01+Lp+\frac{1}{n^2}*L02+\frac{1}{n^2}*Ls)\frac{di_{ap}}{dt} = -(Rp+R1+ \\ \qquad \frac{1}{n^2}*Rs+\frac{1}{n^2}*R5)*i_{ap}-Vc4-\frac{1}{n}*Vo+Vs \\ Co\frac{dvo}{dt} = \frac{1}{n}*i_{ap}-\frac{vo}{Ro} \end{cases} \tag{8}$$

(2) Sub-stage of $Tr1/D3$ Conduction in Stage 4
This is another freewheeling sub-stage in primary power circuit; according to the equivalent circuit Fig. 13, the necessary equations can be built as following:

$$\begin{cases} (L01+Lp+\frac{1}{n^2}*L02+\frac{1}{n^2}*Ls)\frac{di_{ap}}{dt} = -(Rp+R1+ \\ \qquad \frac{1}{n^2}*Rs+\frac{1}{n^2}*R5)*i_{ap}-\frac{1}{n}*Vo \\ Co\frac{dvo}{dt} = \frac{1}{n}*i_{ap}-\frac{vo}{Ro} \end{cases} \tag{9}$$

The necessary equations for other two very short sub-stages in this stage and left four stages can be built similarly according to the working process analysis.

V. Voltage Ratio, Active Power And Efficiency Of Forward Bidirectional Dual Full Bridge Converter With Novel Triple-Phase-Shift Control

It is well known that the converter loss mainly includes conduction loss and switching loss [10], [15]. The switching loss of the converter is eliminated because this converter can realize ZVS very well in large load scope. In the following power and efficiency expressions, only the conduction loss of power MOSFETs and the loss of the winding resistance of the transformer are considered.

A. The Expression of Voltage Ratio Vo/Vs

In order to be convenient to see clearly the major role of triple phase-shift control method, the power MOSFETs and diodes are treated as ideal. The winding resistance of the transformer is neglected. From the working process analysis and the simulation waveforms shown in Fig. 5, it can be found the inductor current iap crosses zero half period of Ts. The first stage $(t_0 - t_1)$ and the fifth stage $(t_4 - t_5)$ are due to the dead band effect. They are neglected here. In order to be convenient, write:

$$L_{eq} = L01+Lp+\frac{1}{n^2}*L02+\frac{1}{n^2}*Ls \tag{10}$$

Because the time interval of snubber capacitors charge/discharge is very short compared with the stage time duration, it can be neglected, too. From Fig. 5, it can be found the corresponding stages are equal to:

$$\begin{cases} t2-t0 = D1*Ts \\ t3-t2 = (0.5-D3)*Ts \\ t4-t3 = D2*Ts \end{cases} \tag{11}$$

Apply Volt-second balance and small ripple approximation to equivalent inductor L_{eq}, there is:

$$Vs*D1+(-\frac{vo}{n}+Vs)*(0.5-D3)+(-\frac{vo}{n})*D2 = 0 \tag{12}$$

The output voltage can be got from this equation as following:

$$\frac{vo}{vs} = \frac{n*(1+2D1-2D3)}{(1+2D2-2D3)} \tag{13}$$

This formula suggests that the output voltage depends on three control variables. This will make the output voltage more robust to parameter changes. With novel triple-phase-shift control, the output voltage behaves very well when the first reference voltage is equal to $5/6/7/8Volts$ or other values in the control circuit. With dual or single phase-shift control, the average output voltage will be always equal to zero when the first reference voltage in the control circuit is equal to or higher than $6Volts$, Fig. 16 and Fig. 17.

B. The Expression of Primary Current in First Half Period

According to the primary current differential equation listed in section IV, there are three main current expressions in the first half period. The current expressions in ZVS sub-stages need not to be considered because the time for ZVS sub-stages are very short and there is no active power in ZVS sub-stages theoretically.
(1)The Expression of Primary Current in Stage $t_0 - t_2$ Write:

$$Req1 = Rp+R1+R4+\frac{1}{n^2}*Rs+\frac{1}{n^2}*R6 \tag{14}$$

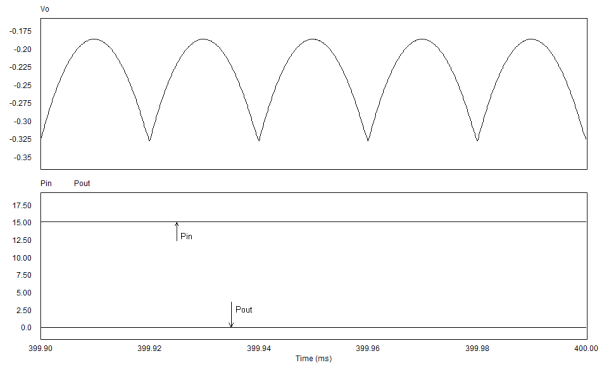

Fig. 16: Forward Simulation Results with Dual Phase-shift Control When Vref1¿=6V

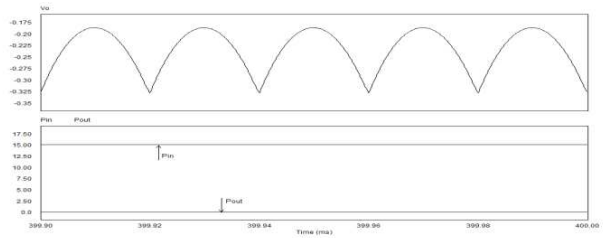

Fig. 17: Forward Simulation Results with Single Phase-shift Control When Vref1¿=6V

Primary current in this stage can be solved out as:

$$i_{ap} = \frac{vs}{Req1} * (1 - e^{\frac{-Req1*t}{Leq}}) \tag{15}$$

(2)The Expression of Primary Current in Stage $t_2 - t_3$ Write:

$$Req2 = Rp + R1 + R4 + \frac{1}{n^2} * Rs + \frac{1}{n^2} * R5 + \frac{1}{n^2} * R8 \tag{16}$$

Primary current in this stage can be solved out as:

$$\begin{cases} i_{ap}(t2+) = iap(t2-) = \frac{vs}{Req1} * (1 - e^{\frac{-Req1*D1*TS}{Leq}}) \\ i_{ap} = \frac{vs - \frac{vo}{n}}{Req2} + [i_{ap}(t2+) - \frac{vs - \frac{vo}{n}}{Req2}] * e^{\frac{-Req2*t}{Leq}} \end{cases} \tag{17}$$

(3)The Expression of Primary Current in Stage $t_3 - t_4$ Write:

$$Req3 = Rp + R1 + \frac{1}{n^2} * Rs + \frac{1}{n^2} * R5 \tag{18}$$

Primary current in this stage can be solved out as:

$$\begin{cases} i_{ap}(t3+) = i_{ap}(t3-) = i_{ap}(t3-) = \dfrac{vs - \frac{vo}{n}}{Req2} + [i_{ap}(t2+) \\ \qquad - \dfrac{vs - \frac{vo}{n}}{Req2}] * e^{\frac{-Req2*(0.5-D2)*TS}{Leq}} \\ i_{ap} = \frac{-vo}{n*Req3} + [i_{ap}(t3+) + \frac{vo}{n*Req3}] * e^{\frac{-Req3*t}{Leq}} \end{cases} \tag{19}$$

The primary current expressions in the second half period are equal to the negative of the corresponding expressions listed above.

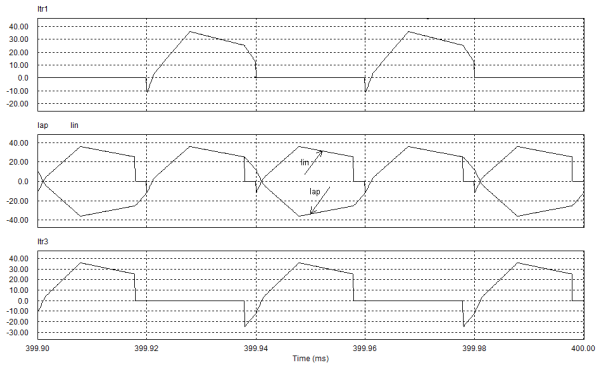

Fig. 18: Forward Simulation Waveforms of Input Current, Primary Current and Power Switch Currents

C. The Expression of Average Input Power

From the working process of the bidirectional converter and the above simulation results Fig. 18, it can be found the primary power circuit does not transfer power to the secondary side during the freewheeling stage $(t_3 - t_4)$ in the first half working period, the situation is similar in the second half working period. Therefore, the average input active power is equal to:

$$Pin = \frac{2}{Ts} \int_0^{\frac{Ts}{2}} Vs * i_{in}\, dt = \frac{2vs}{Ts} \int_0^{\frac{Ts}{2}} i_{ap}\, dt \tag{20}$$

Substituting the corresponding expressions of iap into above equation, the average input active power can be got as following:

$$\begin{aligned} Pin = \frac{2 * Vs^2}{Ts} * Y_2 = \frac{2 * Vs^2}{Ts} * [& \frac{D1 * Ts}{Req1} + \frac{Leq}{Req1^2} \\ & * e^{\frac{-Req1*D1*tS}{Leq}} - \frac{Leq}{Req1^2} + \frac{Ts}{Req2} \\ & * \frac{(D2 - D1) * (1 - 2 * D2)}{(1 + 2 * D2 - 2 * D3)} \\ & - \frac{2 * D1 * (D2 - D1) * Ts}{(1 + 2 * D2 - 2 * D3) * Req2} \\ & - \frac{Leq}{Req1 * Req2} * (1 - e^{\frac{Req1*D1*Ts}{Leq}}) \\ & * e^{\frac{-Req2*(0.5-D2)*Ts}{Leq}} + \frac{Leq}{Req1 * Req2} \\ & * (1 - e^{\frac{-Req1*D1*Ts}{Leq}}) * e^{\frac{-Req2*D1*Ts}{Leq}}] + \frac{2 * vs^2}{Ts} \\ * [& \frac{2 * Leq * (D2 - D1)}{(1 + 2 * D2 - 2 * D3) * rEQ2^2} * e^{\frac{-Req2*(0.5-D2)*Ts}{Leq}} \\ & * [\frac{2 * Leq * (D2 - D1)}{(1 + 2 * D2 - 2 * D3) * rEQ2^2} * e^{\frac{-Req2*D1*Ts}{Leq}} \end{aligned} \tag{21}$$

It can be found the average input active power is decided by three phase-shifts, working period Ts, power switch conduction loss, equivalent inductance and winding resistance of the transformer.

D. The Expression of Average output Power

From the working process of the bidirectional converter and the above simulation results Fig. 19, it can be found the secondary power circuit does not transfer power to the load during the freewheeling stage $(t_0 - t_2)$ in the first half working period, the situation is similar in the second half working period. Therefore, the average output active power is equal to:

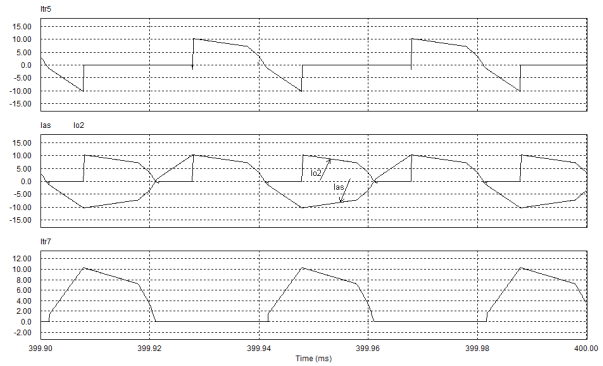

Fig. 19: Forward Simulation Waveforms of Output Current, Secondary Current and Power Switch Currents

$$Pout = \frac{2}{Ts}\int_0^{\frac{Ts}{2}} Vo * i_o\, dt = \frac{2vo}{nTs}\frac{2vs}{Ts}\int_0^{\frac{Ts}{2}} i_{ap}\, dt \tag{22}$$

Substituting the corresponding expressions of iap into above equation, the average output power can be got.

$$\begin{aligned}
Pout = {} & \frac{2 * vs^2 * (1 + 2 * D1 - 2 * D3)}{Ts * (1 + 2 * D2 - 2 * D3)} * Y1 \\
Y1 = {} & [\frac{(D2 - D1) * (1 - 2 * D2) * Ts}{(1 + 2 * D2 - 2 * D3) * Req2} \\
& - \frac{2 * D1 * (D2 - D1)}{(1 + 2 * D2 - 2 * D3) * Req2} \\
& - \frac{Leq}{Req1 * Req2} * (1 - e^{\frac{Req1 * D1 * Ts}{Leq}}) \\
& * e^{\frac{-Req2 * (0.5 - D2) * Ts}{Leq}} \\
& + \frac{Leq}{Req1 * Req2} * (1 - e^{\frac{Req1 * D1 * Ts}{Leq}}) \\
& * e^{\frac{-Req2 * D1 * Ts}{Leq}} \\
& + \frac{2 * (D2 - D1) * Leq}{(1 + 2 * D2 - 2 * D3) * Req2^2} \\
& * e^{\frac{-Req2 * (0.5 - D2) * Ts}{Leq}} \\
& - \frac{2 * (D2 - D1) * Leq}{(1 + 2 * D2 - 2 * D3) * Req2^2} \\
& * e^{\frac{-Req2 * D1 * Ts}{Leq}} \\
& - \frac{(1 + 2 * D1 - 2 * D3) * Ts}{2 * (1 + 2 * D2 - 2 * D3) * Req3} \\
& + \frac{(1 + 2 * D1 - 2 * D3) * (0.5 - D2) * Ts}{2 * (1 + 2 * D2 - 2 * D3) * Req3} \\
& - \frac{2 * (D2 - D1) * Leq}{(1 + 2 * D2 - 2 * D3) * Req2 * Req3} \\
& * e^{\frac{-Req3 * Ts}{2 * Leq}} \\
& + \frac{2 * (D2 - D1) * Leq}{(1 + 2 * D2 - 2 * D3) * Req2 * Req3} \\
& * e^{\frac{-Req3 * (0.5 - D2) * Ts}{Leq}} \\
& - \frac{Leq}{Req1 * Req3} \\
& * e^{\frac{-Req2 * (0.5 - D2) * Ts - 0.5 * Req3 * Ts}{Leq}} \\
& + \frac{Leq}{Req1 * Req3} \\
& * e^{\frac{-Req1 * D1 * Ts - Req2 * (0.5 - D2) * Ts - 0.5 * Req3 * Ts}{Leq}} \\
& + \frac{2 * (D2 - D1) * Leq}{(1 + 2 * D2 - 2 * D3) * Req2 * Req3} \\
& * e^{\frac{-Req3 * (0.5 - D2) * Ts - 0.5 * Req3 * Ts}{Leq}} \\
& + \frac{Leq}{Req1 * Req3} * e^{\frac{-Req2 * (0.5 - D2) * Ts - 0.5 * Req3 * Ts}{Leq}} \\
& - \frac{Leq}{Req1 * Req3} \\
& * e^{\frac{-Req1 * D1 * Ts - Req2 * (0.5 - D2) * Ts - 0.5 * Req3 * Ts}{Leq}} \\
& + \frac{2 * (D2 - D1) * Leq}{(1 + 2 * D2 - 2 * D3) * Req2 * Req3} \\
& * e^{\frac{-Req2 * (0.5 - D2) * Ts - 0.5 * Req3 * Ts}{Leq}} \\
& + \frac{Leq}{Req1 * Req3} \\
& * e^{\frac{-Req2 * (0.5 - D2) * Ts - Req3 * (0.5 - D2) * Ts}{Leq}} \\
& - \frac{Leq}{Req1 * Req3} \\
& * e^{\frac{-Req1 * D1 * Ts - Req2 * (0.5 - D2) * Ts - (0.5 - D2) * Req3 * Ts}{Leq}} \\
& - \frac{Leq * (1 + 2 * D1 - 2 * D3)}{Req3^2 * (1 + 2 * D2 - 2 * D3)} * e^{\frac{Req3 * Ts}{2 * Leq}} \\
& + \frac{Leq * (1 + 2 * D1 - 2 * D3)}{Req3^2 * (1 + 2 * D2 - 2 * D3)} \\
& * e^{\frac{Req3 * (0.5 - D2) * Ts}{Leq}}]
\end{aligned} \tag{23}$$

It can be found the average output active power is decided by three phase-shifts, working period Ts, power switch conduction loss, equivalent inductance and winding resistance of the transformer, too.

E. The Efficiency of the Bidirectional Converter

$$\eta = \frac{Pout}{Pin} \tag{24}$$

Substitute the expressions of average input power and average output power into the above equation, the efficiency of this bidirectional converter with triple phase-shift control method can be solved out as follows:

$$\eta = \frac{(1 + 2 * D1 - 2 * D3) * Y1}{(1 + 2 * D2 - 2 * D3) * Y2} \tag{25}$$

It can be found clearly that the efficiency of the bidirectional converter with novel triple-phase-shift control mainly depends on three control variables. This will make it more robust to parameter and output power change.

From the simulation waveforms and efficiency comparison data listed in Tab. II, it can be seen clearly the novel triple phase-shift control is much better than other two control methods when magnetizing inductance Lm changes with an unknown rule during the simulation process. This suggests the novel triple phase control will make the efficiency of the bidirectional converter much more robust (insensitive) to parameter change than other existing control methods.

In order to check whether this novel triple phase-shift control method can make the bidirectional converter with high efficiency in large load scope, this bidirectional ZVS DC-DC converter with novel triple-phase-shift control is simulated with PSIM software for four different output powers. The corresponding efficiency is listed

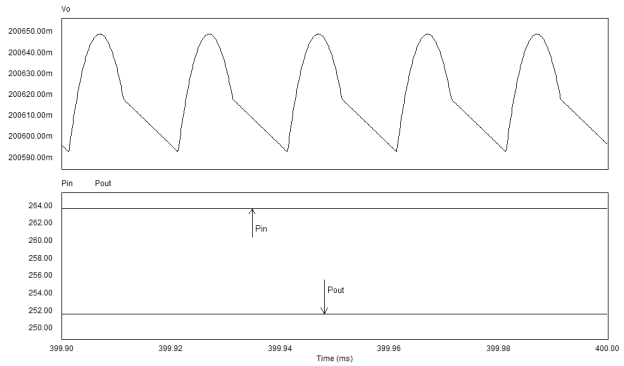

Fig. 20: Simulation Results of Forward Converter with novel Triple-Phase-shift Control (L01=L02=0, Pout=250W)

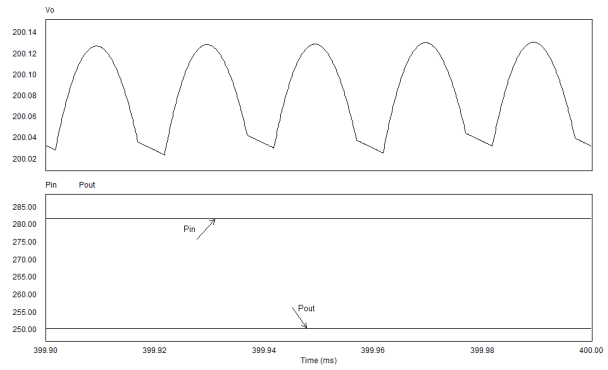

Fig. 21: Simulation Results of Forward Converter with Dual Phase-shift Control (L01=L02=0, Pout=250W)

as following.

VI. Simulation Studies And Discussio

When parameter and output power change, the simulation waveforms and efficiency of the bidirectional converter with three different control methods is attached in the following. They are simulated with PSIM software shown in Fig. 20, Fig. 21 and Fig. 22.

The following table gives the efficiency comparison of the bidirectional dual full bridge converter with three different control methods when parameter and output power change.

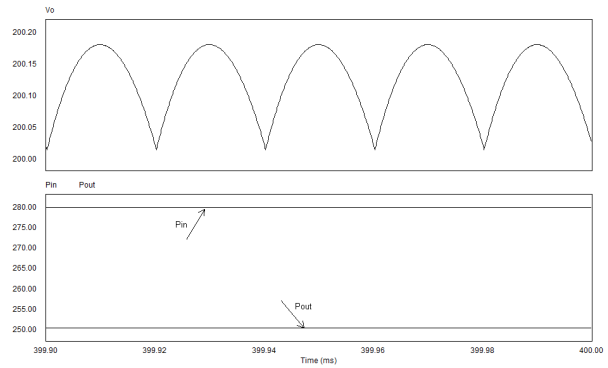

Fig. 22: Simulation Results of Forward Converter with Single Phase-shift Control (L01=L02=0, Pout=250W)

TABLE I: Forward Efficiency Comparison When Parameter Changes ($L01 = L02 = 0$)

Output Power	Single Phase-shift	Dual Phase-shift	Novel Triple Phase-shift
$1kW$	95.4%	95.6%	96.7%
$250W$	89.4%	88.8%	95.4%

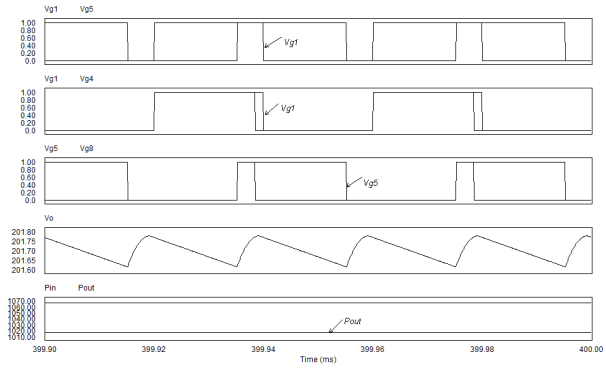

Fig. 23: Simulation Results of Forward Converter with Triple Phase-shift Control When Lm Changes Randomly

TABLE II: Converter Efficiency Comparison When Magnetizing Inductance Lm Changes Randomly

Output Power	Single Phase-shift	Dual Phase-shift	Novel Triple Phase-shift
Forward $1kW$	85%	85.5%	95.3%
Backward $250W$	70.2%	92.5%	96.5%

From these simulation waveforms and the efficiency data listed in Tab. I, it can be found the efficiency of bidirectional power circuit with novel triple phase-shift control is better than the efficiency of the same bidirectional power circuit with other control methods when serial inductance $L01$ changes from $7.3uH$ to $zero$, serial inductance $L02$ changes from $6.9uH$ to $zero$ or output power changes from $1kW$ to $250W$.

If a certain value is not assumed to magnetizing inductance Lm of the transformer, it will change with an unknown rule during the process of simulation with PSIM. This will make the simulation results nearly the same as the real application situation. The forward simulation waveforms of these three control methods with the same bidirectional dual full bridge ZVS converter are attached in Fig. 23, Fig. 24 and Fig. 25.

From the simulation waveforms and efficiency comparison data listed in Tab. II, it can be seen clearly the novel triple phase-shift control is much better than other two control methods when

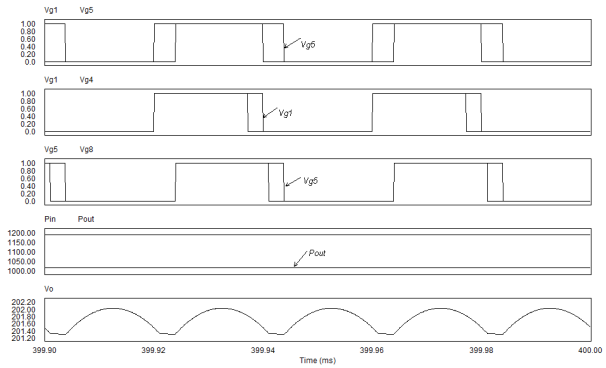

Fig. 24: Simulation Results of Forward Converter with Dual Phase-shift Control When Lm Changes Randomly

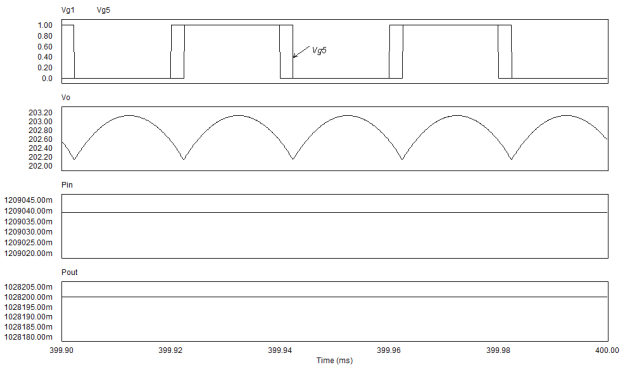

Fig. 25: Simulation Results of Forward Converter with Single Phase-shift Control When Lm Changes Randomly

TABLE III: Forward Output Power and Efficiency

Pout(W)	1003.00	754.75	502.50	252.53
Efficiency	97.6%	97.6%	98.4%	98.5%
Vo(V)	200.30 ±0.019%	200.57 ±0.015%	200.54 ±0.01%	201.01 ±0.006%

TABLE IV: Backward Output Power and Efficiency

Pout(W)	1008.32	751.88	499.84	250.53
Efficiency	96.9%	97.3%	98.0%	98.4%
Vo(V)	48.16 ±0.025%	48.04 ±0.019%	47.95 ±0.015%	48.01 ±0.08%

magnetizing inductance Lm changes with an unknown rule during the simulation process. This suggests the novel triple phase control will make the efficiency of the bidirectional converter much more robust (insensitive) to parameter change than other existing control methods.

In order to check whether this novel triple phase-shift control method can make the bidirectional converter with high efficiency in large load scope, this bidirectional ZVS DC-DC converter with novel triple-phase-shift control is simulated with PSIM software for four different output powers. The corresponding efficiency is listed as Tab. III-Tab. IV.

VII. Conclusion

This paper analyzes the working theory of a bidirectional dual full bridge ZVS DC-DC converter with novel triple phase-shift control method in detail. It separates the nonlinear converter into several linear stages in one period; find its equivalent circuits and build corresponding necessary equations for each stage. The forward output voltage and input voltage ratio, average input active power, average output active power and efficiency are solved theoretically. Relevant simulation demonstrations for this method are provided in this paper.

The simulation results demonstrate that this novel control method makes the efficiency and output voltage of this bidirectional converter more robust (insensitive) to parameter and output power change. Simulation results also show that the forward and backward efficiency of this bidirectional converter for four different output powers are very satisfactory. This suggests this novel triple-phase-shift control method can make the converter realize ZVS and work well in large load scope.

References

[1] L. Zhu, "A novel soft-commutating isolated boost full bridge ZVS-PWM dc-dc converter for bidirectional high power applications," *IEEE Trans. Power Electronics,* vol. 21, No.2, pp. 422-429, March, 2006.

[2] H.J. Chiu and L.W. Lin, "A bidirectional DC-DC converter for fuel cell electric vehicle driving systems," *IEEE Trans. Power Electronics,* vol. 21, no. 4, pp. 950-958, July. 2006.

[3] Shigenori Inoue and Hirofumi Akagi, "A Bidirectional DC-DC Converter for an Energy Storage System with Galvanic Isolation," *IEEE Trans. Power Electronics,* vol. 22, no. 6, Nov. 2007.

[4] Hua Bai and Chris Mi, "Eliminate Reactive Power and Increase System Efficiency of Isolated Bidirectional Dual Active Bridge DC-DC Converters Using Novel Dual Phase Shift Control," *IEEE Trans. Power Electronics,* vol .23, no. 6, Nov. 2008.

[5] Robert W. Erickson, Dragan Maksimovic, "Fundamentals of Power Electronics (Second Edition)," *Springer Science +Business Media,* Inc. 2001.

[6] Gr2aham C. Goodwin , Stefan F. Graebe, Mario E. Salgado , "Control System Design," *Prentice Hall of India,* 2006.

[7] C.W. de Silva, "Modeling and Control of Engineering Systems," *Boca Raton,* FL: CRC Press, 2009.

[8] Y. Hu, J. Tatler and Z. Chen, "A bidirectional dc/dc power electronic converter for an energy storage device in an autonomous power system," *Proc. Power Electronics. Motion Cont. Conf. (IPMEC),* vol. 1. pp. 171-176, 2004.

[9] D.H.Xu, C.H. Zhao and H. F. Fan, "A PWM plus phase-shift control bidirectional DC-DC converter," *IEEE Trans.Power Electronics,* vol. 19, no. 3, pp. 666-675, May. 2004.

[10] Z. Ye, P. Jain, and P. Sen, "Circulating current minimization in high frequency AC power distribution architectures with multiple inverter modules operated in parallel," *IEEE Trans. Industrial Electronics,* vol. 54, no. 5, pp. 2673-2687, Oct. 2007

[11] Kuiyuan Wu and William G. Dunford, "An Unusual Full Bridge Converter to Realize ZVS in Large Load Scope," *Asian Power Electronics Journal,* vol. 2, no. 1, pp. 66-71, Apr, 2008.

[12] K. Lo, Y. Lin, T. Hsieh, "Phase-Shifted Full-Bridge Series-Resonant DC-DC Converters for Wide Load Variations," *IEEE Trans. Industrial Electronics,* pp. 1, 2011.

[13] Jianming Hu, Yuanrui Chen, Zijuan Yang, "Study and Simulation of One Bidirectional DC-DC Converter in Hybrid Electric Vehicle," *Proceedings of Third International Conference on Power Electronics Systems and Applications,* 2009.

[14] R.S. Yang, L.K. Chang, H.C. Chen, "An Isolated Full-Bridge DC-DC Converter with 1MHz Bidirectional Communication Channel," *IEEE Trans. Industrial Electronics,* pp. 1, 2011.

[15] S. Inoue and H. Akagi, "Loss Analysis of a bidirectional isolated dc/dc converter," *Proc. Int. Power Electronics Conf. (IPEC),* 2005.

[16] R. J. Wai, C.Y. Lin, J. J. Liaw, Y. R. Chang, "Newly-Designed ZVS Multi-Input Converter," *IEEE Trans. Industrial Electronics,* pp. 1, 2011.

[17] H. Ribeiro, B. Borges, "New Optimized Full-Bridge, Single Stage AC/DC Converters," *IEEE Trans. Industrial Electronics,* pp. 1, 2011.

[18] B. R. Lin, J. Y. Dong, J. J. Chen, "Analysis and Implementation of a ZVS/ZCS DC-DC Switching Converter with Voltage Step-Up," *IEEE Trans. Industrial Electronics,* pp. 1, 2011.

Performance Comparison of Asymmetric Carrier Random and Dual Random PWM Algorithms for Variable Speed Drives

P. Sadanandam[1] P. Poonam Upadhyay[2] A. Jayalaxmi[3]

Abstract-Pulse Width Modulation (PWM) method is one of the most useful technique for controlling the power switches of inverter fed drives. The existing Asymmetric-Carrier Random PWM (AC-RPWM) method has shaft-torque dynamics issue. This paper presents a Dual Random PWM (DR-PWM) for spreading the harmonic spectrum and to solve the above issue. The DR-PWM is used to achieve better performance like noise reduction for different Modulation Index (M.I) values of modulation region. A DR-PWM uses dithered pulse width and zero vector position, which are simulated with complex calculations. This scheme uses Random Pulse Position (RPP) and Random Career Frequency (RCF) PWM. Lead - Lag random bit and random triangular carrier are used. Time for zero voltage is randomized to get enhanced outcomes for vector controlled Induction Motor drives. The proposed DR-PWM with spread spectrum modulation provides less harmonic distortion in the signal compared to the existing AC-RPWM method.

Keywords-Power converter, resonant converter, motor drives, vector control

I. Introduction

Currently all the modern Power Electronic Converters (PEC), the Voltage Source Inverter (VSI) is probably the most extensively used device among power ratings ranging from fraction of a kilowatt to megawatt level. It converts a fixed DC voltage to three phase AC voltage with controllable frequency and magnitude. To maneuver the power switches from the converter, a number of modulation ways have been proposed from which the PWM approach is perhaps the most used scheme. Power flow is controlled by the inverter switching device gate alerts by generating pulses to obtain high performance, improved efficiency and reliable process. Gate pulses can be obtained by comparing a high frequency carrier signal with a modulating signal. Between the carrier and modulation signals, synchronization was mandatory to achieve high waveform quality with the limited switching frequency capacity of the inverters. Numerous Adjustable Speed Drive (ASD) applications need medium or high bandwidth torque control in order to achieve sufficient control performance. Recent research shows that the Pulse Width Modulation (PWM) is used to provide adjustable frequency sine wave currents to AC machine stators. These drives provide excellent speed control but do not have direct torque control capability.

PWM schemes are categorized into two types such as Current Controlled and Voltage Controlled PWM. Also these schemes are classified as either carrier based or carrier less based PWM schemes.

The paper first received 08 Oct 2017 and in revised form 22 Jun 2018. Digital Ref: APEJ-2017-10-0522

[1]**Department of Electrical and Electronics Engineering,JNTU, Hyderabad (Email: sadi_p901@yahoo.co.in)**

[2]**Department of EEE, VNR-VJIET, JNTU, Hyderabad, (Email: upadhyay_p@vnrvjiet.in)**

[3]**Department of Electrical and Electronics Engineering, JNTU, Hyderabad, (Email: ajl1994@jntuh.ac.in)**

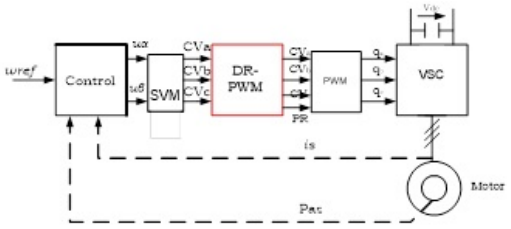

Fig. 1: Block diagram of a motor control using DR-PWM in open and closed loops

For carrier based PWM techniques, a typical harmonic spectrum shows prominent harmonics around the carrier frequency.

When the machines are controlled through such techniques generates acoustic noise. From the current spectrum of the motor, a cost effective strategy to distribute the discrete components is known as Random PWM (RPWM). RPWM also achieves spreading of the energy spectrum through random switching frequency, randomly switching and random pulse position PWM schemes rise to the harmonic spikes and causing unwanted effects in the power converter for example torque ripple, acoustic noise and Electromagnetic Interference (EMI). A variety of RPWM algorithms are reported in the literature [1]–[4]. Till now, research on RPWM schemes was mostly focused on a carrier based implementation [5]. PWM scheme has fixed switching frequency and it causes power spectrum designate and focuses at multiples of the switching frequency.

To obtain effectiveness of PECs, the unwanted effects like torque ripple and EMI need to be reduced. For that reason, this paper is proposed on Dual Random PWM. To reduce the torque ripple time for zero voltage is randomized to get enhanced outcomes. For the torque control of induction motor DTC algorithm was developed and presented by I. Takahashi [6] and it is useful for low and medium power range applications. DTC is produced for very fast torque and flux control and also robust with respect to drive parameters [7], [8]. Though, during steady state process, flux, a notable torque and current pulsations are reflected in speed estimation and it increases acoustical noise. At present, the Space Vector PWM (SVPWM) algorithm is used to overcome these anomalies [9], [10]. SVPWM algorithm is applied to decrease the steady state ripple and to obtain constant switching frequency operation of the inverter DTC in [11]–[13]. Though, the SVPWM algorithm gives good performance, it produces more acoustical noise and harmonic distortion. Existing AC-PWM provides poor performance in torque because of the variation in the frequency components of modulated signal. The peaks are less in the modulated waveform [14]. This problem is reduced in DR-PWM which provides constant variation in the output. The output waveform has many high frequency components. When the operating modulation index is less, the proposed PWM algorithm uses zero voltage as zero voltage vectors. Otherwise, when the operating modulation index is high, the proposed PWM algorithm uses highest voltage as zero voltage vectors. The DR-PWM algorithm is used for Zero Vector Distribution (DRZVD) PWM [15]. It is simple and easy

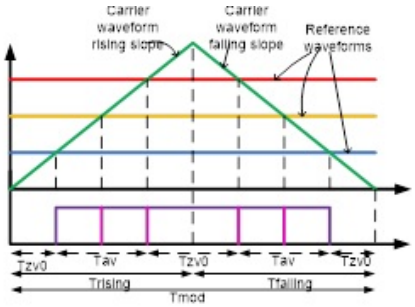

Fig. 2: PWM carrier waveform: symmetrical carrier wave in the modulation period.

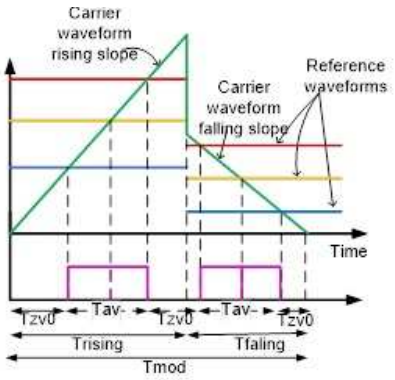

Fig. 3: PWM carrier waveform: Asymmetric carrier wave in the modulation period.

for implementation. In this proposed system, whenever the carrier (dithered) signal changes from negative to positive, Random Carrier Frequency PWM technique is used. For opposite direction, Random Pulse Position PWM (RPP-PWM) is used. The digital information contained in the bits need to be mapped to the analog pulses which are transmitted and this is done by the Pulse Position Modulation (PPM).

II. Asymmetric Carrier Random PWM

In traditional modulation methods like space vector modulation (SVM), called symmetric carrier PWM, the time required for up-counting mode (T_{rising}) is equal to the time required for down-counting mode $(T_{falling})$, as it is shown in the Fig. 2. By changing the ratio between (T_{rising}) and $(T_{falling})$ the resultant voltage vector is generated in the modulation period. This method has a drawback; it gives rise to discrete frequency components in the currents spectrum which leads to EMI [13]. This section presents a new FCF-RPWM technique called Asymmetric-Carrier random PWM technique. The advantage of this method is that, it has good performance for both low and high modulation index values and does not require any external circuits for digital implementation as shown in Fig. 3.

By changing the ratio between (T_{rising}) and $(T_{falling})$, the resultant voltage vectors generated in the conventional and in the AC-PWM is similar in position and magnitude for given modulation period, the only difference is that the voltage vector is created with different modulation frequencies [15]. In this AC-PWM the modulation period is maintained constant, but the distribution of the time length between raising and falling slopes are not equal as it is shown in Fig. 3. By choosing a random time length for raising and falling slopes in every modulation period, the time length for active vector regions will vary randomly. In other words, the voltage vector generated in the raising slope period is generated at different switching frequencies than the voltage vector generated in the falling slope period. The spreading effect of discrete components from the motor current spectrum using this AC-PWM method is good even at high modulation index values. Here the total time spent for generation of active voltage vectors as longer than the time spent for generation of zero vectors. The main advantage of this method is that it is very straightforward to include into an existing closed loop and open loop control algorithms without changing the control structure or adding hardware components, but the problem is that the PWM module has to updated twice during the modulation period and the nonlinearities like minimum dead time and minimum pulse filter have been neglected in the simulation. The AC-PWM is also suffering with shaft torque dynamics issue at low modulation index values are to avoid this problem the sampling period has to be improved. In this paper a new random PWM technique is proposed for reduction of shaft torque dynamics and considering the acoustic noise issue.

III. Proposed Dual Random PWM

A typical motor control structure in open or closed loop block diagram is shown in Fig. 1. In this section, the proposed DR-PWM is discussed. The achievement of efficient spread spectrum modulation is explained as follows.

A. Type sizes

Fig. 1 shows the block diagram of a typical motor control structure in open or closed loop. The result of the control block is calculated with reference voltage vector in the $-$ plane. This output voltage vector U_s from [21] is decomposed into two adjacent active voltage vectors when compared with the values for PWM module using the SVM blocks based calculated values. Within a modulation period, the DR-PWM block is obtained by randomization of the active and zero series vectors time length. In DR-PWM, PR_{rising} and $PR_{falling}$ are also computed with the function ratios are converted into compared values of the PWM module based o existing method and it can be seen from the block diagram in Fig. 1. The main advantage of DR-PWM is easy to implement digitally, without changing the existing control structure and addition of any external hardware modules. This modulation can be used in both open and closed-loop motor control applications. The PWM unit is used for motor control of a commercial microcontroller and it consists of an updown counter, PR and three CRs. For generating the carrier wave for the PWM unit an up-down counter is used. In traditional Space Vector Modulation (SVM), the time required for PR_{rising} up-counting mode is equal to the time required for $PR_{falling}$ down-counting mode, as it is in the existing AC-PWM. The ratio changes between PR_{rising} and $PR_{falling}$, the resultant voltage vectors generated in the first and the second part of the modulation period are similar in position and amplitude, and the difference being the resultant voltage vector which is created with different modulation frequency of active and zero voltage vector times can be calculate from equation (1)-(3).

$$T_1 = \frac{2\sqrt{3}}{pi} M_i sin(60^\circ - \alpha) T_s \tag{1}$$

$$T_2 = \frac{2\sqrt{3}}{pi} M_i sin(\alpha) T_s \tag{2}$$

$$T_z = T_s - T_1 - T_2 \tag{3}$$

where M_i is modulation index and is defined as

$$M_i = \frac{piV_{ref}}{2V_{DC}}$$

In this proposed function, step by step process is explained in system overview section.

B. System Overview

The overall process of DR-PWM system is illustrated in Fig. 1. In this proposed DR-PWM, whenever the dithered signal changes from negative to positive, RPP-PWM technique is used. For opposite direction zero vectors Pulse Position Modulation (PPM) is used. For the digital information contained in the bits needs to be mapped to the analog pulses which are transmitted and it is done by the Pulse Position

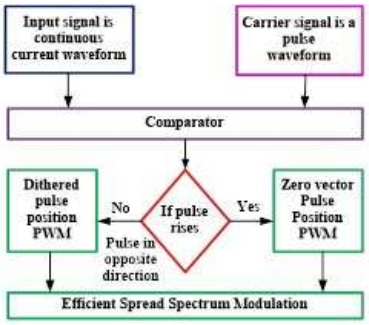

Fig. 4: Overall algorithm of proposed DR-PWM system

Modulation (PPM). The modulation method has randomly updated the frequency, which has the advantage of easy implementation and integration into an existing algorithm of open- or closed loop motor control.

C. Dithering based PWM

Dithering is done by adding noise of a level less than the least-significant bit or signal. The added noise has the significance of spreading the many short-term errors across the signal spectrum as broadband noise Dither is a small ripple frequency that is applied to convert the PWM signal to the current that causes the desired vibration and thereby increases the linearity of the motor and improves motor response.
In proposed method Dither signals are used to perform one part of Random PWM. The popular Dither wave types are triangular, rectangular and three Power modes. In Triangular, default triangular is selected, which is the safest mode for doing additional process of proposed file. Here the triangular based dither wave is used.

Conventional method of dither generation has different dithering frequency ranges with different sweep frequencies which are used to find the best sweep frequency and that would give the minimum peak value of the FFT spectrum of the switch voltage. Here the sinusoidal pulse width modulation is used to simulate the multilevel inverter of three levels. The different dithering frequency ranges for which the inverter is simulated are $19-21kHz$, $18-22kHz$ and $16-24kHz$. The different sweep frequencies considered for each dithering range are $120Hz$, $240Hz$, $480Hz$ and $960Hz$. The above said frequencies are static frequency method. Then in random PWM, dithering frequencies are generated randomly to reduce the high level noise in the form of peak frequency.

D. Zero vector Pulse Position PWM

In PPM modulation, each pulse is delayed or sent in advance of a regular time scale. A binary communication system can be ascertained with a forward or backward shift of the pulse in time. Then the data is encoded with adding an extra time shift θ_{shift} to the impulse. The binary PPM signal is given by equation (4)

$$s(t) = \sum_{k=-\infty}^{\infty} \alpha_k p(t - k_f \pm \theta_{shift}) \tag{4}$$

where the data modulation is done by small shifts in the pulse position shift $p(t)$ is the UWB pulse and T_f is the frame duration.

IV. Simulation Results

In this section, the proposed Dual Random PWM is evaluated and simulations have been carried out for both the PWM algorithms AC-RPWM and DR-PWM in MATLAB/Simulink software for different M.I values. Fig. 5 shows the periodogram power spectrum estimation. Fig. 6(a) show the phase voltage Van Fig. 6(b) and

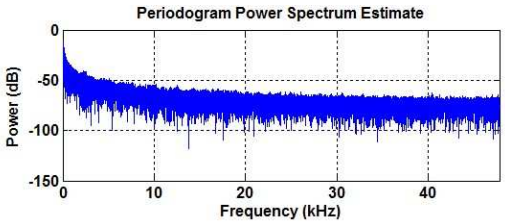

Fig. 5: Periodogram Power Spectrum estimation

Fig. 6(c) shows the motor currents spectrum of AC-PWM and DRPWM for a modulation index of 0.1. When m.i is 0.1 there are some spikes concentrated at 4, 8 and 12 kHz in the AC-PWM but these are completely disappeared in the proposed DR-PWM. The current ripple is increased in the AC-RPWM, by eliminating the discrete components from the currents spectra, the acoustic noise in the case of DR-PWM becomes close to white noise. Fig. 7(a) show the phase voltage Van Fig. 7(b) and Fig. 7(c) shows the magnitude response of AC-PWM and DRPWM for a modulation index of 0.5. Fig. 8(a) shows the phase voltage Van. Fig. 8(b) and Fig. 8(c) shows the magnitude response of AC-PWM and DRPWM for a modulation index of 0.8. When m.i value increases the spikes in the motor currents spectrum are also increases when it is controlled by AC-RPWM. These discrete components completely disappeared when it is controlled by DR-PWM. Fig. 9 shows the wave forms for t_{ga}, t_{gb} and t_{gc}. Fig. 10 shows the comparison of total harmonic distortion for different values of modulation index. The THD is less for all values of m.i in the proposed DRPWM in comparison with AC-PWM. It shows that the proposed DRPWM technique gives superior performance in comparison with the existing random PWM techniques.

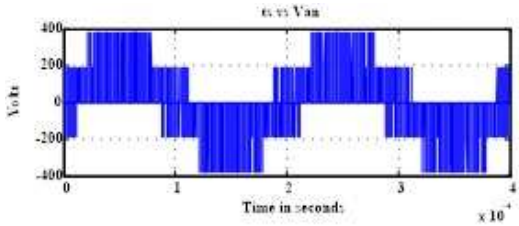

(a)

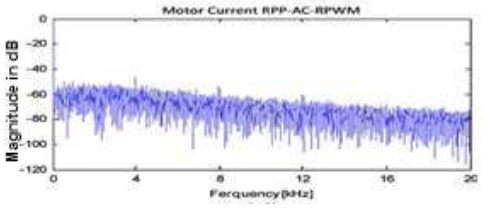

(b)

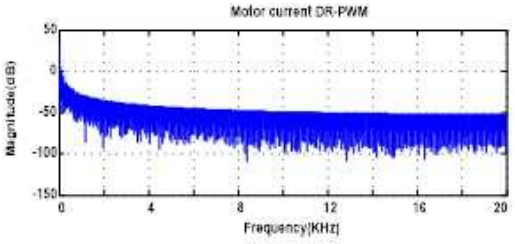

(c)

Fig. 6: (a) Phase voltage Van of DR-PWM Inverter at 0.1 M.I (b) Motor currents spectrum with RPP-AC-RPWM at 0.1 M.I (c) Motor current spectrum with DR-PWM at 0.1 M.I

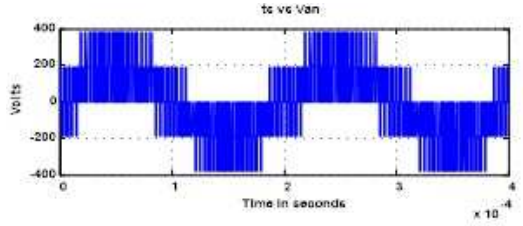

(a)

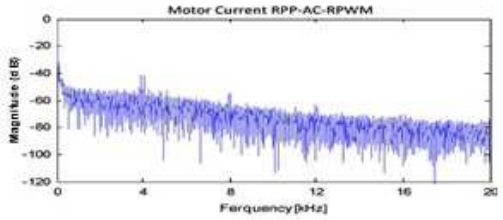

(b)

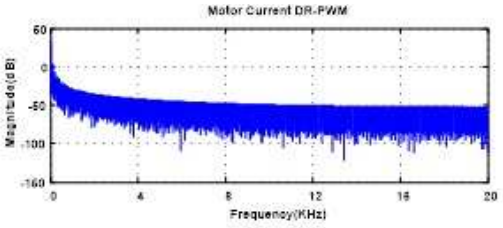

(c)

Fig. 7: (a) Phase voltahe Van of DR-PWM inverter at 0.5 M.I (b) Motor current spectrum with RPP-AC-RPWM at 0.5 M.I (c) Motor current spectrum with DR-PWM at 0.5 M.I

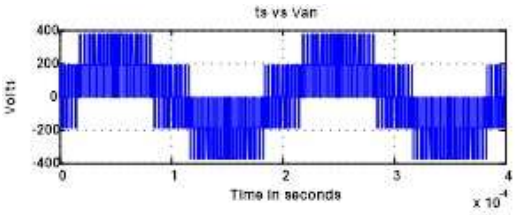

(a)

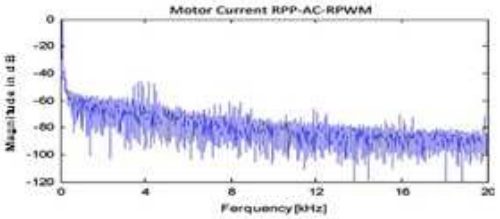

(b)

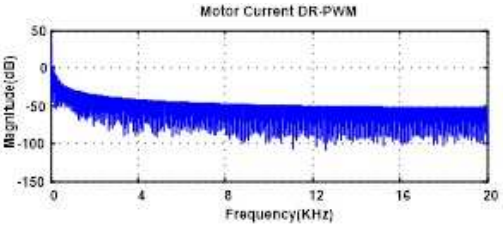

(c)

Fig. 8: (a) Phase voltage Van of DR- PWM inverter at 0.9 M.I (b) Motor current spectrum with RPP-AC-RPWM 0.9 M.I (c) Motor current spectrum with DR-PWM at 0.9 M.I

V. Conclusion

A new Random PWM method called Dual Random PWM is compared with the simulation results of existing AC-PWM method. This scheme uses random pulse position and random carrier frequency PWM to reduce the acoustical noise and the shaft torque dynamics. Time for zero voltage is randomized to get enhanced outcomes for vector controlled Induction Motor drive. The simulation results show that the proposed Dual Random PWM method effectively spreads the discrete components of the current with less noise for various values of modulation index values; it gives less total harmonic distortion and reduces the shaft torque dynamics when compared with the existing AC-RPWM algorithm.

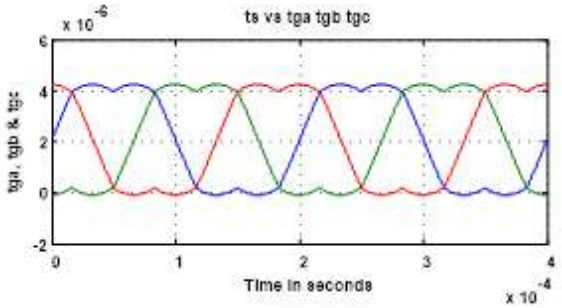

Fig. 9: Time vs t_{ga}, t_{gb} and t_{gc}

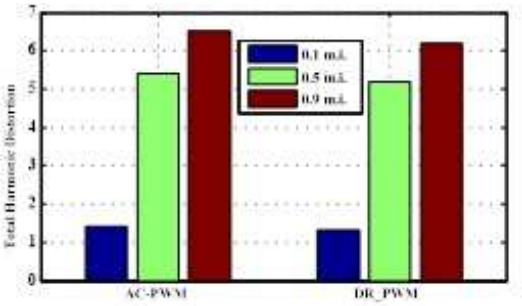

Fig. 10: Total Harmonic Distortion comparison

VI. Acknowledgment

We would like to thank the UGC for sanctioning the research grant under Minor Research Project to carry out this work, also we thank the Management of Vaagdevi College of Engineering for their support and encouragement.

References

[1] Aktaibi, A., Rahman, M., and Razali, A. "A critical review of modulation techniques," 2010.

[2] M. M. Bech, F. Blaabjerg and J. K. Pedersen, "Random modulation techniques with fixed switching frequency for three-phase power converters," *IEEE Trans. Power Electronics,* vol. 15, no. 4, pp. 753-761, July 2000.

[3] S. -. Na, Y. -. Jung, Y. -. Lim and S. -. Yang, "Reduction of audible switching noise in induction motor drives using random position space vector PWM," *IEE Proceedings - Electric Power Applications,* vol.149, no.3, pp. 195-200, May 2002.

[4] Zhao Jinghong and Zhang Junhong, "Random Pulse Width PWM Modulation for Induction Motor," *The 4th International Power Electronics and Motion Control Conference, 2004. IPEMC 2004,* Xi'an, 2004, pp. 684-687, 2005.
[5] Rajendrasinh Jadeja, Amithdilip kumar Vedy, Sidhardhasingh K.Chouhan. "An investigation on the performance of Random PWM Controlled converters," Journal of Engineering Technology and Applied Science Research. Vol.No.5 and 6, 2015 pp.876-884. 2015.
[6] H.F. Abdul Wahab and H. Sanusi, "Simulink Model of Direct Torque Control of Induction Machine," *American Journal of Applied Sciences,* 5 (8): pp.1083-1090, 2008.
[7] D. Casadei, G. Grandi, G. Serra and A. Tani, "Effect of flux and torque hysteresis band amplitude in direct torque control of Induction Machine," *Proceedings of IECON'94 - 20th Annual Conference of IEEE Industrial Electronics,* Bologna, Italy, pp. 299-304 vol.1, 1994.
[8] T. G. Habetler, F. Profumo, M. Pastorelli and L. M. Tolbert, "Direct Torque Control of Induction Machines Using Space Vector Modulation," *IEEE Trans. Industrial Electronics,* vol. 28, no.5, Sep/Oct 1992.
[9] Y. -. Lai, Wen-Ke Wang and Yen-Chang Chen, "Novel Switching Techniques For Reducing the speed ripple of ac drives with direct torque control," *IEEE Trans. Industrial Electronics,* vol. 51, no. 4, pp. 768-775, Aug 2004.
[10] T. G. Habetler, F. Profumo, M. Pastorelli and L. M. Tolbert, "Direct Torque Control of Induction Machines Using Space Vector Modulation," *IEEE Trans. Industry Applications,* vol. 28, no.5, pp. 1045-1053, Sep/Oct 1992.
[11] L. Tang, L. Zhong, A. F. Rahman and Y. Hu, "An investigation of a modified direct torque control strategy for flux and torque ripple reduction for induction machine drive system with fixed switching frequency," *IEEE Proc. Industry Applications Society,* pp.837-844, 2002.
[12] A. Carlosena, W. Chu, B. Bakkaloglu and S. Kiaei, "Randomized carrier PWM with exponential frequency mapping," *IEEE Trans. Power Electronics,* vol. 22, no. 3, pp. 960-966, May 2007.
[13] Aurasopon, A., and Sa-ngiavibool, W, "Synchronization Technique for Random Switching Frequency Pulse-Width Modulation," *International Journal of Electrical Systems Science and Engineering,* vol. 1, no. 2, pp.73-78, 2008.
[14] L. Mathe, F. Lungeanu, D. Sera, P. O. Rasmussen and J. K. Pedersen, "Spread Spectrum Modulation by using Asymmetric-Carrier Random PWM," *IEEE Trans. Power Electronics,* vol. 59, no. 10, pp.3710-3718, 2012.
[15] P.Nagashekara Reddy, Dr.J.Amarnath, P.Linga Reddy, "Space Vector Based Dual Zero-vector Random Cantered Distribution PWM Algorithm for Direct Torque Control of Induction Motor Drive for Reduced Acoustical Noise," *International Journal of Engineering Research and Technology,* vol. no.1, Issue. 8, 2012.
[16] Satyanarayana, K., Amarnath, J., and Rao, A. K, "Random PWM Algorithms for VSI FED Induction Motor Drives with fixed switching frequency," *International Journal of Engineering Science and Technology,* vol. no. 2, pp.6968-6975, 2012.
[17] L. Mathe, "Product Sound: Acoustically pleasant motor drives," *PhD thesis, Department of Energy Technology, Aalborg University,* 2010.
[18] S. E. Schulz and D. L. Kowalewski, "Implementation of variable-delay random PWM for automotive applications," *IEEE Trans. Vehicular technology,* vol. 56, no. 3, pp.1427-1433, 2007.
[19] G. Shiny and M. R. Baiju, "A Fractal based Space Vector PWM Scheme for General n-Level Inverters," *The 2010 International Power Electronics Conference - ECCE ASIA -,* Sapporo, 2010, pp. 847-854.
[20] Wu, Z, chen, G, zhu, Y, and Tian, G, "Harmonic analysis of random zero-vector distribution space vector pulse-width modulation," *Journal of Tongji University (Natural Science),* vol. 6, 2011.
[21] Guoqiang Chen, Jianli Kang and Junwei Zhao, "Study on a New Hybrid Random Space Vector Pulse Width Modulation Strategy," *Information Technology Journal,* vol, 13, no. 5, pp. 816-823, 2014.
[22] Baruah, A. D, and Patel, R. M, "Development of Random Pulse Width Modulation in Power Electronic Converters," *Development,* vol. 2, no. 5, 2015.
[23] L. Mathe, F. Lungeanu, D. Sera, P. O. Rasmussen and J. K. Pedersen, "Spread spectrum modulation by using asymmetric-carrier random PWM," *IEEE Trans. Industrial Electronics,* vol. 59, no. 10, pp.3710-3718, 2012.

P.Sadanandam obtained B.Tech Degree in Electrical and Electronics Engineering from Kakatiya University Waragal and M.Tech Degree in Power Electronics specialization from JNTUH Hydearbad. Currently pursuing Ph.D. in the area of Power Electronics and Drives. Department of Electrical and Electronics Engineering at JNTU, Hyderabad, Telangana State, India. Research interests are Electric Machine Drives, Modeling and control of Power Switching Converters, Pulse Width Modulation Techniques and Renewable Energy Sources. Presently working in Vaagdevi College of Engineering.

Dr.P.Poonam Upadhyay obtained B.E. (EE) degree from Govt College of Engineering Raipur, Ravishankar University, Raipur in 1992. M.Tech (Integrated Power Systems) from Nagpur University, Nagpur in 1996. Ph.D. Degree from Jawaharlal Nehru Technological University, Hyderabad in 2008. Research interests are High Voltage Engineering, Power Systems and Artificial Intelligence.

Dr.A.Jayalaxmi Completed B.Tech., (EEE) Degree from Osmania University, Hyderabad in 1991. M.Tech., (Power Systems) from REC Warangal presently NIT Warangal in 1996. Completed Ph.D. degree (Power Quality) from Jawaharlal Nehru Technological University, Hyderabad in 2007. Has 5 years of Industrial Experience and 16 years of Teaching Experience. Worked as visiting faculty in Osmania University College of Engineering, Hyderabad. Published 80 papers in International Journals and published 120 papers in various International and National conferences at India and also abroad. Research interests are Neural networks, Power Systems, Power Quality and Electric Machine Drives, Distributed Generation, Smart Grid and Deregulation.

Performance of Modular PFC Boost Converter using Average Current Control Technique for improving EMI

Syed Mujtaba Mahdi Mudassir [1] Gulam Amer[2] Shaik Mohammed Mukassir[3]

Abstract-The modular power system is best suited for high power applications and high power is achieved by paralleling multiple small power stages in a single package. In this paper, proposed PWM active clamped boost converter in modular approach is compared with other topologies. The modular converters operating in continuous conduction mode allow high power factor and less EMI. Both modular boost converter topologies use average current control technique and operates in continuous conduction mode where as full-bridge converter operates in discontinuous conduction mode. The proposed converter maintains an input power-factor almost unity, regulated output voltage and improved efficiency of 92% when compared with the other boost derived topologies. Control circuit used is average controller IC UC3854. High power factor is achieved using the proposed converter. The simulation results of different boost converter topologies are presented and compared.

Keywords-Modular converters, active clamp, power factor correction, Boost converter, Full-bridge converter and soft switching.

I. INTRODUCTION

Motivated by the forthcoming stringent power- quality regulations, power-factor correction (PFC) has been an active research topic in power electronics. The single phase PFC is already a common practice, and the industrial application of three-phase PFC techniques has also emerged. Up to this point, the research of three-phase converters has been heavily focused on inverter applications. Although most techniques developed in the inverter area can be used in PFC applications, a PFC circuit has its unique characteristics and, therefore, deserves some special treatment. The primary differences between PFC and inverter applications include the following aspects. Special attention has to be paid to the quality of input current to reduce the pollution to the utility, usually measured by the input current total harmonic distortion (THD). Although there are no specific limits on the input current distortion of general high-power three-phase converters at present, it is a common practice to limit the input current THD of three-phase PFC converters at least below 10%. This makes control design more critical than in inverters.

Efforts on reducing power harmonics have led to the development of some new ”power factor correction (PFC) circuits which draw almost pure sinusoidal current from the AC power supply in the AC-DC power conversion process. The technique used is to control the switching action of the PFC circuit so that the input line current is shaped into a sinusoidal waveform. Because the input current is near- sinusoidal, the amount of harmonics is small and can be filtered easily. Harmonics pollution can thus be minimized. For three-phase AC-DC power converters with step-down ability some investigations concentrate on the novelty of new topology, theory and operation of the converters, whilst reports from industry prefer to extend existing and well proven single-phase technology to the development of high power systems. This modular approach has recently been tested with boost converters. The industry-preferred approach favors the paralleling of single-phase converter units to form high-power converter systems. Such modular development approach has the following advantages:

- well proven and reliable single-phase converter technology can be used immediately,
- no major change of existing production line is required,
- power expandability offers great flexibility in the development of power converter products for different power levels, less requirements for maintenance and repair of power converter modules because of the use of standard single-phase converter units,
- Standard single-phase converter units do not require high-voltage devices that are normally needed in specially designed three-phase converters.

II. STATE ART

Usage of power electronic (PE) converters is ever increasing in the processing of electrical energy in industrial applications such as adjustable speed drives (ASD), SMPSs, UPSs, etc [1]. Therefore, the converters with high power factor are increasingly required in industries. In high-power range, mainly a three-phase system is employed.

Most of the PE systems which get connected to ac utility mains use diode rectifiers at the input [2].The active power line conditioners (APLCs) used for harmonic reduction are generally hard switched; hence, the components are subjected to high-voltage stresses which increases further with increase in the switching frequency. Also, hard switching results in low efficiency, large EMI, etc. as discussed in [3]. In soft-switched resonant converters, some of their characteristics such as large conduction losses, high component stresses, load limitation, and high cost restrict the practical use of these converters as discussed in [4]. Such converters are usually operated in variable frequency mode, and thus components are required to be designed at the lowest operating frequency. Also, resonant tank circuits are required to be designed at a much higher kVA/kW rating. The active clamp technique is one of the most attractive zero voltage- switching (ZVS) topologies [5], [6]. Medium and high power acdc converters usually make use of continuous conduction mode (CCM) boost topology as it gives near to unity

The paper first received 30 Nov 2017 and in revised form 06 July 2018. Digital Ref: APEJ-2017-11-0523

[1, 3]**Department of Electrical & Electronics Engineering, Engineering Deccan College of Engineering & Technology, Darusalaam, Hyderabad-01,Telangana, India, (Email: smmmudassir@yahoo.co.in)**

[2]**Department of Electronics & Instrumentation, Engineering Deccan College of Engineering & Technology, Darusalaam, Hyderabad-01,Telangana, India,**

power factor (UPF) at the AC input [7].

Industries are focusing on extension of existing and well-proven single-phase technology for the development of high power converters. A modular approach provides a convenient paralleling of modules, thus facilitating power expandability. Modules being identical, reserve inventory requirement, manufacturing cost, and time are also reduced. It would also reduce a problem like arduous heat dissipation and expensive components of high rating which may occur in single high power design [8]. The parallel operations of the modular design for boost-type power factor correction circuits are presented in [9]. A near unity power factor of the ac input along with a well regulated dc output voltage is obtained by constant-frequency variable duty-ratio control. By operating the inductors at DCM operation, not only the switching loss is reduced, but also balanced current sharing is achieved by controlling equal duty-ratio for all modules. The frequency of the input current ripple is increased, and its magnitude is reduced by phase-shift control. Phase shift control circuit is used to generate the gate signals for active power switches of operating parallel modules.

Modular approach is also presented in [10].The main characteristics of the proposed system are: its modularity, the employment of simple and well-known techniques, high quality of the input currents and of the output voltage, good efficiency and possibility of continuity in the operation with fall of phase or module fail. The rectifier unit is composed of three single-phase modules without neutral connection and independent power factor pre-regulation stages. The same current in each module is ensured by the current mode control technique. In [11], there exist interactions between different modules which causes boost inductor current of the same module to be different during the off interval of the main switches. In this a 3-Ph rectifier employing three 1-Ph boost PFC circuits is analyzed. Each converter operates in continuous conduction mode. ZVT technique is applied to each converter, to obtain zero turn-on losses and soft turnoff of the freewheeling diodes. Current sharing is ensured by common voltage loop driving individual current loops of 3-converter.Each converter works in CCM. To limit interaction among phases suitable modifications made. Analysis of converter in star and delta connections is analyzed.

In the converter [12], no such interaction takes place between modules. In this paper, a three-phase acdc converter with input power factor almost unity and soft- switching topology in modular approach is presented. An identical single-phase boost type active clamped acdc converter is connected in each line of a three-phase AC source. Outputs of all the three converter modules are connected in parallel to raise the power level. As a separate PFC-PWM controller is provided for each module, the independent control is facilitated even under unbalanced input voltages. The PFC-PWM controllers are not very costly; therefore, increase in the cost is marginal. A comparative performance of resonant, soft switched and hard switched 1- ph PFC rectifier circuits for telecommunication applications is presented in [13]. In this resonant rectifier has higher efficiency than other two rectifiers. Soft switched rectifier uses a phase-shift modulation technique. Resonant rectifier is similar to soft switch rectifier circuit except that it uses a resonant circuit at the output of full-bridge. The Boost pre- regulator used for PFC uses avg. current control technique, to achieve high input P.f. The modular development of single- stage AC-DC power converters is presented in [14]. Features are simple switching control, electrically isolated output, inherent PFC, flexibility for expansion of power capability and a simplification of design.

DC characteristics of the three-phase modular power-factor-correction (PFC) converters using single-phase pulse width modulation (PWM) dc-to-dc converter modules for high-power application are studied in [15]. A single-stage three-phase PFC circuit is developed using three isolated single-phase SEPIC-based PFC circuits operating in continuous-current mode [16]. This approach is found to be attractive for low to medium power applications. Use of isolated single-phase circuits also avoids the problems associated with the interaction among three phases. Detailed design criteria for the power and control stages of the single- phase SEPIC power-factor-correction circuit are presented. Issues specific to the three-phase implementation, such as current sharing at the input, are discussed. The three single- phase modules are connected in delta at the input and in parallel at the output. The individual modules have independent average-mode current controllers driven by a common outer voltage loop.

A single-stage PFC ac/dc converter based on ZVS full bridge topology with two series-connected transformers is proposed in [18]. The converter offers a very wide ZVS range due to the configuration of two series-connected transformers, without auxiliary circuits by just complementarily controlling the duty ratio of switches. High efficiency over wide load ranges, high Pf, low input current harmonics. Integrating the boost stage operated in the DCM in order to achieve the PFC. The steady state equations have been derived according to the large signal modelling. The practical aspects of building modular power supply for telecom application are described in [19]. A single-ended PWM three-phase rectifier is presented in, which is capable of high power factor and wide output voltage regulation while using high-frequency transformer insulation. A single-stage 3-phase AC-DC step-down converter without neutral connection is presented in. In this paper, the modular approach allows well-established singlephase converter modules to be paralleled to form high-power 3- phase converters. The modular approach allows well- established singlephase converter modules to be paralleled to form high-power three-phase converters. This approach greatly enhances the flexibility and power expansibility of power converters and significantly simplifies the production and maintenance procedures of such power products. The transfer function of the modular system is similar to that of a DC-DC converter. In addition, all switches in the modules are controlled simultaneously. Thus, the AC-DC modular system can be controlled as if it is a DC-DC converter. With the development of soft-switching technique, the proposed modular converter approach offers an alternative solution for reducing both low and high frequency EMI emission from power converter systems.

III. Proposed Modular PFC Boost Converter

Fig. 1 shows simplified block-diagram of a three-phase acdc converter in a modular system. Fig. 2 shows circuit diagram of the proposed single-phase module. The proposed converter consists of a small line filter comprising of L_f and C_f followed by single-phase line rectifier ($D_1 - D_4$) and a very small high- frequency bypass capacitor C_{in}. Unlike the conventional boost converter, in addition to the boost inductor Lb and the high-frequency (HF) rectifier output diode D; the resonant inductor L_r in series and resonant capacitor C_r in parallel are connected to the main switch S_m . The auxiliary switch S_a with series connected clamping capacitor C_c is connected between the drain of the S_m and the cathode of the D . The small capacitor C_n is used as a high-frequency bypass filter at the output of each module. Both the switches are driven in a complementary manner. The single output filter capacitor C_o is used at the output of the three-phase.

By sensing boost inductor current, output dc and input ac voltages, gating pulses are generated accordingly using PFC-PWM IC (UC3854) and fed to Driver IC (UC3706). Drive IC provides complementary gate drive pulses with sufficient dead band. A PCB-mounted miniature current LEM is used for sensing the boost inductor current. When boost inductor current exceeds the set limit, drive pulses are disabled, hence the converter is protected. Proposed converter uses average current mode control. In average current mode control, boost inductor current is continuously monitored

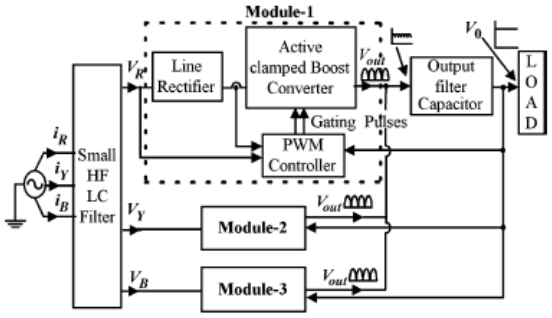

Fig. 1: Three-phase modular converter system

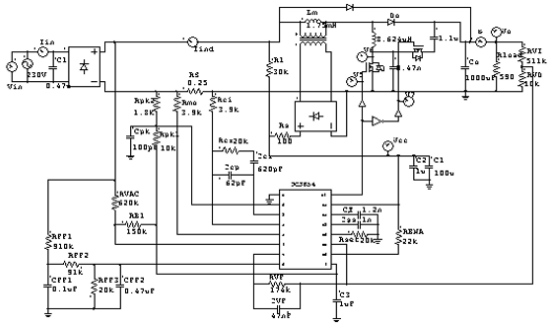

Fig. 2: Simulation circuit of proposed boost topology-1

and controlled to follow the reference signal proportional to ac line voltage. Thus, input current is sinusoidal. To regulate output voltage, a multiplier circuit controls the amplitude of the sinusoidal current reference signal in accordance with the voltage error signal generated using the output voltage and rectified input ac voltage. When the load decreases, the output voltage increases. To maintain constant load voltage, the control circuit senses the load voltage and the pulse width is automatically reduced in the switching cycle and the output voltage is regulated and maintained almost constant. The control circuit varies the duty ratio in switching cycles over the input supply voltage cycle, as the instantaneous input supply voltage is varying over the cycle.

IV. Design of Modular Converters

A. Proposed Boost Converter Topology-1

From different modes of operation of circuit, we get the following equations:

$$i_{L_b}(t) = i_{L_b}(t_0) + \frac{(V_{in} - V_o)(t - t_0)}{L_b} \quad (1)$$

$$i_{L_b}(t) = i_{L_b}(t_1) + \frac{(V_{in} - V_o)(t - t_1)}{L_b} \quad (2)$$

$$i_{L_b}(t_3) = i_{L_b}(t_3) \approx \frac{V_{in}(D_m - D_s)T}{L_b + L_r} \quad (3)$$

$$i_{L_b}(t) = i_{L_b}(t_4) + \frac{(V_{in} - V_o)(t - t_4)}{L_b} \quad (4)$$

$$i_{L_b}(t) = i_{L_b}(t_5) + \frac{(V_{in} - V_o)(t - t_5)}{L_b} \quad (5)$$

Neglecting transition intervals between two switches and based on voltage-second balance of the boost inductor Lb, from (1)(3) and (4) and (5); we get

$$\frac{V_{in} - V_o}{L_b}(D_s) + \frac{V_i n}{L_b + L_r}(D_m - D_s) + \frac{V_{in} - V_o}{L_b}(1 - D_m) = 0$$

Therefore, output voltage is given by,

$$V_o = \frac{V_{in}}{1 - D_m + D_s}[1 - \frac{L_r}{L_b + L_r}(D_m - D_s)]$$

If $L_b \gg L_r$ and $D_m \gg D_s$, we get $V_o \approx \frac{V_{in}}{1-D_m}$.
If peak to peak ripple current of the boost inductor $L_b = \Delta I_{L_b}$ $\Delta I_{L_b} \approx i_{L_b}(t_4) - i_{L_b}(t_2)$, Neglecting Ds interval

$$\Delta I_{L_b} \approx \frac{V_{in}}{L_b + L_r}\dot{D}_m T$$

From above two equations we get,

$$\Delta I_{L_b} \approx \frac{V_o}{L_b}(1 - D_m)D_m$$

$$L_b \approx \frac{V_o}{\Delta I_{L_b} f_s}(1 - D_m)D_m$$

L_b will be maximum for $D_m = 0.5$. L_b should be greater than the value calculated by above equation at $D_m = 0.5$; therefore, minimum value of boost inductor (L_{bmin}) is,

$$L_{bmin} = \frac{V_o}{4\Delta I_{L_b} f_s}$$

Energy stored in the resonant inductor L_r must be greater than the energy stored in the resonant capacitor C_r to achieve ZVS for the main switch S_m . Thus.

$$L_r \geq \frac{C_r(V_o + V_c c)^2}{(i_{L_r}(t_6))^2}$$

At the end of Mode 7, the resonant capacitor C_r discharges to zero in the quarter cycle of the resonant frequency $\omega_3 = \frac{1}{\sqrt{L_r C_r}}$, thus, the time required for discharging C_r completely is given by $t_d = (\frac{\pi}{2}\sqrt{L_r C_r})$, thus, $L_r = \frac{4{t_d}^2}{\pi^2 C_r}$.
By choosing a suitable value of C_r and t_d, the required value of L_r can be found out.

The duration required to reach to $V_{cc(max)}$ is approximately one half of the off period of the main switch, thus V_{cc} can be expressed as

$$V_{cc} \approx L_r \frac{2I_{L_r}}{(1 - D_m)T} \approx 2L_r f_s \frac{V_o}{V_{in}}^2 I_o$$

Where f_s is the switching frequency Peak-to-peak ripple voltage of clamp capacitor ΔV_{cc} can be expressed as

$$\Delta V_{cc} \approx \frac{1}{C_o}\int_0^{[(1-D_m)/2]T} i_{L_r}\, dt \approx \frac{I_o}{4C_o f_s}$$

If $\Delta V_{cc} = kV_{cc(max)}$ the value of clamp capacitor C_c can be obtained as

$$C_c = \frac{(V_{in(min)})^2}{8kL_r {f_s}^2 {V_o}^2}$$

The value of the output filter capacitor C_o is dependent on allowable peak-to-peak value of output voltage ripple V_{p-p} and maximum

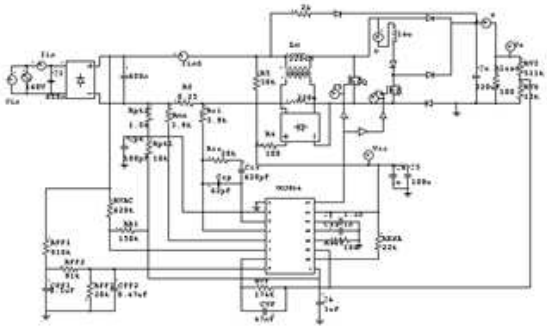

Fig. 4: Single-phase simulation circuit of boost topology-2

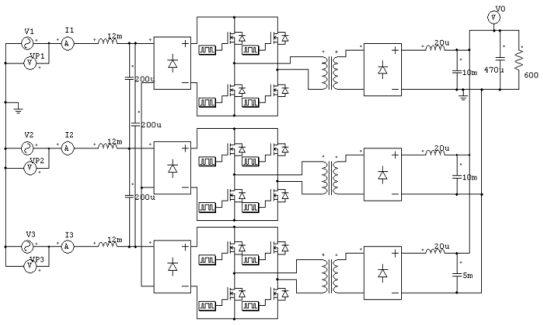

Fig. 6: Three-phase simulation circuit of boost topology-2

load current I_o and input line frequency f and is given by

$$C_o = \frac{2(2I_o/35)}{6\omega V_{p-p}} = \frac{I_o}{105\pi f V_{p-p}}$$

B. boost Converter Topology-2

Besides the ZVT network composed by L_r, D_r and S_r, each circuit differs from the normal boost topology by the presence of a split input inductor L_{ja}, L_{jb} and a split freewheeling diode D_{ja}, D_{jb} (j=1,2,3).Input voltage of 160V,50Hz is given. Power rating is 500W.Control circuit UC3854 is shown. Three phase modular connection of boost topology-2 is shown in Fig. 5 Three-single phase modules are connected in parallel.

C. Full-Bridge Modular Circuit

A simulation diagram of Full-Bridge modular converter is shown in Fig. 6 Input voltage = 160V, Output power = 1500W, Output voltage = 500V .Inputs are star connected and outputs are paralleled.

V. Simulation Results

Proposed boost converter topology-1, boost converter topology-2 and Full-Bridge converters are simulated for three phase in modular approach. Control circuit used is UC3854 PFC IC, which uses average current control technique. Output voltage, rectified input voltage and rectified input current are taken as reference values to the control circuit. Simulation is done for the following specifications:

- for 3-phase circuit: Input voltage=400V (rms), 50 Hz, Output voltage=500V, Output Power=1500W,
- for 1-phase circuit: Input voltage=160V (rms), 50 Hz, Output voltage=500V, Output Power=500W.

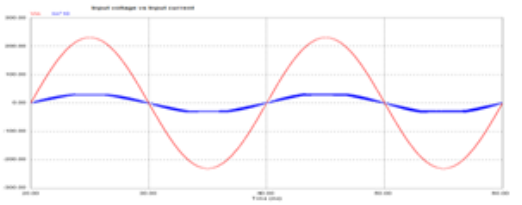

Fig. 7: Input Voltage and current waveforms of 1-ph circuit

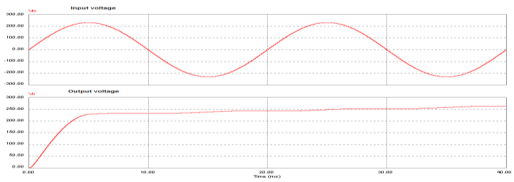

Fig. 8: Input and Output voltage waveforms of 1-ph circuit

A. Simulation of Boost Converter Topology-1

Fig. 7 shows single phase input voltage vs current waveforms. There is no phase difference between current and voltage thus, input power-factor is almost unity.

Fig. 8 shows single phase input voltage vs output voltage. It is observed that the output voltage is almost constant DC and does not have many disturbances. Fig. 9 shows 3 phase input voltages and input currents and output voltage of boost topology-1. AC input line currents follow their input voltages; thus, input power-factor is almost unity. Output voltage is almost constant DC.

B. Simulation of Boost Converter Topology-2

Fig. 10 shows 3 phase input voltages and input currents of boost topology-2. It is observed that ac input line currents are little phase-shifted with respect to sinusoidal input voltages thus, input power-factor is less compared to boost topology-1.

C. Simulation of Full-Bridge Modular Converter

Fig. 11 shows 3 phase input voltages, input currents and output voltage of Full-Bridge modular converter. The input currents follow

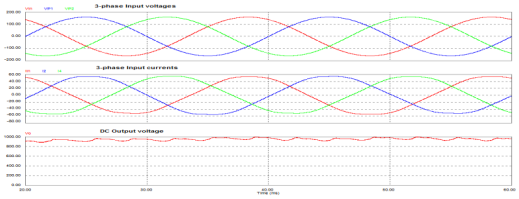

Fig. 9: Input and Output voltage waveforms of 1-ph circuit

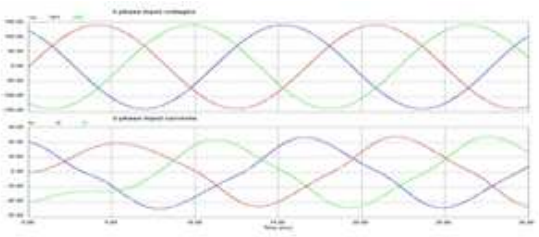

Fig. 10: Input and Output voltage waveforms of 1-ph circuit

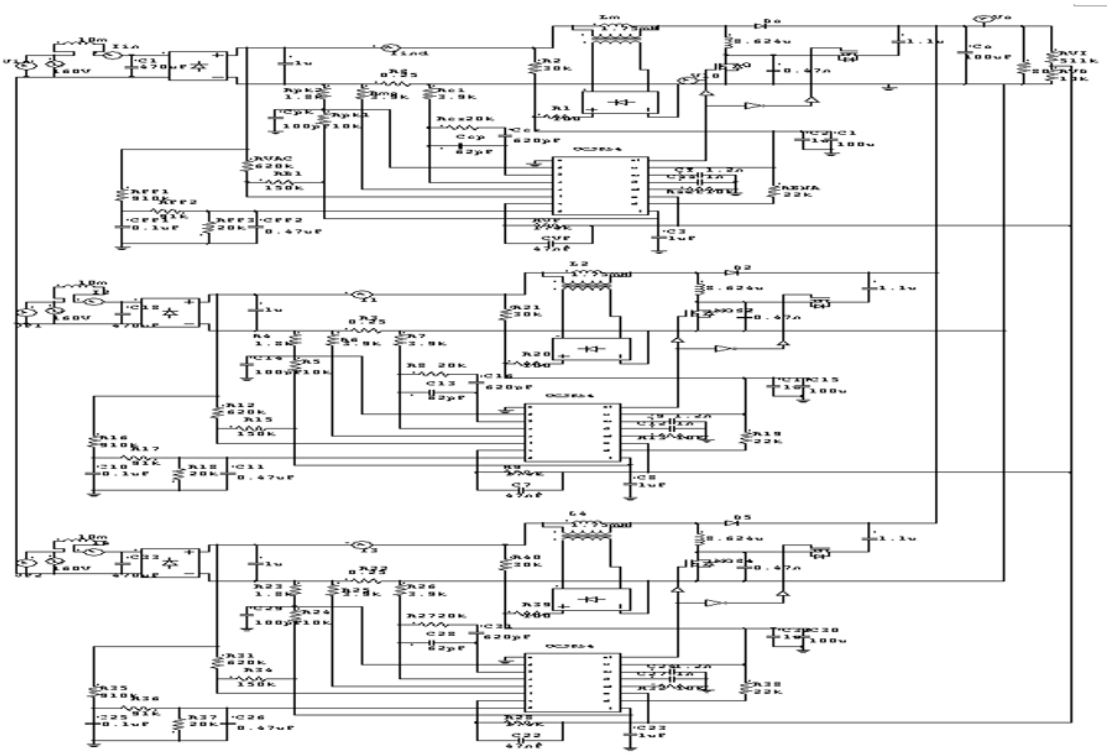

Fig. 3: Three phase circuit diagram of proposed boost converter topology 1

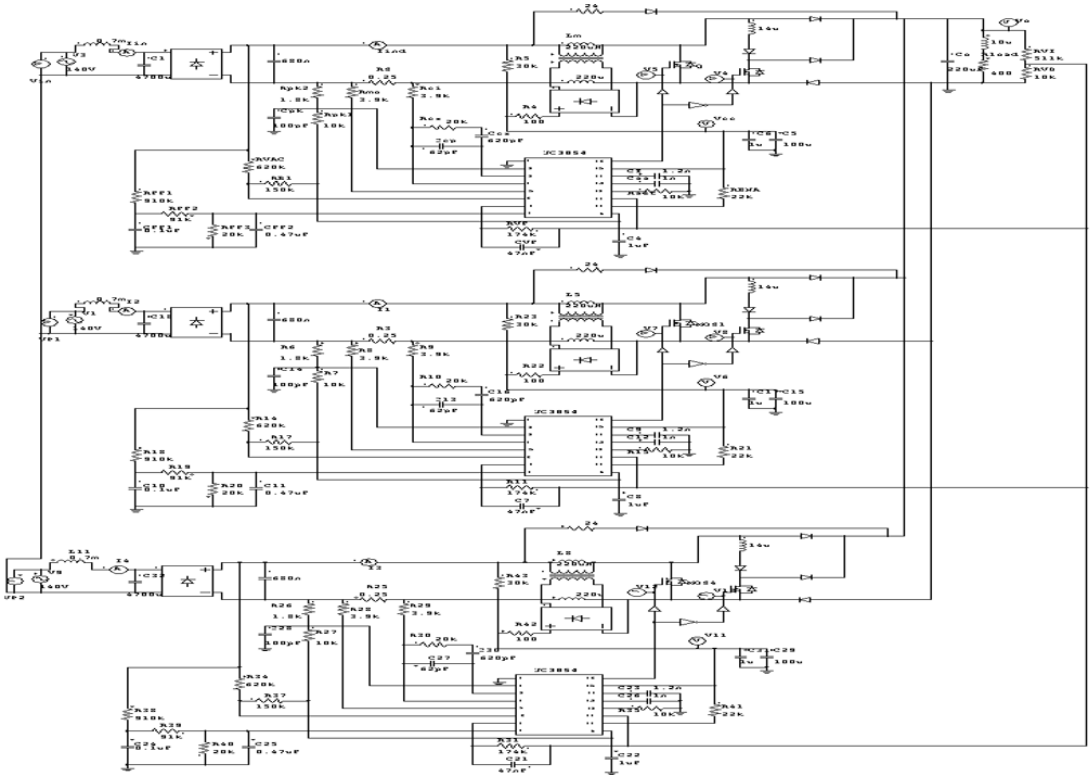

Fig. 5: Three-phase simulation circuit of boost topology-2

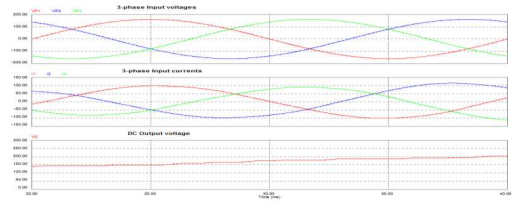

Fig. 11: Input and Output voltage waveforms of 1-ph circuit

input voltages but not exactly. Power factor is less than boost topology-1 and almost same as that of boost toplogy.

VI. Conclusion

Three-phase acdc converter using three single-phase dc-dc converters in modular approach is studied. Proposed boost converter topology-1 in modular approach is compared with other topologies. For proposed boost topology, P.f=0.99 and THD=7.8 for 1-Ph and P.f=0.99 and for 3-Ph P.f=0.99, 0.98, 0.99 and THD=5.56%, 12.9% and 4.5% respectively for 3-Ph currents. For other topologies Power factor is less and THD more compared to proposed topology. Efficiency is highest for proposed topology. It is found that efficiencies are 92%, 90% and 88% and power factors are around 0.99, 0.9 and 0.89 respectively for proposed boost topology-1; boost topology-2 and full-bridge converters.

Boost topology is better than other topologies as it operates in Continuous conduction mode and has highest power factor compared to others. Control circuit used is UC3854 PFC which uses average current control technique to control the pulses. Boost topology has less number of switches compared to others. It operates at almost unity power factor, low THD, and high efficiency and less number of components. As number of switches is more in Full-Bridge converter, switching losses are more in it compared to other converter topologies. The only disadvantage in boost converter is high output voltage, which is to be stepped down, as low voltages are required in telecommunication applications.

References

[1] B. Singh, B. N. Singh, A. Chandra, K. Al-Haddad, A. Pandey, and D. P. Kothari, "A review of three-phase improved power quality acdc converters," *IEEE Trans. Ind. Electron,* vol. 51, no. 3, pp. 641660, Jun, 2004.

[2] B. M. Saied and H. I. Zynal, "Minimizing current distortion of a three-phase bridge rectifier based on line injection technique," *IEEE Trans. Power Electron,* vol. 21, no. 6, pp. 17541761, Nov, 2006.

[3] M. R. Ramteke, H. M. Suryawanshi, and K. L. Thakre, "Single-phase resonant converter in three-phase system in modular approach," *EPE J,* vol. 16, no. 4, pp. 513, Dec, 2006.

[4] T.-F. Wu and S.-A. Liang, "A systematic approach to developing single-stage soft switching PWM converters," *IEEE Trans. Power Electron,* vol. 16, no. 5, pp. 581593, Sep, 2001.

[5] R. Watson, F. C. Lee, and G. C. Hua, "Utilization of an active clamp circuit to achieve soft switching in flyback converters," *IEEE Trans. Power Electron,* vol. 11, no. 1, pp. 162169, Jan, 1996.

[6] J. A. Cobos, O. Garcia, J. Uceda, J. Sebastian, and E. Cruz, "Comparison of high efficiency low output voltage forward topologies," *Proc. IEEE PESC,* pp. 887894, 1994.

[7] M. M. Jovanovic, "A technique for reducing rectifier reverse recovery related losses in high power boost converter," *IEEE Trans. Power Electron,* vol. 13, no. 5, pp. 932941, Sep, 1998.

[8] R. Ayyanar, R. Giri, and N. Mohan, "Active input voltage and load current sharing in input-series and output parallel connected modular dc-dc converter using dynamic input-voltage reference scheme," *IEEE Trans. Power Electron,* vol. 19, no. 6, pp. 14621473, Nov, 2004.

[9] C. S. Moo, H. L. Cheng, and P. H. Lin, "Parallel operation of modular power factor correction circuits," *IEEE Trans. Power Electron,* vol. 17, no. 3, pp. 398404, May, 2002.

[10] M. L. Heldwein, A. Ferrari de Souza, and I. Barbi, "A simple control strategy applied to three-phase rectifier units for telecommunication applications using single-phase rectifier modules," *Proc. IEEE PESC,* pp. 795800.

[11] G. Spiazzi and F. C. Lee, "Implementation of single-phase boost power-factor correction circuits in three-phase applications," *IEEE Trans. Ind. Electron,* vol. 44, no. 3, pp. 365371, Jun, 1997.

[12] H. M. Suryawanshi, Member, IEEE, M. R. Ramteke, K. L. Thakre, and V. B. Borghate, "Unity-Power-Factor Operation of Three-Phase AC DC Soft Switched Converter Based On Boost Active Clamp Topology in Modular Approach," *IEEE Trans. Power Electron,* vol. 23, no. 1, Jan, 2008.

[13] Praveen Jain, Jim Valerio and Pankaj Jain, "A Review of Single Phase Power Factor Correction Circuits For Telecommunication Applications," *16th International Telecommunications Energy Conference, INTELEC,*

[14] S.Y.R. Hui, H. Chung, Y.K.E. Ho and Y.S. Lee', "Modular development of single-stage 3-phase pfc using single-phase step-down converters," *29th IEEE Power Electronics Specialists Conference, PESC 98,* vol. 1.

[15] Y. K. Eric Ho, S. Y. R. Hui, and Yim-Shu Lee, "Characterization of Single-Stage Three-Phase Power-Factor-Correction Circuit Using Modular Single-Phase PWM DC-to-DC Converters," *IEEE Trans. Power Electron,* vol. 15, no. 1, Jan, 2000.

[16] Rajapandian Ayyanar and Ned Mohan, "Single-Stage Three-phase Power-Factor-Correction Circuit Using Three Isolated Single-phase SEPIC Converters Operating in CCM," *31st Power Electronics Specialists Conference, PESC 2000 IEEE,* vol. 1.

[17] Sewan Choi and Youngsang Bae, "A New Unity Power Factor Telecom Rectifier System by an Active Waveshaping Technique," *Industry Applications Conference, Fourtieth IAS Meeting. Conference Record 2005,* vol. 2.

[18] Tae-Sung Kim, Gwan-Bon Koo, Gun-Woo Moon, and Myung-Joong Youn, "A Single-Stage Power Factor Correction AC/DC Converter Based on Zero Voltage Switching Full Bridge Topology With Two Series-Connected Transformers," *IEEE Trans. Power Electron,* vol. 21, no. 1, Jan, 2006.

[19] T. Thandapani and R. Arumugam, "Modular Power Supply for Telecom Application (54V/100A)," *IEEE ISIE 2006, Montreal, Quebec, Canada,* pp. 9-12, July, 2006,

Investigation of Modulation Strategy for Cascaded H-bridge Multi level inverter fed Induction Motor Drive

Ravi kumar Bhukya[1] P. Satish kumar[2]

Abstract-In this paper a new SPWM technique using a trapezoidal triangular multicarrier space vector PWM for a 11 level cascaded H bridge multilevel inverter is simulated and compared with other types of carrier based PWM technique for performance evaluation. Different triangular carrier modulation techniques such as constant switching frequency level shift (LS) PWM technique viz, phase disposition (PD), phase opposition disposition (POD), alternative phase disposition (APOD), clamping space vector carrier based (CSVPWM), and weighted function based space vector carrier (WCSVPWM) are compared with proposed technique for symmetric structure of cascaded H bridge MLI. Simulation for 11 level CHB inverter has been carried out in MATLAB/Simulink and simulation results for voltage waveform and harmonic spectrum are presented and compared. The variation of THD with modulation index and frequency modulation for output voltages are analyzed.

Keywords-11-level cascaded inverter, CSV-PDPWM, CSV-PODPWM, CSV-APODPWM, CSV-PSPWM, TTMC-SVPDPWM, TTMC-SVPODPWM, TTMC-SVAPODPWM, TTMC-PSSVPWM, Induction motor drives, THD.

I. Introduction

Multilevel inverter (MLI) offers several advantages that make it preferable over the conventional voltage source inverter (VSI). These include the capability to handle higher DC link voltage, reduced power device stress and improved harmonics performance [1]. By using a multilevel structure, the stress on each switching device can be reduced in proportional to the higher voltages. In some applications, it is possible to avoid expensive and bulky step-up transformer [2]. Another significant advantage of a multilevel output is better and more sinusoidal voltage waveform as well as lowers THD [3]. Further, high dv/dt of semiconductor devices increases the electromagnetic interference (EMI) problem, resulting more common mode voltage and hence the stresses on the motor bearings are increased leads to possibilities of failure of motor. Thus by increasing the number of levels in the output waveform, the switching dv/dt stress is reduced in the multilevel inverter [4].

Multilevel inverters have achieved increasing acceptance in high power and high performance applications. Recently, multilevel inverters are widely used as static var compensators, active power filters and in motor drive applications. The advantages of multilevel inverters are good power quality, low switching loss and high voltage capability [5].

The paper first received 21 Oct 2017 and in revised form 17 July 2018. Digital Ref: APEJ-2017-12-0525

[1]**Department of Electrical Engineering, Osmania University, Hyderabad, Telangana, (Email: rkpurnanaik2014@gmail.com)**

[2]**Department of Electrical Engineering, Osmania University, Hyderabad, Telangana, (Email: Satish$_8$020@$yahoo.co.in$)**

The topologies of multilevel inverters are classified into three types: flying capacitor, diode clamped and cascaded multilevel inverters [6].

The cascaded H-bridge (CHB) multilevel inverter (MLI) is widely used due to the modularity and simplicity of the control. A single-phase five level cascaded multilevel inverter is contain Each dc source connected with its H-bridge generates three different output voltages, $+Vdc$, 0, and Vdc using various combinations of switching with the 4 switches. With two symmetric H-bridges in cascade, five level $+2Vdc$, $+Vdc$, 0, $-Vdc$, $-2Vdc$ of output voltage can be produced. The overall output voltage of CHB MLI is given by: $Vo1 = Vdc1 + Vdc2 + ... + Vdcn$.

In this paper, constant low switching frequency based on carrier pulse width modulation methods are presented and compared. A new modulation method called trapezoidal triangular multi carrier space vector PWM (TTMC-SVPWM) SPWM is implemented and compared with other methods. This new modulation method gives advantages in multilevel inverter to minimize the percentage of total harmonic distortion (THD) and to increase the output voltage.

II. Multi Carrier Based PWM Techniques

By implementing modulation technique, low frequency voltage harmonics are removed perfectly. This modulation technique produces nearly perfect sinusoidal wave forms, with lower THD.A very wide spread method in industrial applications is the classic carrier-based Si-up to $2N_{th}$ carrier group, where N_c is the number of H-bridges in each phase. Phase Shifted Carrier PWM (PSCPWM) is the common PWM for cascaded MLI. The switching transitions for PSCPWM are 2N times the number of switching transitions for APOD. The vertically shifted carrier scheme can be easily realizable on any digital controller. This scheme comes with three different techniques:

- All carrier signals are in phase (Phase Dispositions (PD)).
- In which each carrier is phase shifted by 1800 from its neighboring carrier(Alternative Phase Opposition Dispositions (APOD)).
- All carriers above the sinusoidal reference zero point are $180\circ$ out of phase with those bellow the reference zero point (Phase Opposition Dispositions (POD))

In the APOD, the sideband harmonics corresponding to first set are centered around the carrier frequency. In the APOD and the POD, harmonics will not exist at pulse number mf, due to odd symmetry of their PWM waveforms [7]. The APOD and the POD strategies provide similar performance for three level converters [8]. In PD, the triplen harmonics of voltage will be removed because the waveforms are asymmetric and thus harmonics at mf are removed if mf is chosen as a multiple of three. So the PD is more expedient due to minute values of other harmonics. The PD strategy is now well recognized for attaining the lowest line-to-line harmonic voltage distortion [9].

A. Modulation index

The modulation index is the ratio of peak magnitudes of the modulating signal V_m and the carrier signal:

$$m = \frac{Vm}{Vc} \tag{1}$$

The modulation index in SPWM technique for cascaded multilevel inverter configuration is given by:

$$m = \frac{Vm}{(N-1)Vc} \tag{2}$$

where N is number of levels. For under modulation $0 < m < 1$. For over modulation $m > 1$.

Generally, over modulation is not desired because of the presence of the lower frequency harmonics in the output voltage and subsequent distortion in the load current.

B. Frequency modulation

It is the ratio of frequency of the triangular carrier signal f_c to the frequency of sinusoidal reference signal f_s. It controls harmonics in the output voltage.

$$mf = \frac{f_c}{f_s} \tag{3}$$

III. Generaltized TTMC-SPACE Vector PWM For Cascaded Multi Level Inverter

This paper presents a modified Space vector Pulse width modulation technique so called Clamping Space vector Pulse width modulation(CSV-PWM) technique, In this paper the reference sine wave generated as in case of conventional off set injected SVPWM technique is modified by down sampling the reference wave by order of 10. Thus the waveform will be discretised reference modified Sine wave which when compared with the carrier techniques such as PD, POD, APOD and PS will generated the accurate PWM pulses for the proposed cascaded multi-level inverter. The problem DC bus unbalance has suppressed to maximum extent. And this paper presents weighted clamping Space vector Pulse width modulation(WCSV-PWM) technique, in this techniques gives the some weight function down sampling the reference waves. Thus the waveform will be discretised reference modified Sine wave which when compared with the carrier techniques such as PD, POD, APOD and PS will generated the accurate PWM pulses for the proposed cascaded multi-level inverter.

The modified SVPWM method offers a good opportunity for the realization of the Three-phase inverter control. In case of the eleven level inverters it is better to use the modified SVPWM method and with three reference waves compared to PD, POD, APOD and PS-PWM carrier waves with each phase . In such case the motor harmonic losses will be considerably lower [10].In the SPWM scheme for two-level inverters, each reference phase voltage is compared with the triangular carrier and the individual pole voltages are generated, independent of each other [11]. To obtain the maximum possible peak amplitude of the fundamental phase voltage, in linear modulation, a common mode voltage, T_{offset}, is added to the reference phase voltages. where the magnitude of T_{offset} is given by,

$$T_{offset} = \frac{-(T_max + T_min)}{2} \tag{4}$$

In this paper, a simple technique to determine the offset voltage (To be added to the reference phase voltage for PWM generation for the entire modulation range) is presented, based onely on the sampled amplitudes of the reference phase voltages [12]. The proposed modified reference PWM technique presents a simple way to determine the time instants at which the three reference phases cross the triangular carriers. To obtain the maximum possible peak amplitude of the fundamental phase voltage in linear modulation, the procedure for this is given in [13]. An offset time, offset T , is added to the reference phase voltages where the magnitude of T_{offset} given by,

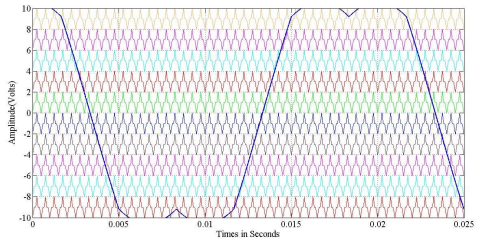

Fig. 1: TTMC-PDSVPWM

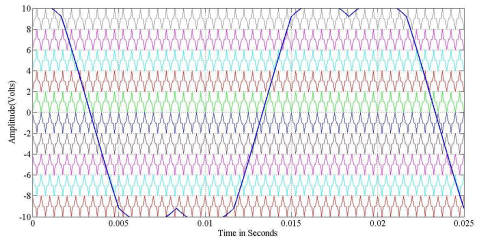

Fig. 2: TTMC-PDSVPWM

$$T_a = \frac{-(V_a * T_s)}{Vdc} \tag{5}$$

$$T_b = \frac{-(V_b * T_s)}{Vdc} \tag{6}$$

$$T_c = \frac{-(V_c * T_s)}{Vdc} \tag{7}$$

T_a, T_b and T_c are the imaginary switching time periods proportional to the instantaneous values of the reference phase voltages.

$$T_{offeset} = [\frac{T_o}{2} - T_{min}] \tag{8}$$

$$T_o = [T_s - T_{offeset}] \tag{9}$$

$$T_{offeset} = [T_{max} - Tmin] \tag{10}$$

The pulse generation of the different carried based SVPWM techniques shown in bellows figures. Fig. 1: Indicates the TTMC-PDSVPWM techniques, Fig. 2: Indicates the TTMC-PODSVPWM techniques, Fig. 3: Indicates the TTMC-APODSVPWM techniques, Fig. 4: Indicates the PD-SVPWM techniques, Fig. 5: Indicates the CSV-PDPWM techniques and Fig. 6: Indicates the weighted CSV-PDPWM techniques,

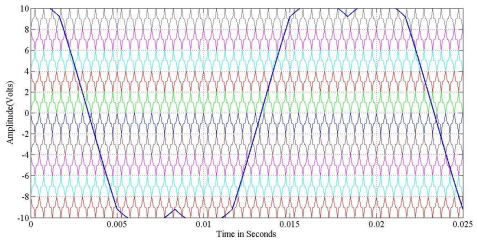

Fig. 3: TTMC-APODSVPWM

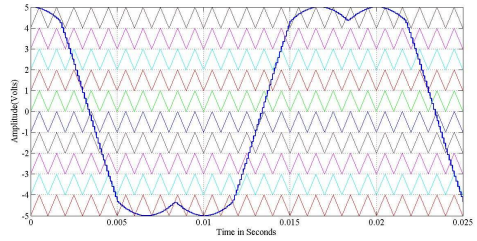

Fig. 4: PD-SVPWM

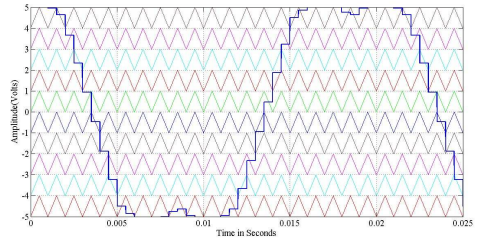

Fig. 5: CSV-PDPWM

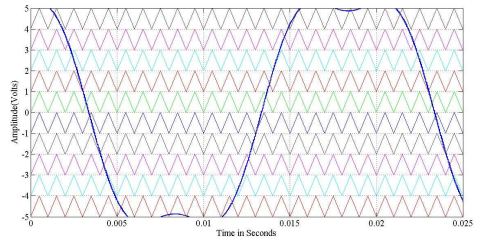

Fig. 6: CSV-PDPWM

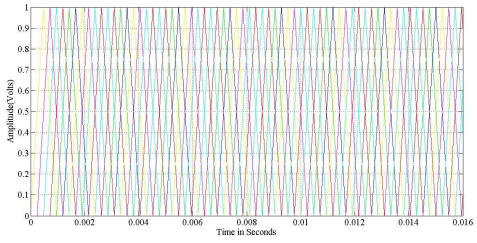

Fig. 7: CSV-PDPWM

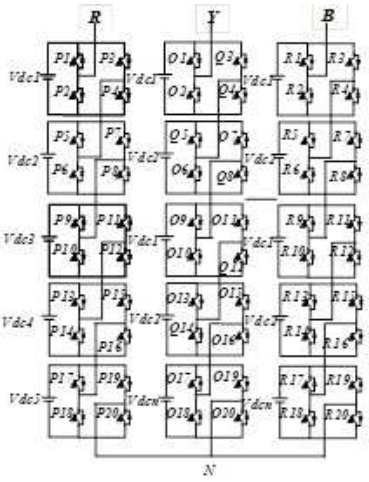

Fig. 8: 11-Level cascaded H-bridge inverter

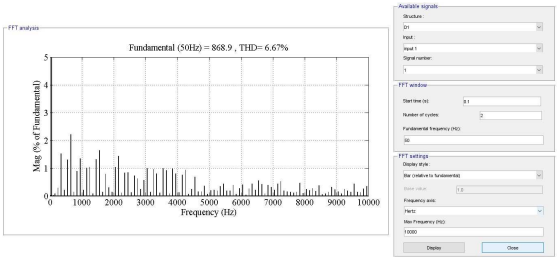

Fig. 9: PD-SPWM

IV. Simulation Results And Discussion

The simulation of cascaded H-bridge multi-level inverter with proposed comparison of control strategies applied to three phase eleven level cascaded multi-level inverter is simulated by MATLAB/SIMULINK. The output line voltages are of $398V$ magnitude peak to peak as for the DC input of $400V$. The number level in phase voltage is $2N_c + 1$, where Nc is number of single phase inverter cells used in a phase and the number of level in line voltage is $2m - 1$, where m is the number of levels in phase voltage. CMLI researches the higher output voltage and power levels. Fig. 8.Showns 11-level cascaded H-bridge inverter.

Fig. 9, Fig. 10, Fig. 11 and Fig. 12 show the harmonic analysis of inverter output line voltage for dierent SPWM techniques with the triangular carrier wave having mf of 21. The fundamental component of output voltage in all the PWM techniques is almost the same but 15% more than all the SPWM techniques. The performance of PODPWM and APODPWM techniques is almost the same in terms of THD. The PDPWM technique gives 6.67% of THD, which gives better performance with respect to all other techniques. If the carrier frequency increases, the THD in PDPWM, PODPWM,APODPWM and PSPWM techniques reduces, whereas no change is observed in

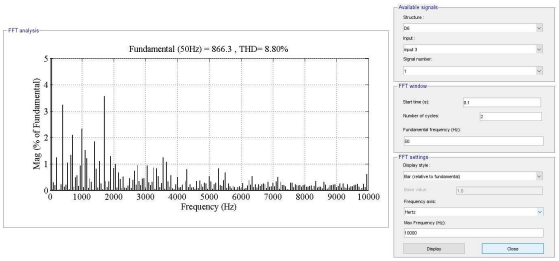

Fig. 10: POD-SPWM

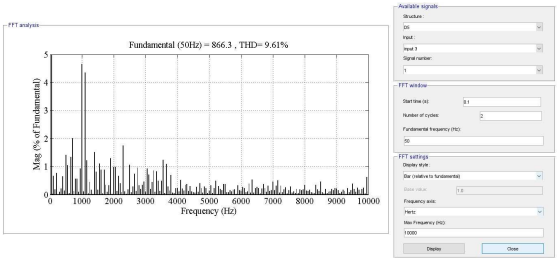

Fig. 11: APOD-SPWM

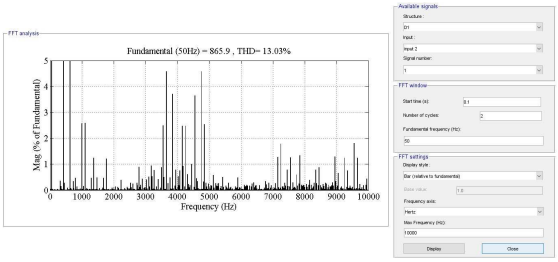

Fig. 12: PS-SPWM

the magnitude of fundamental component.

Fig. 13, Fig. 14, Fig. 15 and Fig. 16 show the harmonic analysis of inverter output line voltage for dierent modified SVPWM techniques with the triangular carrier wave having mf of 21. The fundamental component of output voltage in all the PWM techniques is almost the same but 15% more than all the SPWM techniques. The performance of PODSVPWM and APODSVPWM techniques is almost the same in terms of THD. The PDSVPWM technique gives 5.35% of THD, which gives better performance with respect to all other techniques. If the carrier frequency increases, the THD in PDSVPWM, PODSVPWM,APODSVPWM and PSSVPWM techniques reduces, whereas no change is observed in the magnitude of fundamental component.

Fig. 17, Fig. 18, Fig. 19 and Fig. 20 show the harmonic analysis of inverter output line voltage for dierent CSVPWM techniques with the triangular carrier wave having mf of 21. The fundamental component

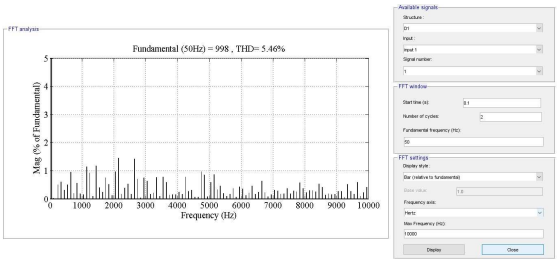

Fig. 13: PD-SVPWM

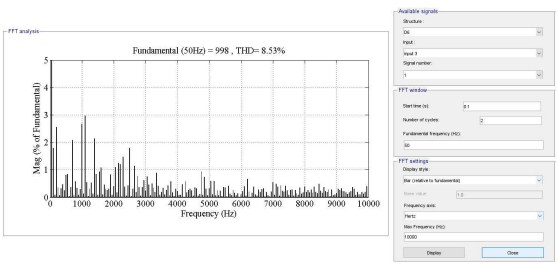

Fig. 14: POD-SVPWM

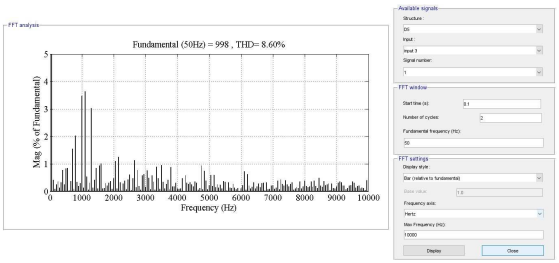

Fig. 15: APOD-SVPWM

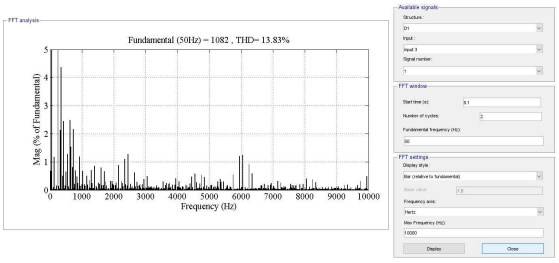

Fig. 16: PS-SVPWM

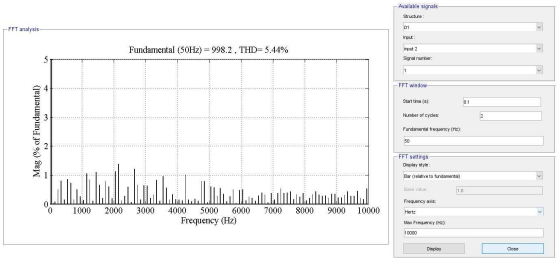

Fig. 17: CSV-PDPWM

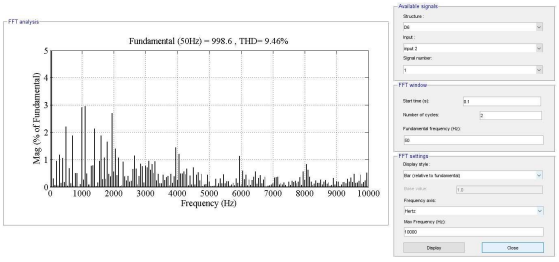

Fig. 18: CSV-PODPWM

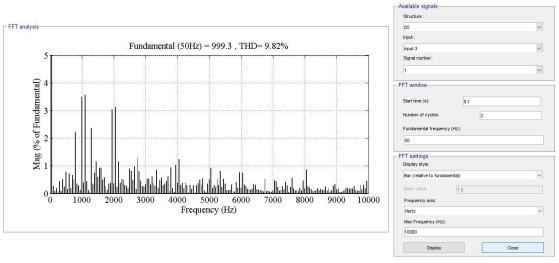

Fig. 19: CSV-APODPWM

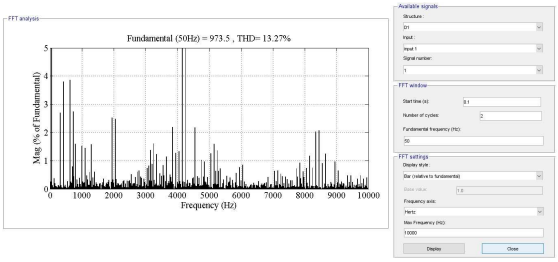

Fig. 20: CSV-PSPWM

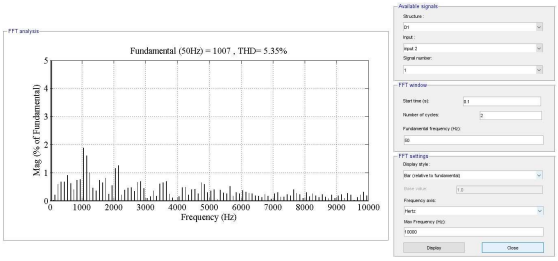

Fig. 21: WCSV-PDPWM

of output voltage in all the PWM techniques is almost the same but 15% more than all the SPWM techniques. The performance of CSVPODSVPWM and CSVAPODSVPWM techniques is almost the same in terms of THD. The CSVPDSVPWM technique gives 6.77% of THD, which gives better performance with respect to all other techniques. If the carrier frequency increases, the THD in CSVPDSVPWM, PODSVPWM APODSVPWM and PSSVPWM techniques reduces, whereas no change is observed in the magnitude of fundamental component.

Fig. 21, Fig. 22, Fig. 23 and Fig. 24 show the harmonic analysis of inverter output line voltage for dierent weighted function of CSVPWM techniques with the triangular carrier wave having mf of 21. The fundamental component of output voltage in all the PWM techniques is almost the same but 15% more than all the SPWM techniques. The performance of PODSVPWM and APODSVPWM techniques is almost the same in terms of THD. The PDSVPWM technique gives 5.35% of THD, which gives better performance with

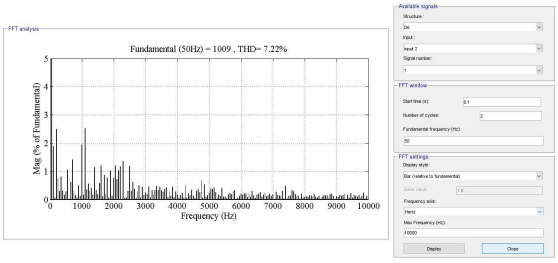

Fig. 22: TTMC-PDSVPWM

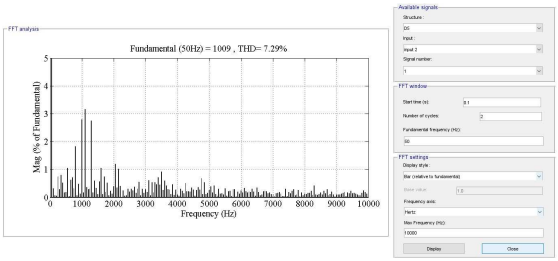

Fig. 23: WCSV-APODPWM

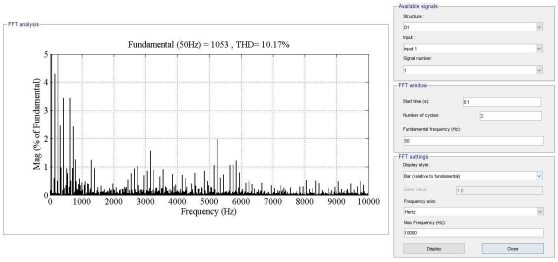

Fig. 24: WCSV-PSPWM

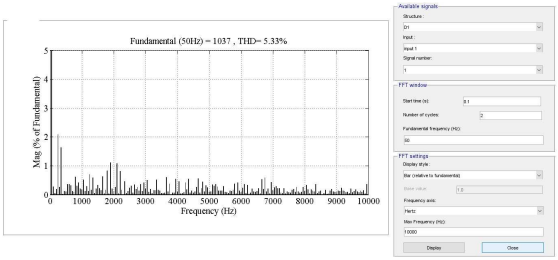

Fig. 25: TTMC-PDSVPWM

respect to all other techniques. If the carrier frequency increases, the THD in WPDSVPWM, PODSVPWM,APODSVPWM and PSSVPWM techniques reduces.

Fig. 25, Fig. 26, Fig. 27 and Fig. 28 show the harmonic analysis of inverter output line voltage for dierent modified trapezoidal triangular carrier based TTMC-SVPWM techniques with the triangular carrier wave having mf of 21. The fundamental component of output voltage in all the PWM techniques is almost the same but 15% more than all the SPWM techniques. The performance of TTMC-PDSVPWM and TTMC-PODSVPWM techniques is almost the same in terms of THD. The TTMC-PDSVPWM technique gives 5.35% of THD, which gives better performance with respect to all other techniques. If the carrier frequency increases, the THD in TTMC-PDSVPWM, TTMC-PODSVPWM TTMC-APODSVPWM and TTMC-PSSVPWM techniques reduces, whereas no change is observed in the magnitude of fundamental component.

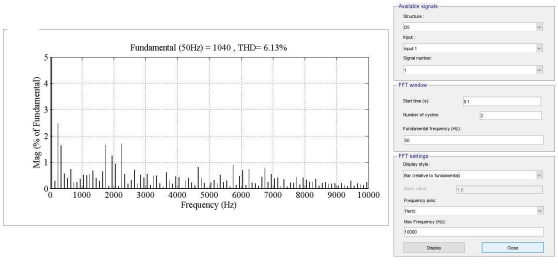

Fig. 26: TTMC-PODSVPWM

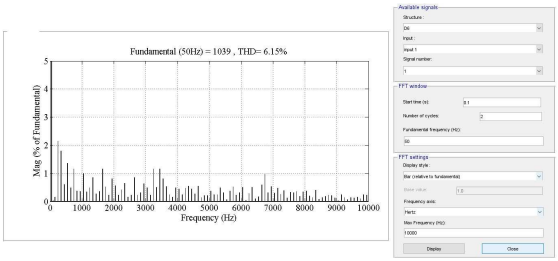

Fig. 27: TTMC-APODSVPWM

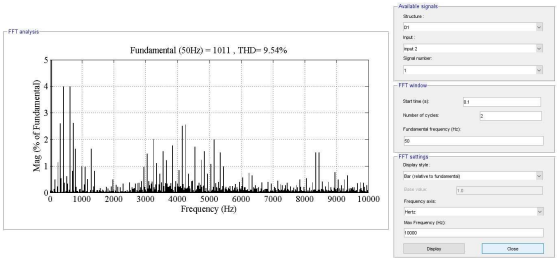

Fig. 28: TTMC-PSSVPWM

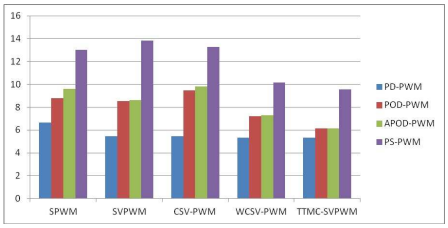

Fig. 29: THD comparison for different modulation strategy

The eleven level CMLI was simulated with induction motor load, and the DC voltage given is $100V$. In the eleven level single phase CMLI contain five H-bridges with series connections with the output phase voltage is 11 level and line voltage is 21 level of the inverter. Fig. 1. shows the circuit arrangement for 11-level CMLI with PWM generator. With perfect voltage and current shapes of the eleven level CMLI. The comparison of total harmonic distroction of different modulation strategy SPWM, modified SVPWM, clamping based CSV-PWM, weighted function based CSV-PWM and trapezoidal triangular carrier based TTMC-SVPWM techniques. In PSCPWM techniques for all different modulation strategy the harmonics are shifted towards higher frequency and compared the THD for different modulation techniques show in bellow graph (Fig. 29).

V. Conclusion

This paper present simulation results for a Eleven level cascaded H bridge inverter in symmetric configuration using various types of PWM like level shift constant switching frequency (PD, POD, APOD) PWM, phase shift PWM, modified SVPWM, clamping space vector based PWM (CSVPWM), weighted function based space vector PWM (WCSVPWM) and trapezoidal triangular carrier based space vector PWM (TTMC-SVPWM) techniques. The based on simulation results are compared. The proposed trapezoidal triangular carrier space vector PWM wave as new multi carrier for sinusoidal pulse width modulation technique gave minimum THD of 5.33%, whereas corresponding values are high in triangular LS- PWM, PSC-PWM, CSV-PWM, and WCSV-PWM for the symmetrical structure. The output voltage with the proposed TTMC SVPWM is also second highest, just next to phase shift PWM, but PSC PWM has major disadvantage of highest THD. So, the TTMC SVPWM is the best choice for minimum THD and maximum output voltage.

VI. Acknowledgment

We thank the University Grants Commission (UGC), Govt. of India, New Delhi for providing Major Research Project to carry out the Research work on Multi-Level Inverters.

References

[1] Samir Kouro, Pablo Lezana, Mauricio, Angulo, and Jos Rodrguez, "Multicarrier PWM with DC-link ripple feedforward compensation for multilevel inverter," *IEEE Trans. Power Electronics,* vol.23, n.1, pp.52-59, Jan. 2008 .

[2] Jose Rodriguez, Jih-sheng lai, and F.Zheng peng, "Multilevel Inverters-A Survey of Topologies, Controls, and Applications," *IEEE Trans. Industrial Electronics,* vol.49, n.4, pp.724-738, Aug. 2002.

[3] Jun Mei, Bailu Xiao, Ke Shen, Leon M. Tolbert and Jian Yong Zheng, "Modular Multilevel Inverter with New Modulation Method and Its Application to Photovoltaic Grid-Connected Generator," *IEEE Trans. Power Electronics,* vol.28, n.11, pp.5063-5073, Nov. 2013.

[4] L. G. Franquelo, J. Rodriguez, J.I. Leon, S. Kouro, R. Portillo and M.A.M. Parts, "The Age of Multilevel Converters arrives," *IEEE Industrial Electronics Magazine,* vol.2, n.2, pp.28-39, June 2008.

[5] J.S. Lai, , F.Z. Peng, "Multilevel converters a new bread of converters," *IEEE Trans. Industrial Appllication,* vol. 32, pp. 509517, 1996.

[6] P. Palanivel, S.S. Dash "Analysis of THD and output voltage performance for cascaded multilevelinverter using carrier pulse width modulation technique," *IET Power Electronics,* vol. 4, no. 8, pp. 951-958, 2010.

[7] B. P. McGrath, D. G. Holmes, and T. Lipo, "Optimized space vector switching sequences for multilevel inverters," *IEEE Trans. Power Electronics,* vol. 18, pp. 12931301, Nov. 2003.

[8] S. Busquets-Monge, J. Bordonau, D. Boroyevich, and S. Somavilla, "The nearest three virtual space vector Pwm- A modulation for the comprehensive neutral point balancing in the three-level npc inverter," *IEEE Power Electronics. Lett,* vol. 2, no. 1, pp. 1115, Mar, 2004.

[9] Tzou, Y.Y., Hsu, H.J, "FPGA realization of space-vector PWM control IC for three-phase PWM inverters," *IEEE Trans. Power Electronics,* vol. 12, no. 6, pp. 953963, 1997.

[10] Naderi, R. and A. Rahmati, "Phase-Shifted Carrier PWM Technique for General Cascaded In- verters," *IEEE Trans. Power Electronics,* vol. 23, no. 3, pp. 12571269, 2008.

[11] Celanovic, N.and D.Boroyevich, "A fast space-vector modulation algorithm for multilevel three-phase converters," *IEEE Trans.In dustry Applications,* vol. 37, no. 2, pp. 637641, 2001.

[12] Reddy,T. B., B.K. Reddy, J. Amarnath and D. S. Rayudu, "New Hybrid SVPWM Techniques for Direct Torque Controlled In- duction Motor Drive to Reduce Current and Torque Ripples without Angle and Sector Es- timation," *IEEE International Conference on Industrial Technology (ICIT 2006),* pp. 16241629, 2006.

[13] Reddy,C. L.,P. S. Kumar and M.Sushama, "Modified Modulation Techniques for Cascaded Multilevel Inverter Fed Induction Motor Drive," *Global Journal of Research in Engineering. 2015,* vol. 15, no. 9, pp. 1724, 2015.

Ravi kumar Bhukya was born in Warangal, Telangana, India. He obtained B.Tech. in Electrical and Electronics Engineering from JNTU University, Hyderabad in 2010 and M.Tech. in Power and induristal drives Engineering in 2013 from Jawaharlal Nehru Technological University, Hyderabad. His research interests include Power Electronics Drives and Multilevel inverters. Presently he is pursuing Ph. D. in Osmania University Telangana INDIA.

P. Satish kumar was born in Karimnagar, Telangana, India. He obtained B.Tech. in Electrical and Electronics Engineering from JNTU College of Engineering, Kakinada, India in 1996. He obtained M.Tech. in Power Electronics in 2003 and Ph.D. in 2011 from Jawaharlal Nehru Technological University, Hyderabad. He has more than 21 years of teaching experience and at present he is an Assistant Professor in the Department of Electrical Engineering, University College of Engineering, Osmania University, Hyderabad, India. His research interests include Power Electronics, Special machines and Drives and Multilevel inverters and guiding eight research scholars.

Comparison of Aircraft System Using Fuzzy Logic Control and Traditional Control Scheme

Saifullah Khalid

Abstract-Sinusoidal Current Control technique for extracting reference currents for shunt active power filters has been assessed for 400Hz aircraft electric power system. From that point forward, its performance has been compared when optimized using fuzzy logic control. Critical analysis of Comparisons of the compensation ability of these two techniques based on THD and compensation time will be done, and suggestions will be given for the selection of the best method to be used. The simulated results are presented. That will prove the importance of the proposed control method of aircraft shunt SAF in the aviation industry.

Keywords-aircraft electrical system; shunt Active Filter (SAF); sinusoidal current control strategy; fuzzy logic control; total harmonic distortion.

I. Introduction

More advanced aircraft power system [1]–[3] are now day requirement due to the vast application of electrical power in place of different other alternate power sources. The subsystems like flight control, passenger entertainment, flight surface actuators, are driven using electric power that consecutively increased the demand for creating aircraft power system much more advanced and intelligent. These subsystems have considerable issues of stability and power quality problems.

Aircraft AC power system uses source frequency and source voltage of 400 Hz and 115/200V respectively [1]–[3]. The loads with the aircraft ac system are quite dissimilar from the normal loads used in general 50 Hz supply system [1]. Whenever we consider it as the generation portion; aircraft system will be AC driven from the engine for general aircraft primary power. However, when considering the distribution of general primary power, whether AC or DC; each approach has its merits. In DC distribution, HVDC power distribution systems permit the most resourcefulemploy of generated power by antithetical loss from skin effect. It allows paralleling and load sharing among the generators. In AC distribution, Switching of AC is very clear-cut even at high levels as it logically has a zero crossing point. Due to its high reliability over HVDC system, the full range of Contactors, Relays can be exploited.

While talking about Aircraft Power Systems we also need to consider increased power electronics application in aircraft. It creates harmonics, mainly neutral currents, waveform distortion of both supply voltage and current, poor power factor and excessive current demand. Besides if a number of non-linear loads are impressed upon a supply their effects are additive. Due to these troubles, there may be nuisance tripping of circuit breakers or increased loss and thermal heating effects that may provoke early component failure.

Today, advanced computing techniques are used very popularly in automatic control system and also for optimization of the system.

The paper first received 01 Oct 2017 and in revised form 20 Aug 2018. Digital Ref: APEJ-2016-03-0477

Member, IEEE, India,

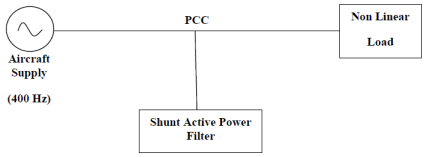

Fig. 1: Aircraft system using Shunt Active Power Filter

Some of them are GA used optimization of active power filter [9]–[12], fuzzy logic [4]–[8], neural network control [14]–[18], power loss minimization using PSO (Particle swarm optimization) [13], applied in machinery and filter devices.

Fuzzy logic controller has been used to improve the overall performance of active filter for reduction of harmonics and other related problems generated by the aircraft electrical system due to the non-linear loads [1]. The simulation results clearly show their effectiveness. The simulation results obtained with a novel optimized model will prove its superiority over traditional sinusoidal current control technique.

The paper has been designed in the following steps. The SAF configuration and the loads under consideration are discussed in Section II. The control algorithm for SAF is discussed in Section III. MATLAB/ Simulink based simulation results are presented in Section IV, and finally Section V concludes the paper.

II. System Information

The aircraft system is a 3-phase power system using source frequency of 400 Hz. From Figure 1, we can see that Shunt Active Power Filter specifically improves the power quality and compensates the most of the harmonic currents in the system [22], [24], [25], [27], [28]. The SAF is uses one voltage source inverters (VSIs) connected at PCC with a DC link voltage [20]–[23].

The set of loads for aircraft system consist of three loads. First load is a three-phase rectifier in parallel with inductive load and an unbalanced load connected in a phase with midpoint (Load 1). Second one is a three-phase rectifier connects a pure resistance directly (Load 2). Third one is a three-phase inductive load linked with the ground point (Load 3). A combination of all three loads connected with the system together at different time interval has been done. So, that we can study the effectiveness of the control schemes used. That, in turn, verifies the functionality of the SAF and its ability to harmonics compensation. For the case, Load 1 is always connected; Load 2 is initially connected and is disconnected after every 2.5 cycles. Load 3 is connected and disconnected after every half cycle. All the simulations have been done for 15 cycles. The circuit parameters values are given in Appendix.

III. Control Theory

The proposed control of SAF depends on Sinusoidal Current Control strategy. It has also been optimized for artificially intelligent technique i.e. fuzzy logic control. Sinusoidal Current Control

strategy has been discussed in brief in this section. The following section also deals with primary application of fuzzy logic in control scheme on Sinusoidal Current Control strategy [19], [20].

A. Sinusoidal Current Control Strategy (SCC)

With some modification in Constant Instantaneous Power Control strategy [19], the new approach can be used under unbalanced conditions too. The new strategy has been named as Sinusoidal current control strategy.

Fig. 2 shows the control diagram of shunt active filter using sinusoidal current control strategy that is modified a version of Constant Instantaneous Power Control strategy and under unbalanced conditions able to compensate load currents too. The modification uses a positive sequence detector that replaced the 6.4 KHz cutoff frequency LPFs and found the correct phase angle, as well as the frequency, of the component of fundamental positive sequence voltage. Thus, SAF compensates the most reactive power of the load. While designing this detector, utmost care should be taken so that shunt active filter produces ac currents orthogonal to the voltage component, otherwise it will produce active power. i_α, i_β, p' and q' are obtained after the calculation from $\alpha - \beta - 0$ transformation block and send to the $\alpha - \beta$ voltage reference block, which calculates v_α and v_β.

Finally, $\alpha - \beta - 0$ inverse transformation block calculates the V'_a,, V'_b, and V'_c. In place of the filtered voltages used previously, V'_a,, V'_b, and V'_c, are inputs to the main control circuit. Now fundamental negative sequence power, harmonic power, and the fundamental reactive power, are also included in the compensating powers.

The sinusoidal current control strategy makes the active filer to compensate the current of a nonlinear load to guarantee balanced, sinusoidal current drawn from the network, even under an unbalanced and/or distorted system voltage. We know that neutral current is a big problem for aircraft system and this strategy compensates also the neural current of the load.

Fig. 2 shows the complete control block diagram of the shunt active filter that realizes the sinusoidal current control strategy for aircraft systems. One simplification was done in the positive-sequence detector shown in Fig. 3, and included as part of the controller of the aircraft shunt active filter. Fig. 4 presents the MATLAB/Simulink model of control block diagram of shunt active filter.

It is important to remark that the voltage regulator of Fig. 2 that generates the signal p_{loss} has received an additional ask besides those listed in the last sections: to correct errors in power compensation. This occurs because the feed forward control circuit is now unable to supervise the zero-sequence power. Since the active filer compensates the whole neural current of the load in the presence of zero-sequence voltages, the shunt active filter eventually supplies. pis replaced simply by $p_{l\bar{o}ss}$. Therefore, if t-he active filer supplies $\bar{p_0}$ to the load, this causes dc voltage variations, which are sensed by the PI controller of the dc voltage regulator. Hence, an additional amount of average real power, numerically equal $\bar{p_0}$, is automatically added to the signal plot that is mainly used to provide energy to cover for losses in the power circuit of the SAF.

B. Fuzzy Logic Control Application inSinusoidal Current Control Strategy (FUZZY-SCC)

The fuzzy logic control is generally used in the dc voltage control loop of the SAF. In fuzzy logic, the design uses standard centrifugal de-fuzzification method. The steps involved in the design of a controller using the fuzzy logic require a particular set of

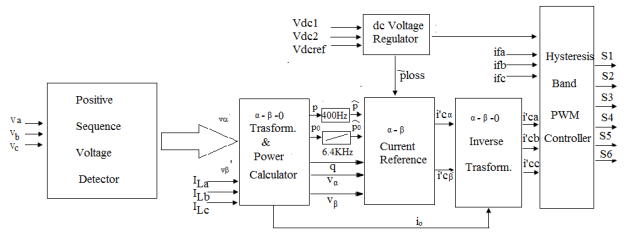

Fig. 2: Control Diagram for Shunt Active Filter Controller using Sinusoidal Current Control Strategy

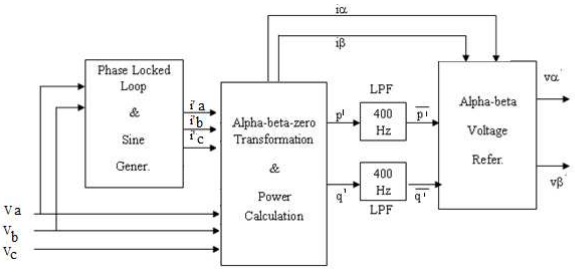

Fig. 3: Block Diagram of the Fundamental Positive-Sequence Voltage Detector for Sinusoidal Current Control Strategy

TABLE I: Fuzzy Control Rule

Errorde/dt	Negative	Zero	Positive
Negative	Big Negative	Positive	Big Positive
Zero	Big Negative	Zero	Big Positive
Positive	Big Negative	Negative	Big Positive

information. The algorithm is simple once the design problem is identified i.e. number of input and output variables required and the kind of output desired.

Two inputs; error (e)& its derivative (de/dt) and one output, which are the command signal are applied. The inputs are normalized values of capacitor voltage deviation as e and its derivative (de/dt). The two inputs uses familiar Gaussian membership functions. The output uses the triangle membership function. Tab. I shows the fuzzy control rule. Fig. 4 displays the membership functions used.

IV. Simulation Results and Discussions

The proposed scheme of SAF is simulated to estimate its performance. The load applied with the aircraft system consists of three-phase rectifier connected a pure resistance directly. To make an active compensation by SAF, a small inductance is connected at the terminals of the load. The simulation results reveal that the control scheme is comfortably able to reduce the considerable amount of THD in source voltage and source current within limits.

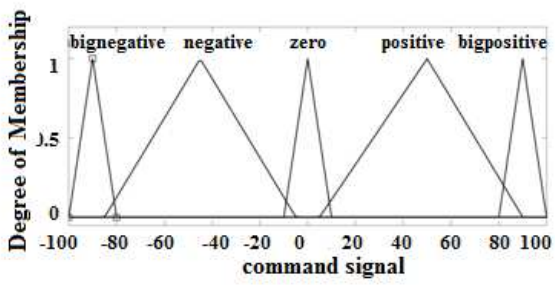

Fig. 4: Membership functions

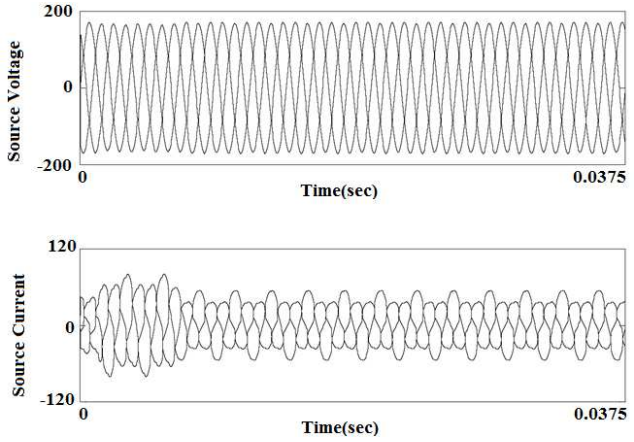

Fig. 5: Waveforms of source voltage and source current for load 1, 2 and 3 connected together at different time interval

A. Uncompensated system

From the simulation results shown in Fig. 5, it has been observed that that the THD of source current & source voltage was 9.5% and 1.55% respectively, which is obviously not within the limit of the international standard.

B. Performance of SAF

In this section, performance of SAF has been discussed for Sinusoidal Current Control Strategy alone and along with Fuzzy Logic Control. Simulation results using MATLAB show the affectivity of control schemes.

1) For Sinusoidal Current Control Strategy : The results from simulation are shown in fig. 6. THD block available in MATLAB has been used to calculate the THD of source current and voltage. From the MATLAB simulation results, THDs of source current & source voltage were 2.72% and 1.65% respectively. At t=0.01 sec, we can see that the waveforms for source voltage and source current have become sinusoidal. The observed compensation time was 0.01 sec.

The waveforms of compensation current, dc capacitor voltage and load current can be seen from Fig. 6. There is variation in dc voltage which can be seen clearly in the waveforms. If there is a need for increasing the compensation current for fulfilling the demand of load current, it releases the energy and after that it charges and tries to regain its set value.

After close observation, we can find out that the compensation current is completing the demand of load current. After using SAF, the source current, and voltage forcefully becomes sinusoidal. Comparative performance of compensation current, source current and source voltage for various loads used for different control strategies are discussed in further chapters. After the comparison with the uncompensated system, it has been observed that the system using active filter has compensated the supply system. The results are within the limit of IEEE 519-1992 standard defined for voltage and current harmonics.

2) For Sinusoidal Current Control techniquesusing Fuzzy Controller (SCC-Fuzzy): The results from simulation are shown in Fig. 7. From the MATLAB Simulation results,THDs of source current & source voltage were 2.22% and 1.01% respectively. At t=0.0066 sec, we can see that the waveforms for source voltage and source current have become sinusoidal. The observed compensation time was 0.0066 sec.

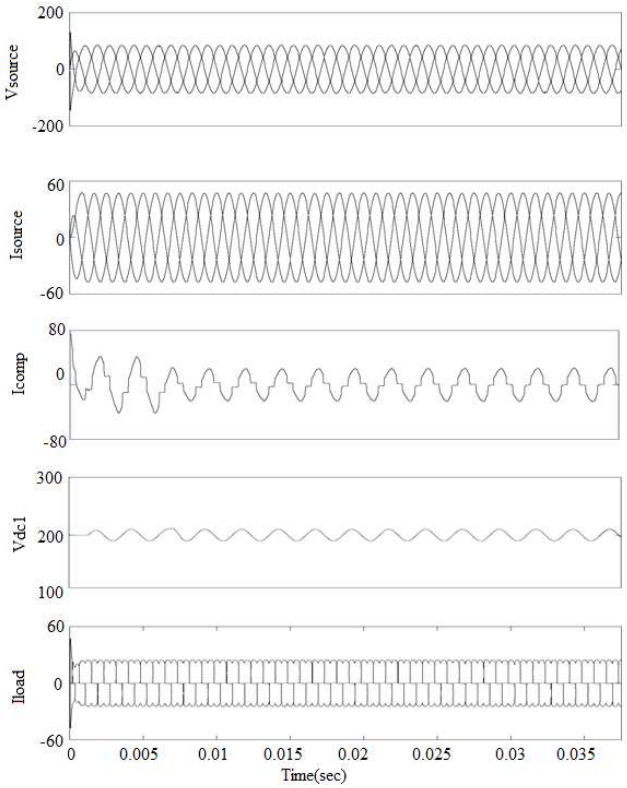

Fig. 6: Source Voltage, Source Current, Compensation Current, DC Link Voltage and Load Current Waveforms of Active Power Filter using SCC Strategy for Aircraft System

TABLE II: Summaries of Simulation Results Using SAF

Strategy Used Compensation Time(sec)	THD-I (%)	THD-V (%)
SCC 0.0100	2.72	1.65
SCC-FUZZY 0.0066	2.22	1.01

The waveforms of compensation current, dc capacitor voltage, and load current can be seen from Fig. 7. There is variation in dc voltage which can be seen clearly in the waveforms. If there is a need for increasing the compensation current for fulfilling the demand of load current, it releases the energy and after that it charges and tries to regain its set value.

After close observation, we can find out that the compensation current is completing the demand of load current and after applying the SAF, the source current and voltage forcefully becomes sinusoidal. Comparative performance of compensation current, source current and source voltage for various loads used for different control strategies are discussed in further chapters. After the comparison with the uncompensated system, it has been observed that the system using active filter has compensated the supply system. The results are within the limit of IEEE 519-1992 standard defined for voltage and current harmonics.

C. Comparative Analysis of the Simulation Results

Simulation results, shown in Fig. 6 and Fig. 7, have been tabulated in Tab. II. From the table, we can conclude that SCC-Fuzzy strategy is better than conventional SCC approach.

Figure 8 presents the bar chart for total harmonic distortion calculated for source current and source voltage. We can clearly

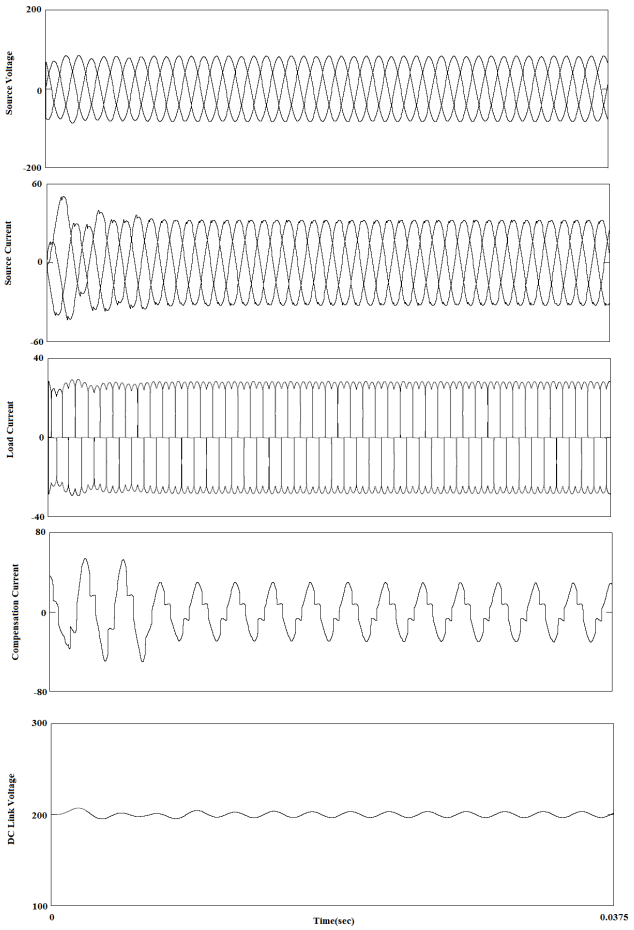

Fig. 7: Source Voltage, Source Current, Load Current, Comp Current and DC Link Voltage Waveforms of Active Power Filter using SCC Strategy using Fuzzy Logic Control for Aircraft System

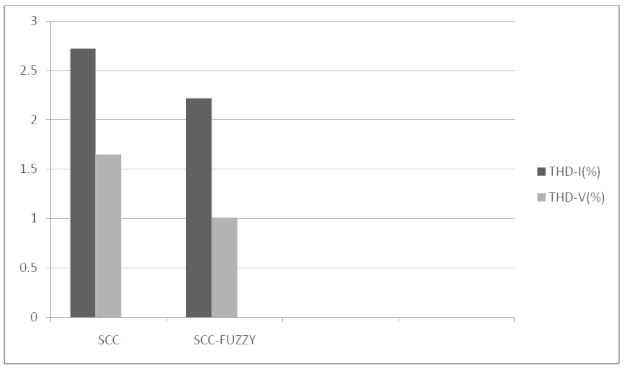

Fig. 8: THD of Source Current and Source voltage for SCC and SCC-Fuzzy strategy

observe the significant reduction in THD of both source voltage and source current for SCC-Fuzzy from SCC strategy. Current THD is reduced from 2.72% to 2.22%. Voltage THD is reduced from 1.65% to 1.01%. The compensation time for SCC-Fuzzy is less than SCC strategy, which clearly proves that SCC-Fuzzy is fast and overall better than traditional SCC strategy.

V. Conclusion

This paper has done a critical analysis of traditional (SCC) and soft computing control strategies (SCC-Fuzzy) for shunt SAFs installed in aircraft power utility of 400 HZ. The ideas have been given for the optimum selection of strategy based on compensation time and THDs of source current and voltage. Sinusoidal Current Control Strategys performance has been improved like anything when modified using Fuzzy Logic control. SCC-Fuzzy has been observed better and fast as compare to SCC control strategy discussed.

VI. Appendix

The system parameters used are as follows [1]:

Three-phase source voltage: $110V/400Hz$
Filter capacitor= $5F$
Filter inductor=$0.25mH$
Dc voltage reference: $400V$
Dc capacitor: $4700F$

References

[1] Chen Donghua, Tao Guo, Shaojun Xie, Bo Zhou, "Shunt Active Power Filters Applied in the Aircraft Power Utility," *36th Power Electronics Specialists Conference, PESC '05, IEEE,* pp. 59-63, 2005.

[2] Zixin Li,Yaohua Li, Ping Wang, Haibin Zhu, Congwei Liu, and Fanqiang Gao, "Single-Loop Digital Control of High-Power 400-Hz Ground Power Unit for Airplanes," *IEEE Trans. Industrial Electronics,* vol. 57, no. 2, pp. 532- 543, Feb, 2010.

[3] E.Lavopa, P.Zanchetta, " Real-time estimation of Fundamental Frequency and harmonics for active shunt power filters in aircraft Electrical Systems," *IEEE Trans. Industrial Electronics,* vol. 56, no. 8, Aug, 2009.

[4] Ahmed A. Helal, Nahla E. Zakzouk, and Yasser G. Desouky, "Fuzzy Logic Controlled Shunt Active Power Filter for Three-phase Four-wire Systems with Balanced and Unbalanced Loads," *World Academy of Science, Engineering and Technology,* vol. 58, pp. 621-626, 2009.

[5] Bimal K. Bose, "Expert System, Fuzzy Logic, and Neural Network Applications in Power Electronics and Motion Control," *IEE Proceedings of the IEEE,* vol. 82, no. 8, pp. 1303-1323. Aug, 1994.

[6] S. Jain, P. Agrawal, and H. Gupta, "Fuzzy logic controlled shunt active power filter for power quality improvement," *IEE Proceedings of the Electric Power Applications,* vol. 149, pp. 317-28. 2002.

[7] B. Mazari and F. Mekri, "Fuzzy Hysteresis Control and Parameter Optimization of a Shunt Active Power Filter," *Journal of Information Science and Engineering,* vol. 21, pp. 1139- 1156, 2005.

[8] H. Henao, G. A. Capolino, and J. A. Martinez-Velasco, "A new structure of fuzzy-hysteresis current controller for vector controlled induction machine drives," *Proceedings of the IEEE Power Electronics Specialist Conference (PESC),* pp. 708-712, 1996.

[9] Babak Keshavarz Hedayati, Abdolreza Rahmati, "Genetic Algorithm Application in Controlling Performance and Power Dissipation of Active Power Filters," *Canadian Journal on Electrical & Electronics Engineering,* vol. 1, no. 1, pp. 15-19, Feb, 2010.

[10] Parmod Kumar, and Alka Mahajan, "Soft Computing Techniques for the Control of an Active Power Filter," *IEEE Trans. Power Delivery,* vol. 24, no. 1, pp. 452-461, Jan, 2009.

[11] Marco Liserre, Antonio Dell Aquila, and FredeBlaabjerg, "Genetic Algorithm-Based Design of the Active Damping for an LCL-Filter Three-Phase Active Rectifier," *IEEE Trans. Power Electronics,* vol. 19, no. 1, pp.76-86, Jan, 2004.

[12] M. El-Habrouk and M. K. Darwish, "A New Control Technique for Active Power Filters Using a Combined Genetic Algorithm/Conventional Analysis," *IEEE trans. Industrial Electronics,* vol. 49, no. 1, pp. 58-66, Feb, 2002.

[13] RadhaThangaraj, Thanga Raj Chelliah, Millie Pant, Ajit Abraham and CrinaGrosan, "Optimal gain tuning of PI speed controller in induction motor drives using particle swarm optimization," *Logic Journal of IGPL Advance Access,* pp.1-14, July, 2010.

[14] Avik Bhattacharya, ChandanChakraborty, "A Shunt Active Power Filter With Enhanced Performance Using ANN-Based Predictive and Adaptive Controllers," *IEEE Trans. Industrial Electronics,* vol. 58, no. 2, pp. 421-428, Feb, 2011.

[15] Whei-Min Lin, Chih-Ming Hong, "A New Elman Neural Network-Based Control Algorithm for Adjustable-Pitch Variable-Speed Wind-Energy Conversion Systems," *IEEE Trans. Power Electronics,* vol. 26, no. 2, pp. 473-481, Feb, 2011.

[16] Jiang You-Hua, Chen Yong-Wei, "Neural Network Control Techniques of Hybrid Active Power Filter," *Proceedings of International Conference on Artificial Intelligence and Computational Intelligence,* pp. 26-30, 2009.
[17] BhimSingh,VishalVerma, and Jitendra Solanki, "Neural Network-Based Selective Compensation of Current Quality Problems in Distribution System," *IEEE Trans. Industrial Electronics,* vol. 54, no. 1, pp. 53-60, Feb, 2007.
[18] R. Dehini, A. Bassou, B. Ferdi, "Artificial Neural Networks Application to Improve Shunt Active Power Filter," *International Journal of Computer and Information Engineering,* vol. 3, no. 4, pp. 247-254, 2009.
[19] Maurcio Aredes, Lus. F. C. Monteiro, Jaime M. Miguel, "Control Strategies for Series and Shunt Active Filters," *IEEE Bologna Power Tech Conference, June 23th-26th, Bologna, Italy,* pp. 101-106, 2003.
[20] Mauricio Aredes, Jurgen Hafner, Klemens Heumann, "Three-Phase Four-Wire Shunt Active Filter Control Strategies," *IEEE Trans. Power Electronics,* vol. 12, no. 2, pp. 311-318, March, 1997.
[21] BhimSingh,KamalAl-Haddad andAmbrish Chandra, "Areviewof active filters for power quality improvement," *IEEE Trans. Industrial Electronics,* vol. 46, no. 5, pp. 960-971, Oct, 1999.
[22] F. Z.Peng, , H.Akagi, , and A.Nabae, "A New Approach to Harmonic Compensation in Power Systems a Combined System of Shunt Passive and Series Active Filters," *IEEE Trans. on Industry Applications,* vol. 6, no. 26, pp. 983-990, 1990.
[23] B.K.Bose, "RecentAdvancesinPowerElectronics," *IEEE Trans.on Power Electronics,* vol.7, no.1, pp.2-15, Jan, 1992.
[24] R. C. Dugan, M. F. McGranaghan, and H. W, "Beaty, Electrical Power Systems Quality," New York: McGraw-Hill, 1996.
[25] C. Sankaran, "Power Quality," Boca Raton, FL: CRC Press, 2002.
[26] IEEE Recommended Practices and Requirements for Harmonic Control in Electrical Power Systems, IEEE Standard 519-1992, 1992.
[27] A. Ghosh and G. Ledwich, "Power Quality Enhancement Using Custom Power Devices," Boston, MA: Kluwer, 2002.
[28] N.Mohan, T. Undeland, and Robbins, "W. Power Electronics Converters, Applications, and Design," 2nd. ed. Canada: John Wiley & Sons, 1995.

Performance of PV System for Maximum Power Point Tracking

Bipin Singh[1] Arunima Verma[2] V. K. Giri[3]

Abstract-In this paper, performance of proposed Perturb & Observe (P&O) and Incremental Conductance (IncCond) algorithms to Maximum Power Point Tracking (MPPT) for photovoltaic (PV) systems have been analyzed critically. Based on above design methodologies, a PV module of maximum voltage 32.9V, maximum current 8.2A and maximum power 200W is simulated. The output of a solar panel depends on solar insolation and temperature. Also a power electronic converter is required to interface the solar panel output to the ac grid. A step up DC to DC converter circuit is modeled for simulation implementing algorithms Perturb & Observe and Incremental Conductance. Under different insolation conditions characteristics equations for the output current generated by a solar panel is studied and verified. From results the efficiency of the Incremental Conductance algorithm is slightly more than Perturb & Observe algorithm and it has reached to the maximum value in shorter time duration (0.02 second) while due to high tracking efficiency and simplicity Perturb & Observe algorithm is probably the most preferred maximum power point tracking technique. The work deals with the solar panel to operate at maximum power point and improve the efficiency of photovoltaic system applications.

Keywords-Solar photovoltaic generation module, Perturb & Observe (P&O) algorithm, Incremental Conductance (IncCond) algorithm and DC to Dc converter.

I. INTRODUCTION

In recent developments there is an increased demand of renewable energy in the consumption of electric power. The primary sources of electric power of fossil fuels cause environmental pollution. So, a transition from conventional energy system to more clean and secure energy is the need of the now. From this point of view the renewable energies attract for more and more attention. The most common renewable energy source in use is solar energy [1]. The energy from sunlight is converted in to DC from Photovoltaic cells. Photovoltaic has added advantages to other renewable energy sources that it gives no noise and no requires maintenance [2].

Power generation from solar source provides a realistic form has been carried out. Many studies on the use of renewable energy sources for power generation have been presented already. Due to its unpredictable nature the solar energy system is highly unreliable. To analyze the reduction in the fuel consumed the photovoltaic panel has been incorporated with a diesel electric system. The other energy source can compensate the difference when the sources are unavailable or insufficient in meeting the load demands [3].The renewable energy power sources are connected to the boost converter in the rectification of DC/DC converter by maximum power point tracking controller; due to the environmental factors the above systems have a problem.

In general, the environmental conditions highly depend on the energy generation in PV modules, despite their energy conversion efficiency, manufacturing technology, etc. The fluctuation mainly caused by passing clouds, adequately affects the module characteristics and changes the amount of electrical current generated by the module to the amount of received solar irradiance [3]. For the mentioned variations in the electrical power generated by photovoltaic (PV) module cause their efficiencies to be reduced and therefore larger systems are required to generate the desired amounts of electrical power. Taking the mentioned negative effects into consideration, application and development of appropriate methods to enhance the energy generation by the systems have obtained a significant importance for an efficient use of solar energy generation systems [3], [4]. Maximum power point tracking as one of the reveal methods has been subjected to numerous research and various techniques have been proposed by researchers [4]. Despite the differences in their performance and working principles, the aim of maximum power point tracking techniques is to extract the maximum power from photovoltaic modules under liable to change environmental conditions by operating them at their maximum power point. Perturb and Observe algorithm is the most widely preferred maximum power point tracking technique due to its efficacy and simplicity. The algorithm predominantly compares the photovoltaic power before and after the control parameter due to perturbation and decides on the next perturbation [5]. Therefore, the fixed step size perturbation in the conventional Perturb and Observe algorithm causes the algorithm to suffer from oscillations near maximum power point. Smaller perturbation steps decrease oscillations while larger perturbation steps increase the maximum power point tracking speed. Use of perturbation steps variable has been proposed by numerous researchers to reduce the problem of oscillation and hence enhance the maximum power point tracking efficiency [6].

This paper has implemented the two most common algorithms to evaluate the performance of Perturb and Observe and Incremental Conductance maximum power point tracking. Mathematical model of a solar cell has been simulated to analyze the characteristics of the Photovoltaic module. A boost DC to DC converter is utilized where the main criteria on the selection of this topology has been the appropriateness of this converter for applications of grid connected system. The parameters of photovoltaic (PV) module consider for comparison are input voltage, maximum power and efficiency.

II. MAXIMUM POWER POINT TRACKING (MPPT) ALGORITHM

For efficiency improvement and development methods have been considered by numerous researchers and number of maximum power point tracking techniques has been proposed [7]. By operating the photovoltaic system at its maximum power point (Pmax) the common principle of operation of these methods is that all of them

The paper first received 07 Nov 2018 and in revised form 03 Dec 2018. Digital Ref: APEJ-2018-11-0484

[1]**Electrical Engineering Department, Institute of Engineering & Technology, Lucknow, India, (Email: singhbipin08@gmail.com)**

[2]**Electrical Engineering Department, Institute of Engineering & Technology, Lucknow, India, (Email: arunima_eed@ietlucknow.edu)**

[3]**Director, Resional Engineering College, Sonbhadra, India, (Email: girivkmmm@gmail.com)**

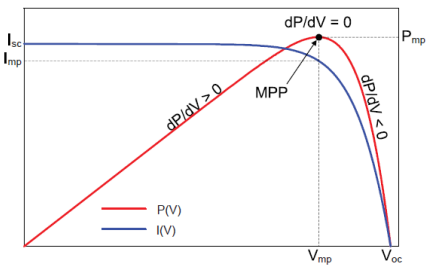

Fig. 1: Variation of $fracdPdV$ on the power and voltage characteristic of a PV module

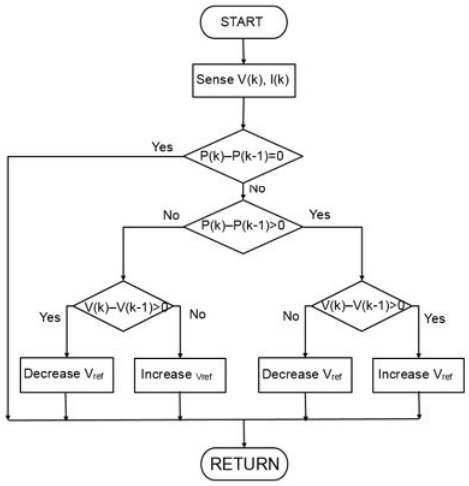

Fig. 2: Flowchart of the Perturb & Observe maximum power point tracking algorithm

enhance the system efficiency. Perturb & Observe and Incremental Conductance find the greatest application among the mentioned methods. The principle of operation of these two methods is briefly described in this section.

A. Perturb & Observe (P&O) Algorithm

Perturb & Observe algorithm is one of the Hill-Climbing maximum power point tracking techniques. Perturb & Observe algorithm tracks the maximum power point of the module with respect to the sign of $fracdPdV$. Fig. 1 shows the variation of $fracdPdV$ on the power and voltage characteristic of a photovoltaic module.

Above characteristics from the Fig. 1, $\frac{dP}{dV} < 0$ for the operating points on the right side of the maximum power point and $\frac{dP}{dV} > 0$ for operating points on the left side of the maximum power point. The variations in $\frac{dP}{dV}$ observes algorithm perturbs voltage by a constant value. If $\frac{dP}{dV} > 0$, it means the perturbation is in a forward direction and it reaches the maximum power point. If $\frac{dP}{dV} < 0$, it means that the operating point is getting far from the maximum power point, therefore, the next perturbation will be in the reverse direction. Above procedure continues the maximum power point until it reached, this means that the module operates at V_{mp} point. Due to high tracking efficiency and simplicity this method is probably the most preferred maximum power point tracking technique in the literature [7]. Low tracking efficiency under rapidly changing solar irradiation conditions and oscillations around the maximum power point are the disadvantages of this technique. In the literature efficiency of this technique has been reported over 90% [6]. Fig. 2 shows the flowchart of the Perturb and Observe maximum power point tracking algorithm.

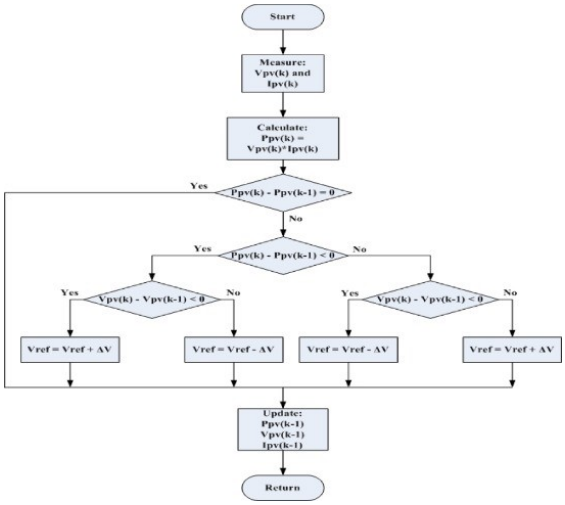

Fig. 3: Flowchart of the Incremental Conductance maximum power point tracking algorithm

B. Incremental Conductance (IncCond) Algorithm

An improvement in the Perturb & Observe algorithm introduced as another Hill-Climbing method is Incremental Conductance method. The maximum power point tracking by this algorithm is comparing the current-voltage characteristics of the module and its incremental conductance $\frac{dI}{dV}$ using by the following expression (1) and (2),

$$\frac{dP}{dV} = \frac{d(IV)}{dV} = I + V\frac{dI}{dV} \tag{1}$$

$$\left|\frac{dP}{dV}\right| I = I_m, V = V_m = 0; \left|\frac{dP}{dV}\right| I = I_m, V = V_m = -\frac{I_m}{V_m} \tag{2}$$

where, V_m -MPP voltage of the array, I_m -MPP current of the array.

The Incremental Conductance uses the photovoltaic array's incremental conductance $\frac{dI}{dV}$ to compute the sign of $\frac{dP}{dV}$ [6]. It does this using an expression derived from the condition that, at the maximum power point, $\frac{dP}{dV} = 0$. Beginning with this condition, it is possible to show that, at the maximum power point $\frac{dI}{dV} = -\frac{I}{V}$ [7].

The Incremental Conductance algorithm has the ability to determine the distance to the maximum power point, therefore stop the perturbation and tracking procedure after reaching the maximum power point [8]. Above mentioned property the oscillations around the maximum power point theoretically reduces by this algorithm. But practically it is observed that still oscillations exist around the maximum power point completely is not always achieved. Although higher accuracies are achieved with respect to the Perturb & Observe algorithm [9], under the fast changing environmental conditions this algorithm still has the low tracking efficiency [10]. Fig. 3 shows the flowchart of the Incremental Conductance maximum power point tracking algorithm.

III. Modeling Blocks of System Components

The main component of modeling system is shown in Fig. 4, for maximum power point tracking algorithm performance evaluation.

A. Mathematical Modelling of Solar Photovoltaic (SPV) cell

The mathematical model of single diode solar cell is used to simulate the photovoltaic module. Due to its simplicity and wide area of application, this model is preferred. The equivalent circuit of

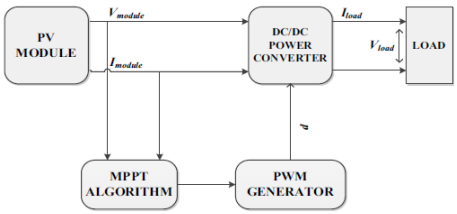

Fig. 4: Model of system components

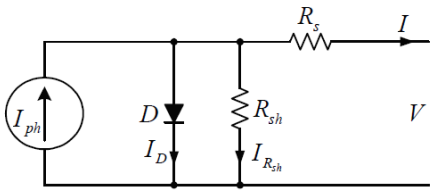

Fig. 5: Equivalent circuit of single diode solar cell

the single diode solar cell model is shown in Fig. 5.

The output current (I) is given by equation (3)

$$I = I_{ph} - I_0(e^{\frac{v+iRs}{NsV_t}} - 1)\frac{v + iRs}{R_{sh}N_s} \tag{3}$$

Thermal voltage:

$$V_t = \frac{AkT_{STC}}{q} \tag{4}$$

The simulated results of power- voltage (P-V) curve, current-voltage (I-V) curve and different insolation of power-voltage (P-V) curve presented in Fig. 6, Fig. 7 and Fig. 8 respectively.

The boost DC to DC converter is used in this paper for suitability of grid connection. The diagram of electrical circuit of a boost DC to DC converter is shown in Fig. 9. From Fig. 9it is clear that boost converter circuit consists of an inductor, a switch, a diode and a capacitor.

The boost DC to DC converter operates in two modes:

The 1^{st} mode operations switch is turned on i.e. t = T_{ON} and the rising input current flows through the inductor and the switch and

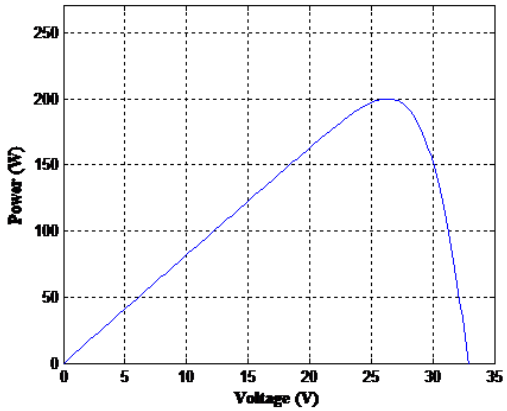

Fig. 6: Power-voltage (P-V) curve of Solar module

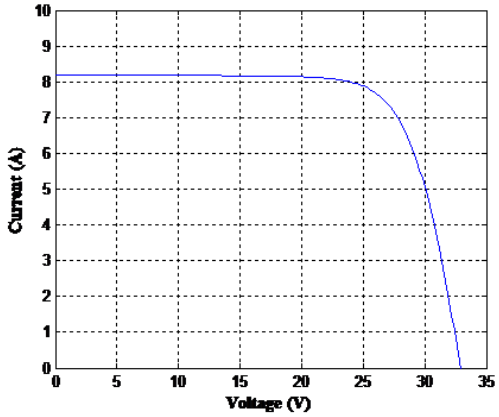

Fig. 7: Current-voltage (I-V) curve of Solar module

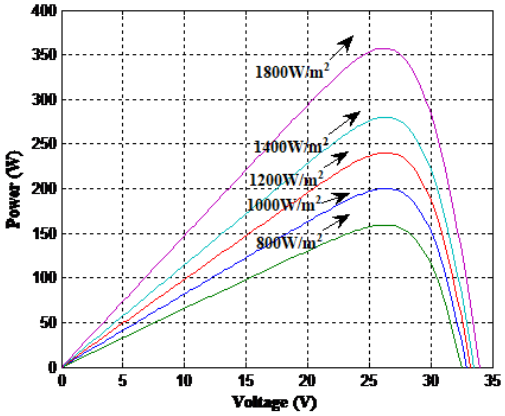

Fig. 8: Different insolation of power-voltage (P-V) curve of solar module

the energy is stored in the inductor.

The 2^{nd} mode operations switch is turned off i.e. t = T_{OFF} and current flows through the inductor, diode, capacitor and the load. The inductor current falls until the beginning of the next cycle of operation and the energy is transferred to the load.

The output voltage can be described in terms of input voltage by the following equation (5),

$$V_O = \frac{V_{in}}{(1-\alpha)} \tag{5}$$

where, α = Duty cycle.

B. Modeling of Maximum Power Point Tracking Algorithm

The proposed models of the Perturb & Observe and Incremental Conductance maximum power point tracking algorithms are

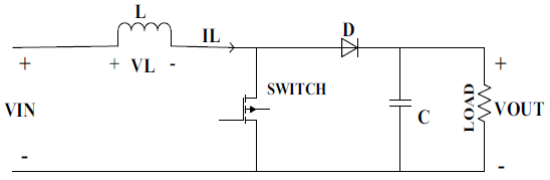

Fig. 9: Electrical circuit diagram of a boost DC to DC converter

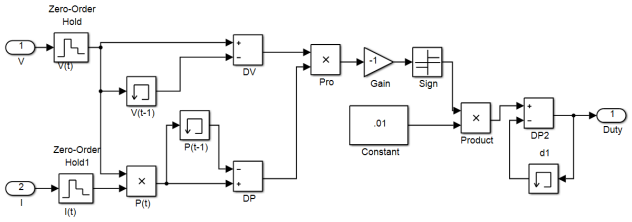

Fig. 10: Model of Perturb & Observe maximum power point tracking algorithm

constructed based on the flowcharts of the mentioned algorithms as explained in Fig. 2 and Fig. 3, respectively. The simulation models are shown in Fig. 10 and Fig. 11, respectively.

IV. Simulation Results

This research paper has carried out the simulation with both Perturb & Observe and Incremental Conductance maximum power point tracking algorithms. The Matlab/simulation model is run for 0.1 second under standard temperature condition (Ambient Temperature =250$^{\circ}C$ and $G = 1000W/m^2$,). Emphasize the value and improving effects of maximum power point tracking application results are compared with the results carried out from the simulation system.

A model of Boost DC to DC converter using Perturb & Observe maximum power point tracking algorithm and complete model is presented in Fig. 12.

Model of Boost DC to DC converter using Incremental Conductance maximum power point tracking algorithm is shown in Fig. 13.

From simulation results, both algorithms have same amount of power delivered to the load while the Incremental Conductance algorithm output power has been slightly higher than the Perturb & Observe algorithm.

The evaluation of efficiency and comparison is performed by given equation (6),

$$= \frac{Pout}{Preal} \tag{6}$$

where, P_{real} = Under test condition available maximum power The simulation results of output power without and with maximum power point tracking algorithm and their efficiencies of the maximum power point tracking algorithms for both Perturb & Observe and Incremental Conductance are shown in Fig. 14 & Fig. 15 respectively.

Simulation result presented in Fig. 14 shows the operating point of the photovoltaic with Incremental Conductance algorithm represents at the right side of the maximum power point while the Perturb & Observe algorithm operates the photovoltaic at the left side of the maximum power point. It is also showed that the operating point without application of maximum power point trackers of open circuit. It is showing that maximum power point tracking algorithms have enhanced the overall efficiency greater than 72% of the system.

Simulation result presented in Fig. 15 shows the efficiency for both of the algorithms is more than 92%. It is also observed that the efficiency of the Incremental Conductance algorithm is slightly more than Perturb & Observe algorithm and it has reached to the maximum value in shorter time duration (0.02 second).

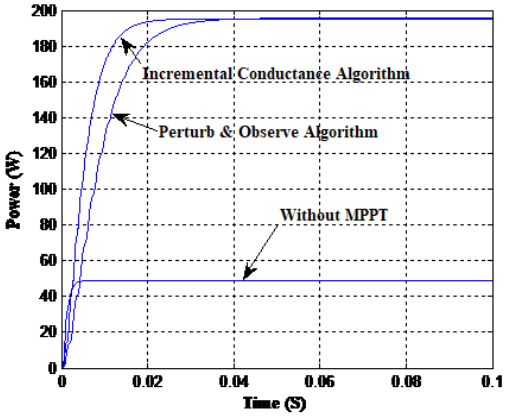

Fig. 14: Output power with and without MPPT Algorithm

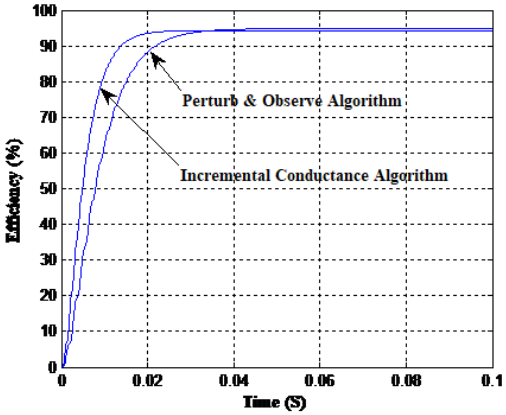

Fig. 15: Efficiency of MPPT Algorithm

TABLE I: Simulation Result (Numerical value)

Parameter	P&O Algorithm	IncCond Algorithm	Without MPPT
V_{in} (V)	32.9	32.9	47
P_{max} (W)	198.6	198.9	48.55
Efficiency ($\eta\%$)	93.49	94.56	22.10

Tab. I shows the numerical data for simulation of Perturb & Observe and Incremental Conductance algorithms. In view of the simulation results together with the advantages and disadvantages of Perturb & Observe and Incremental Conductance algorithms, a tracking system which simultaneously tracks the maximum power point of the photovoltaic modules using both Perturb & Observe and Incremental Conductance algorithms may be indicated as a practical solution. Depending on the application requirement and environmental conditions maximum power point tracking system can control and compare the outputs of the mentioned methods and pick the appropriate maximum power point tracking method. Therefore, most reliable and efficient control can be given to take the merits of each individual maximum power point tracking method under application requirements and environmental conditions.

V. Conclusion

The Perturb & Observe method is the simplest maximum power point tracking method. The Incremental Conductance method is an improvement to the Perturb & Observe method and it has a quite complex structure. The results of simulation verified under identical insolation conditions both of the methods have nearly same efficiencies greater than 92%. The presented simulation results,

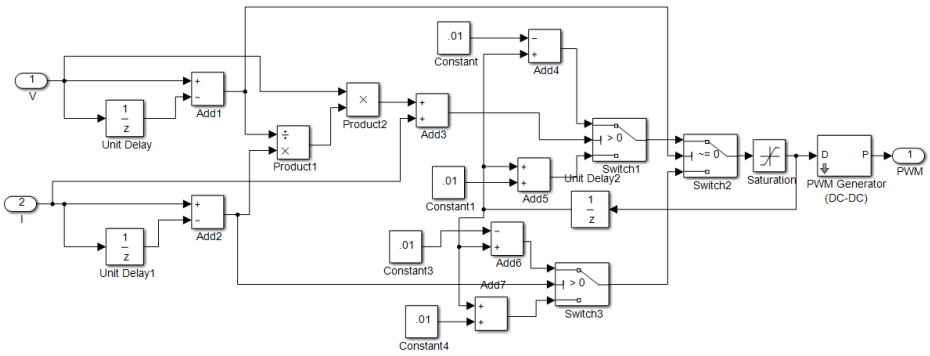

Fig. 11: Model of Incremental Conductance maximum power point tracking algorithm

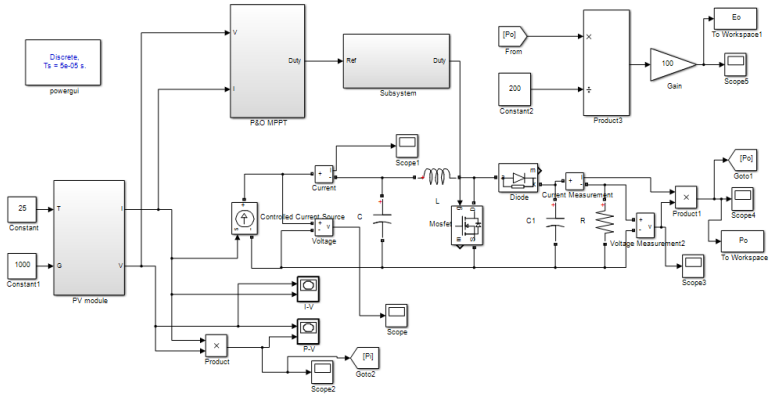

Fig. 12: Model of Boost DC/DC converter using P&O MPPT algorithm

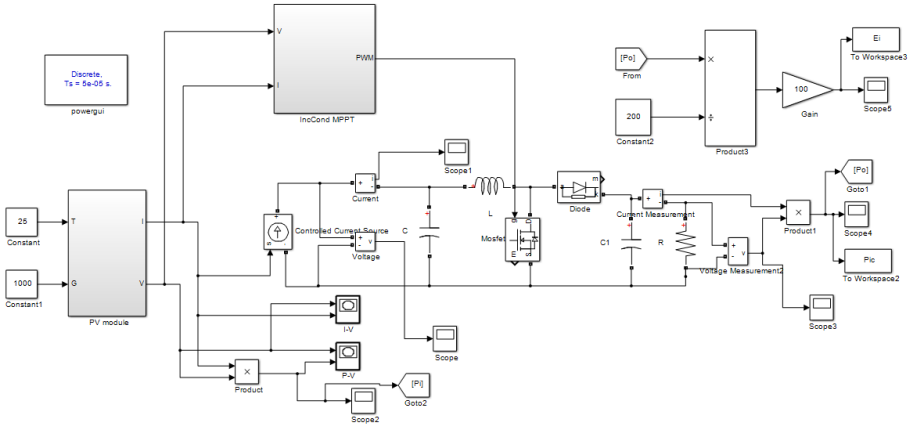

Fig. 13: Model of Boost DC to DC converter using Incremental Conductance maximum power point tracking algorithm

shown slightly better performance by Incremental Conductance method in tracking the maximum power point tracking of the solar photovoltaic (SPV) system. It is shown and observed that the output power of the Incremental Conductance method reaches to the maximum power point in a shorter time duration (0.02 second) as compared with the Perturb & Observe algorithm which takes more time duration (0.03 second). The high tracking and its simple structure efficiency makes the Perturb & Observe algorithm to be the most preferable one and can utilize maximum power point tracker for solar photovoltaic module. The maximum power point trackers application has increased the total output power by greater than 72%, where the simulation results clearly show the enhancing role of the maximum power point tracking in photovoltaic systems.

VI. Appendix

Parameters of Solar Photovoltaic (SPV) module
Open circuit voltage (V_{oc}) = 32.9V
Rated power (V_{mp}) = 200W
Current at maximum power (V_{mp}) = 7.58A
Short circuit current (I_{sc}) = 8.21A
Total number of cells in series (N_s) = 54
Total number of cells in parallel (N_p) = 1
Ideality factor of diode = 1.3
Charge of an electron (e) = 1.610-19C
Insolation = 1000W/M^2
Bandgap energy (E_{g_0}) = 1.1ev
Series resistance (R_s) = 0.221
Shunt resistance (R_{sh}) = 415
Nominal temperature (T_n) = 298K
Short circuit current of cell at 250° C and 1000W/m^2
Boltzmann constant k = 1.3810-23 J/k

References

[1] Shu-Hung et al, "A Novel Maximum Power Point Tracking Technique for Solar Panels Using a SEPIC or Cuk Converter," *IEEE Trans. Power Electronics,* vol. 18, no. 3, May, 2003.

[2] Wies et al., "Simulink Model for Economic Analysis and Environmental Impacts of a PV with Diesel-Battery System for Remote Villages," *IEEE Trans.Power Systems,* vol. 20, no. 2, May, 2005.

[3] Soeren Baekhoej Kjaer, "A Review of Single-Phase Grid-Connected Inverters for Photovoltaic Modules," *IEEE Trans. Industry Applications,* vol. 41, no. 5, Sep/Oct, 2005.

[4] A. K. Abdelsalam, A. M. Massoud, S. Ahmed, and P. N. Enjeti, "High-Performance Adaptive Perturb and Observe MPPT Technique for Photovoltaic-Based Microgrids," *IEEE Trans. Power Electronics,* vol. 26, no. 4, April, 2011.

[5] Q. Zhang, C. Hu, L. Chen, A. Amirahmadi, N. Kutkut, Z.J. Shen and I. Bataresh, "A Center Point Iteration MPPT Method with Application on Frequency-Modulated LLC Microinverter," *IEEE Trans. Power Electronics,* vol. 29, no. 3, March, 2014.

[6] N. Femia, G. Petrone, G. Spagnuolo, and M. Vitelli, "Optimization of Perturb and Observe Maximum Power Point Tracking Method," *IEEE Trans. Power Electronics,* vol. 20, no. 4, July, 2005.

[7] B. N. Alajmi, K. H. Ahmed, S. J. Finney, and B. W. Williams, "Fuzzy-Logic-Control Approach of a Aodified Hill-Climbing Method for Maximum Power Point in Microgrid Standalone Photovoltaic System," *IEEE Trans. Power Electronics,* vol. 26, no. 4, April, 2011.

[8] R. F. Coelho, F. M. Concer and D. C. Martins, "Analytical and Experimental Analysis of DC-DC Converters in Photovoltaic Maximum Power Point Tracking Applications," *Proc. IECON 2010, IEEE Press,* Nov, 2010.

[9] Lin Chen, Ahmadreza Amirahmadi, Qian Zhang, Nasser Kutkut, and Issa Batarseh, "Design and Implementation of Three-Phase Two-Stage Grid-Connected Module Integrated Converter," *IEEE Trans. Power Electronics,* vol. 29, no. 8, Aug, 2014.

[10] Juan David Bastidas-Rodriguez, Edinson Franco, Giovanni Petrone, Carlos Andrs Ramos-Paja and Giovanni Spagnuolo, "Maximum Power Point Tracking Architectures for Photovoltaic Systems in Mismatching Conditions: A Review," *IET Power Electronics,* vol. 7, no. 6, pp. 13961413, 2014.

[11] G Bhuvaneswari and R Annamalai, "Development of a Solar Cell Model in MATLAB for PV Based Generation System," *Proceedings of Annual IEEE India Conference (INDICON),* pp. 1-5, 2011.

[12] Moein Jazayeri, Sener Uysal, Kian Jazayeri, "Evaluation of Maximum Power Point Tracking Technique in PV Systems using MATLAB/Simulink," *Sixth Annual IEEE Green Technologies Conference 2014,* pp. 54-60, 2014.

[13] Tekeshwar Prasad Sahu, T. V. Dixit, "Modelling and analysis of P & O and IncCond MPPT algorithm for PV array using Łuk converter," *IEEE Students' Conference on Electrical, Electronics and Computer Science 2014,* pp. 1 6, 2014.

[14] Kancherla Harini , Syama S., "Simulation and analysis of IncCond and P & O MPPT with DC-DC converter topology for PV array," *International Conference on Electrical, Computer and Communication Technologies (ICECCT) 2015,* pp. 15, 2015.

[15] M Praful Raj, Ann Mary Joshua, "Design, implementation and performance analysis of a LabVIEW based fuzzy logic MPPT controller for stand-alone PV systems," *IEEE International Conference on Power, Control, Signals and Instrumentation Engineering (ICPCSI) 2017,* pp. 1012-1017, 2017.

Author Index

A	Page
A.Jayalaxmi	10
Arunima Verma	38
B	
Bipin Singh	38
C	
Clarence W.de Silva	1
G	
Gulam Amer	15
K	
Kuiyuan Wu	1
P	
P.Sasanandam	10
P.Pooanm Upadhyay	10
P.Satish kuman	21
R	
Ravi kumar Bhukya	21
S	
Syed Mujtaba Mahdi Musassir	15
Shaik Mohammed Mukassir	15
Saifullah Khalid	27

Submission Details

Only online submission will be accepted. Please first register and submit online. The paper is in double column and is similar to most IET or IEEE journal format. There is no page limit. Any number of pages of more than 6 will be subject to additional charge.

The paper guidelines can be downloaded using the link: http://perc.polyu.edu.hk/apejournal/

Any queries, please contact Prof. Eric Cheng, Publishing Director of APEJ, Dept. of Electrical Engineering, The Hong Kong Polytechnic University, Hung Hom, Hong Kong. Email: eeecheng@polyu.edu.hk Fax: +852-2330 1544

Any secretarial support and production related matters, please contact Dr. James Ho, Power Electronics Research Centre, The Hong Kong Polytechnic University, Hung Hom, Hong Kong. Email: eeapej@polyu.edu.hk Tel: +852-3400 3348 Fax: +852-3400 3343

Publication Details

The Journal will be published 2-3 times a year. The first issue was published in 2007. Response time for paper acceptance is within 3 months.

Financial Charge

All the accepted papers will be printed without charge for 6 or less pages. An additional page charge is HK$100 per page. A hardcopy of the journal will be posted to the corresponding author free of charge. Additional copies of the journal can be purchased at HK$200 each. The charge includes postage and packing.

All Chinese Papers will be subjected to a translational fee of HK$350 per page. It will be charged when the paper is accepted for publication.

Advertising

Advertisement is welcome. Full page advertisement is HK$1000. For colour advertisement, the amount is doubled. All the advertisement will be both posted online in the journal website and hardcopy of the journal.

For advertising enquiries and details, please contact Ms. Anna Chang, eeapej@polyu.edu.hk .
Tel: +852-3400 3348 Fax: +852-3400 3343

For payment, please send your cheque, payable to 'The Hong Kong Polytechnic University, address to Ms. Kit Chan, Secretary of APEJ, Dept. of Electrical Engineering, The Hong Kong Polytechnic University, Hung Hom, Hong Kong.